Studies on the effects of regulators of the cholesterol biosynthesis pathway and fatty acid oxidation on the thermogenic adipocyte function

KWON JUNGIN

2024

Abstract

Thermogenic (brown/beige) adipocytes are essential for maintaining whole-body homeostasis by dissipating heat in response to external cues (e.g., cold). Although accumulating evidence indicates that lipid metabolism affects thermogenic adipocyte function, the molecular mechanisms underlying it have not been fully understood. Therefore, this research aims to elucidate the role of lipid metabolism regulators in regulating thermogenic adipocyte function by focusing on 3-hydroxy-3-methylglutaryl-CoA reductase (HMGCR) and peroxisome proliferator-activated receptor alpha (PPARα), which are regulators of the cholesterol biosynthesis pathway and fatty acid oxidation, respectively. In the first part of the study, the effects of the cholesterol biosynthesis pathway on brown adipogenesis and the survival of mature brown adipocytes were elucidated by inhibiting HMGCR, a rate-limiting enzyme in the cholesterol biosynthesis pathway. HMGCR deficiency inhibited brown adipogenesis and mature brown adipocyte survival by inducing apoptosis. It was due to the lack of geranylgeranyl pyrophosphate (GGPP). Mature brown adipocyte-specific *Hmgcr* knockout showed brown adipose tissue (BAT) atrophy and impaired thermogenic capacity in mice. These findings revealed that the cholesterol biosynthesis pathway is important for maintaining BAT mass and its function by producing GGPP. In the second part of the study, the effect of *Ppara* gene expression on thermogenic adipocyte function was elucidated under inflammation. Obesity-associated chronic inflammation diminishes catecholamine responsiveness, resulting in a reduction in thermogenesis in adipocytes; however, the underlying mechanisms remain unclear. It was found that *Ppara* gene expression was downregulated by obesity-induced inflammation. Impaired *Ppara* gene expression suppressed beta adrenergic stimulation-induced thermogenic gene expression in adipocytes. It was revealed that inflammation-induced nitric oxide (NO) downregulated *Ppara* gene expression by suppressing its promoter activity via the suppression of transcriptional activity of specificity protein 1. The findings in Chapter2 suggested that downregulated *Ppara* gene expression by NO may provide a mechanistic link between inflammation-induced catecholamine resistance and a reduction in thermogenesis in adipocytes. Taken together, the present study suggests that proper regulation of lipid metabolism by its regulators in thermogenic adipocytes plays a crucial role in the maintenance of their thermogenic function.

Abbreviations

1400w	*N*-(3-[aminomethyl]benzyl)acetamidine
ACC1	Acetyl-CoA carboxylase
ADIPOQ	Adiponectin
ALK7	Activin receptor-like kinase 7
ANOVA	Analysis of variance
ASM	Acid soluble metabolite
ATF2	Activating transcription factor 2
ATF2	Activating transcription factor 4
ATGL	Adipose triglyceride lipase
ATP	Adenosine triphosphate
ATR	Atorvastatin
ACOX1	Acyl-coenzyme A oxidase 1
ADRB3	Adrenergic receptor beta 3
BAC	Bacterial artificial chromosome
BAT	Brown adipose tissue
BMI	Body mass index
BAX	Bcl-2-associated X
BCL	B-cell/CLL lymphoma
BIP	Binding immunoglobulin protein
BMP7	Bone-morphogenic protein 7
C/EBPα	CCAAT/enhancer-binding protein alpha
C/EBPβ	CCAAT/enhancer-binding protein beta
C/EBPδ	CCAAT/enhancer-binding protein delta
cAMP	Cyclic adenosine monophosphate
CE	Cold exposed
cGMP	Cyclic guanosine monophosphate
CL	CL316,243; 5-[(2*R*)-2-{[(2*R*)-2-(3-Chlorophenyl)-2-hydroxyethyl]amino}propyl]-1,3-benzodioxole-2,2-dicarboxylic acid disodium salt
CM	Conditioned medium
CT	Computed tomography
CASP3	Caspase 3
ChIP	Chromatin immunoprecipitation
CHOP	CCAAT-enhancer-binding protein homologous protein
CIDEA	Cell death-inducing DNA fragmentation factor alpha subunit-like effector

	A
CoA	Coenzyme A
CoQ	Ubiquinone
$CoQH_2$	Ubiquinol
CPT1	Carnitine palmitoyltransferase 1
CPT2a	Carnitine palmitoyltransferase 2a
Ctrl	Control
Cyt	Cytoplasm
DAPI	4',6-Diamidino-2-phenylindole
DEX	Dexamethasone
DI	Differentiation-induced
DMEM	Dulbecco's modified eagle medium
DNL	*De novo* lipogenesis
E10	Embryonic day 10
E18.5	Embryonic day 18.5
E8.5	Embryonic day 8.5
EDTA	Ethylenediaminetetraacetic acid
ER	Endoplasmic reticulum
ER^{T2}	Estrogen receptor T2
EWS	Ewing sarcoma
FA	Fatty acid
FABP4	Fatty acid-binding protein 4
FASN	Fatty acid synthase
FBS	Fetal bovine serum
FDG	Fluorodeoxyglucose
FITC	Fluorescein isothiocyanate
FPP	Farnesyl pyrophosphate
FGF21	Fibroblast growth factor 21
GGPP	Geranylgeranyl pyrophosphate
GGPS1	Geranylgeranyl pyrophosphate synthase 1
GGTI-286	*N*-4-[2(*R*)-Amino-3-mercaptopropyl]amino-2-phenylbenzoyl-L-leucine methyl ester
GGTase I	Geranylgeranyltransferase type 1
GTP	Guanine triphosphatase
GTP	Guanosine-5'-triphosphate
GW	GW7647 (PPARα agonist)
H&E	Hematoxylin and eosin
HDL-C	High-density lipoprotein cholesterol

HEPES	4-(2-Hydroxyethyl)piperazine-1-ethane-sulfonic acid
HFD	High-fat diet
HMGCR	3-Hydroxy-3-methylglutaryl-coenzyme A reductase
HMGCS2	3-Hydroxy-3-methylglutaryl-coenzyme A synthase 2
HRP	Horseradish peroxidase
HSL	Hormone-sensitive lipase
HOXA5	Homeobox A5
IBMX	3-Isobutyl-1-methylxanthine
IFNγ	Interferon gamma
IKK	IκB kinase
IKKε	IκB kinase epsilon
IL6	Interleukin 6
INSIG	Insulin-induced gene
IRS1	Insulin receptor substrate 1
ISO	Isoproterenol
JNK	c-Jun N-terminal kinase
KO	Knockout
LDL-C	Low-density lipoprotein cholesterol
LPL	Lipoprotein lipase
LPS	Lipopolysaccharide
LVS	Lovastatin
LXR	Liver X receptor
MAPK	Mitogen-activated protein kinase
MCE	Mitotic clonal expansion
MCP1	Monocyte chemoattractant protein 1
MCT1	Monocarboxylate transporter isoform 1
mRFP1	Monomeric red fluorescent protein 1
MTA	Mithramycin A
mTOR	Mammalian target of rapamycin
mTORC1	Mammalian target of rapamycin complex 1
MTS	3-(4,5-dimethylthiazol-2-yl)-5-(3carboxymethoxyphenyl)-2-(4-sulfophenyl)-2*H*-tetrazolium
MVA	Mevalonate
NAC	*N*-Acetyl-L-cysteine
NC	Negative control
ND	Normal diet
NF-κB	Nuclear factor kappa B
NIL	N^6-(1-iminoethyl)-L-lysine hydrochloride

NO	Nitric oxide
NOR5	(±)-*N*-{(*E*)-4-Ethyl-3-[(*Z*)-hydroxyimino]-6-methyl-5-nitro-3-heptenyl}-3-pyridinecarboxamide
NOS2	Nitric oxide synthase 2
NOx	Nitrogen oxides
Nuc	Nucleus
ODQ	1*H*-[1,2,4]Oxadiazolo[4,3-α]quinoxalin-1-one
P0.5	Postnatal day 0.5
P2	Postnatal day 2
P2Y6R	Purinergic receptor type 6
PBA	4-Phenyl butyric acid
PBS	Phosphate-buffered saline
PC	Positive control
PDGFRα	Platelet-derived growth factor alpha
PET	Positron emission tomography
PI	Propidium iodide
PI3K	Phosphatidylinositol 3-kinase
PKA	Protein kinase A
PKG	Protein kinase G
PPARα	Peroxisome proliferator-activated receptor alpha
PPARγ	Peroxisome proliferator-activated receptor gamma
PPRE	PPAR-responsive regulatory element
PPARGC1A	Peroxisome proliferator-activated receptor gamma coactivator 1 alpha (gene encoding PGC1α)
pRB	Phosphorylated retinoblastoma
PRDM16	PR domain-containing protein 16
RB	Retinoblastoma
ROS	Reactive oxygen species
RT	Room temperature exposed
RXR	Retinoid X receptor
RAC1	Rac family small GTPase 1
RPLP0	Ribosomal protein lateral stalk subunit P0
SCAP	SREBP cleavage-activating protein
scWAT	Subcutaneous white adipose tissue
SDS	Sodium dodecyl sulfate
SDS-PAGE	Sodium dodecyl sulfate-polyacrylamide gel electrophoresis
SEM	Standard error of the mean
siRNA	Small interfering RNA

SP1	Specificity protein 1
SQ	Squalene
SRE	Sterol regulatory elements
SREBP	Sterol regulatory element binding protein
SREBP1C	Sterol regulatory element binding protein 1c
T2D	Type 2 diabetes
T_3	3,3,5-Triiodothyronine
TAZ	Transcriptional coactivator with PDZ-binding motif
TBK1	TANK-binding kinase 1
TBST	Tris-buffered saline with 0.1% Tween® 20 detergent
TG	Triglyceride
TGFβ	Transforming growth factor beta
TMAO	Trimethylamine-*N*-oxide
TNFR1	Tumor necrosis factor receptor 1
TNFα	Tumor necrosis factor alpha
TUNEL	Terminal deoxynucleotidyl transferase-mediated 2'-deoxyuridine-5'-triphosphate nick-end labeling
Thap	Thapsigargin
Tun	Tunicamycin
UCP1	Uncoupling protein 1
UD	Undifferentiated
Veh	Vehicle
vWAT	Visceral white adipose tissue
WAT	White adipose tissue
WT	Wild-type
YAP	Yes-associated protein
Zol	Zoledronate

Contents

General Introduction

Obesity, the global epidemic, and its impact on metabolic abnormalities

Obesity is still an ongoing epidemic, as its prevalence is continuously and globally increasing. According to the World Obesity Atlas 2023, reported by the World Obesity Federation, the portion of overweight (>30 kg/m² body mass index (BMI) ≥ 25 kg/m²) and obese people (BMI ≥ 30 kg/m²) aged over 5 years is estimated to increase 13% and 10% more from 38% and 14%, respectively, in 2035 than in 2020, and approximately one in four men and women is projected to be obese by 2035 [1]. Obesity is one of the major risk factors for the development of metabolic disorders, such as insulin resistance, hyperglycemia, and dyslipidemia [2]. Individuals with obesity-related metabolic disorder exhibit a substantially higher risk of type 2 diabetes (T2D) and cardiovascular disease (CVD) compared to the healthy population, which consequently impairs quality of life and even increases mortality [3,4]. Therefore, understanding the mechanisms underlying the pathophysiology of obesity is essential for prevention and treatment strategies for obesity and obesity-related diseases.

Obesity is defined as abnormal (ectopic) or excessive fat accumulation in the body and as having body fat greater than 25% for men and more than 30% for women [5]. Obesity often results from a long-term positive energy balance due to excessive energy intake (e.g., increased food consumption) and reduced energy expenditure (e.g., an increased sedentary lifestyle) [6]. Not simply a state of fat accumulation, it increases the probability of having metabolic abnormalities, including dyslipidemia, hyperinsulinemia, and higher plasma free fatty acid and glycerol levels [7–9]. To be specific, approximately 60–70% of patients with obesity have dyslipidemia characterized by at least one of the following: higher total cholesterol (≥ 240 mg/dL), low-density lipoprotein cholesterol (LDL-C; ≥ 160 mg/dL), or triglycerides (TG; ≥ 200 mg/dL), or lower high-density lipoprotein cholesterol (HDL-C; < 40 mg/dL) [7]. Basal and glucose-stimulated insulin secretion rates are > 50% greater, and plasma free fatty acids and glycerol levels are higher by 26% and 47%, respectively, in obese individuals than in

non-obese individuals [8,9]. However, these metabolic disorders can be significantly attenuated by body weight loss, as proven by numerous weight loss studies. Weight loss in obese individuals (~20% body weight loss and an ~30% decrease in fat mass) decreases basal serum insulin and free fatty acid levels by ~35% and ~20%, respectively [8]. Moreover, 5–10% weight loss results in a ~6 mg/dL decrease in TG and ~16 mg/dL decrease in LDL-C [10]. Overall, obesity-associated metabolic disorders can be significantly improved through weight loss, suggesting that body fat and systemic metabolism are closely related.

Distribution and physiological function of adipose tissues

In mammals, there are two distinct classes of adipose tissue: brown adipose tissue (BAT) and white adipose tissue (WAT). In humans, WAT is dispersed throughout the body, with major intra-abdominal depots around the omentum, intestines, and perirenal areas (visceral WAT; vWAT), as well as subcutaneous depots in the buttocks, thighs, and abdomen (subcutaneous WAT; scWAT) [11]. White adipocytes in WAT contain one single lipid droplet and are highly adapted to store energy in the form of TGs. White adipocytes also serve as an energy supply by releasing energy substrates through the lipolysis of TGs stored in lipid droplets when energy is needed [12]. While BAT, in infants, is mainly found in the interscapular area, in adult humans, it is localized in a region extending from the anterior neck to the thorax [12]. BAT is mainly composed of brown adipocytes with a high mitochondrial content and a high capacity for lipid oxidation [12]. Contrary to white adipocyte function, brown adipocytes dissipate energy in the form of heat through a process called non-shivering thermogenesis, via the action of uncoupling protein 1 (UCP1), which uncouples mitochondrial respiration from ATP production in the mitochondrial inner membrane [12]. This energy-consuming futile cycle for thermogenesis makes BAT an attractive target tissue to study obesity and associated metabolic complications [13]. Apart from brown adipocytes, adipocytes in WAT can be converted into thermogenic adipocytes capable of expressing UCP1 induced by certain environmental (e.g., cold), hormonal (e.g., catecholamines), and

pharmacological stimuli (e.g., β-adrenergic receptor agonist), and they are called brown-in-white (beige) adipocytes. The process of converting white adipocytes to beige adipocytes is called browning [14,15]. Altogether, white adipocytes and brown adipocytes have different physiological functions: white adipocytes store energy as triglycerides, while brown adipocytes dissipate energy as heat through non-shivering thermogenesis, making BAT a valuable focus in obesity research.

Contribution of functional thermogenic adipose tissue to systemic metabolism

As thermogenic (brown/beige) adipocytes expend energy to produce heat, the existence of metabolically active thermogenic adipose tissues affects systemic metabolism, as proven by several human studies using 2-deoxy-2-[^{18}F]fluoro-D-glucose (FDG)-positron emission tomography (PET)/computed tomography (CT). Since FDG-PET/CT-detected human adipose depot consists of a mixture of brown and beige adipocytes, adipose tissue containing these adipocytes is hereinafter referred to as thermogenic adipose tissue (AT). Thermogenic AT uptakes circulating glucose at a rate of 90–120 nmol/g/min during acute cold exposure (placing one foot intermittently (5 min in/5 min out) in water at a temperature of 8°C during the PET/CT session) in healthy individuals. The rate is ~8-fold higher than that of skeletal muscles, on average, per gram of tissue during mild cold exposure [16]. Thermogenic AT also metabolizes ~7 μmol/min of plasma free fatty acid in healthy individuals exposed to cold [17]. Intracellular TG in thermogenic AT is hydrolyzed within 1–3 h through sympathetically stimulated intracellular lipolysis. Thermogenic AT TG fraction is reduced from 81 to 76% (i.e., from 136 g to 128 g of TG when assuming a total thermogenic AT mass of 168 g), and ~8 g of TG (~72 kcal) is mobilized from thermogenic AT over 2 h of mild cold exposure [16,18]. This reduction in TG content of thermogenic AT during acute cold exposure is specific to thermogenic AT and does not occur in WAT or in muscles [18]. Moreover, metabolically active thermogenic AT contributes to thermogenesis at 46–211 kcal per day during mild cold exposure in humans [19]. Altogether, this suggests a physiologically significant role of thermogenic AT in regulating whole-body metabolism.

Although it is unclear to what extent thermogenic AT is needed to play a role in energy balance in adult humans, it has been suggested that the decline in metabolic activities of thermogenic AT is associated with body weight gain and reduced metabolic effects in humans [20,21]. Metabolically active thermogenic AT is inversely correlated with the BMI and thermogenic AT prevalence is less in individuals with excessive accumulation of vWAT, which highly contributes to insulin resistance [20,21]. Moreover, the thermogenic AT glucose uptake rate falls to 35 nmol/g/min in obese individuals [16,17]. Thermogenic AT in overweight individuals exposed to cold metabolizes only 0.1 μmol/min of plasma free fatty acid [17]. Consumption of β-blockers that inhibit the sympathetic nervous system, thereby blocking activation of thermogenic adipocytes, reduces the total energy consumption by about 5–10%, which corresponds to 100–200 kcal per day. This reduction can explain the 1 to 3.5 kg weight gain observed in clinical studies [22]. However, 10 days of cold acclimation (14–15 °C) in patients with T2D results in enhanced peripheral insulin sensitivity by ~43% (glucose infusion rate during the hyperinsulinemic-euglycemic clamp) [23]. In addition, cold exposure increases glucose uptake and improves insulin sensitivity [24]. Therefore, activation of thermogenic adipocytes is promising for the improvement of obesity-induced metabolic abnormalities, such as T2D.

Underlying mechanisms of thermogenic adipocyte development and its activation

The protective role of thermogenic AT, in terms of its metabolic consequences prompted the molecular exploration of its activation. For an understanding of thermogenic adipose tissue function, an understanding of their development, as well as the factors that influence the activity of thermogenic adipocytes, is necessarily of importance. The most relevant molecular factor is UCP1, which exists in the inner mitochondrial membrane of thermogenic adipocytes [12]. UCP1 has only been found in thermogenic adipocytes and is, therefore, used as a thermogenic adipocyte marker. Mitochondria in almost all eukaryotic cells are responsible for ATP synthesis by using glucose and fatty acids as fuel. This process is referred to as respiration coupling, where the energy released during the reoxidation of

reduced coenzymes and oxygen consumption is in large part used to phosphorylate ADP into ATP. Due to the presence of UCP1, mitochondria in thermogenic adipocytes respire to dissipate energy as heat without being forced to phosphorylate ADP [12].

Under conditions of increased thermogenic demand, the number of thermogenic adipocytes increases through the process of adipogenesis to fulfill the demand. Adipogenesis is the process by which undifferentiated precursor cells differentiate into adipocytes. Sustained cold or β-adrenergic stimulation induces the adipogenesis of brown/beige adipocytes to increase the thermogenic capacity of AT [25,26]. The cellular process of adipogenesis involves three well-defined stages, as shown in **Figure 0-1**: (1) commitment of multipotent precursor cells to the thermogenic adipocyte lineage; (2) mitotic clonal expansion; and (3) terminal differentiation, involving the expression of adipocyte-specific genes and transcriptional factors such as the CCAAT/enhancer-binding protein alpha (C/EBPα) and peroxisome proliferator-activated receptor gamma (PPARγ) [26,27]. Brown and beige adipocytes arise from different precursor cells; most brown adipocytes originate from myogenic factor 5-positive (Myf5+) progenitor cells, similar to skeletal myocytes [26]. In contrast, beige adipocytes originate from Myf5-negative (Myf5−) progenitor cells, similar to white adipocytes [28,29]. The PRD1-BF1-RIZ1 homologous domain containing 16 (PRDM16) is a key transcriptional coactivator responsible for determining the brown/beige adipocyte lineage from progenitor cells in mice [26]. In culture cells, growth-arrested preadipocytes synchronously reenter the cell cycle after hormonal induction of differentiation and undergo mitotic clonal expansion (MCE), approximately two rounds of mitosis, which is required for terminal differentiation of adipocytes [27]. As the quiescent preadipocytes in G0/G1 phase across the G1/S checkpoint, transcription factor CCAAT/enhancer-binding protein beta (C/EBPβ) acquires DNA-binding activity, initiating MCE with transcription factor CCAAT/enhancer-binding protein delta (C/EBPδ) and inducing transcription factors such as CCAAT/enhancer-binding protein alpha (C/EBPα) and PPARγ, which are master transcription factors for adipogenesis [27,30,31]. C/EBPα can bind to the PPARγ promoter and activate the expression of PPARγ, thereby creating a pro-

adipogenic feed-forward loop [32]. PPARγ then activates transcription of many adipocyte genes whose expression produces thermogenic adipocyte phenotypes, such as *Ucp1*, adiponectin (*Adipoq*), and fatty acid synthesis-related genes such as fatty acid synthase (*Fasn*), acetyl-CoA carboxylase (*Acc1*), sterol regulatory element-binding protein 1 (*Srebp1*), fatty acid binding protein (*Fabp4*), and lipoprotein lipase (*Lpl*) [33–35]. PPARγ also plays an important role in activating its coactivator, peroxisome proliferator-activated receptor-gamma coactivator 1 alpha (*Ppargc1α*), to enhance *Ucp1* expression [36].

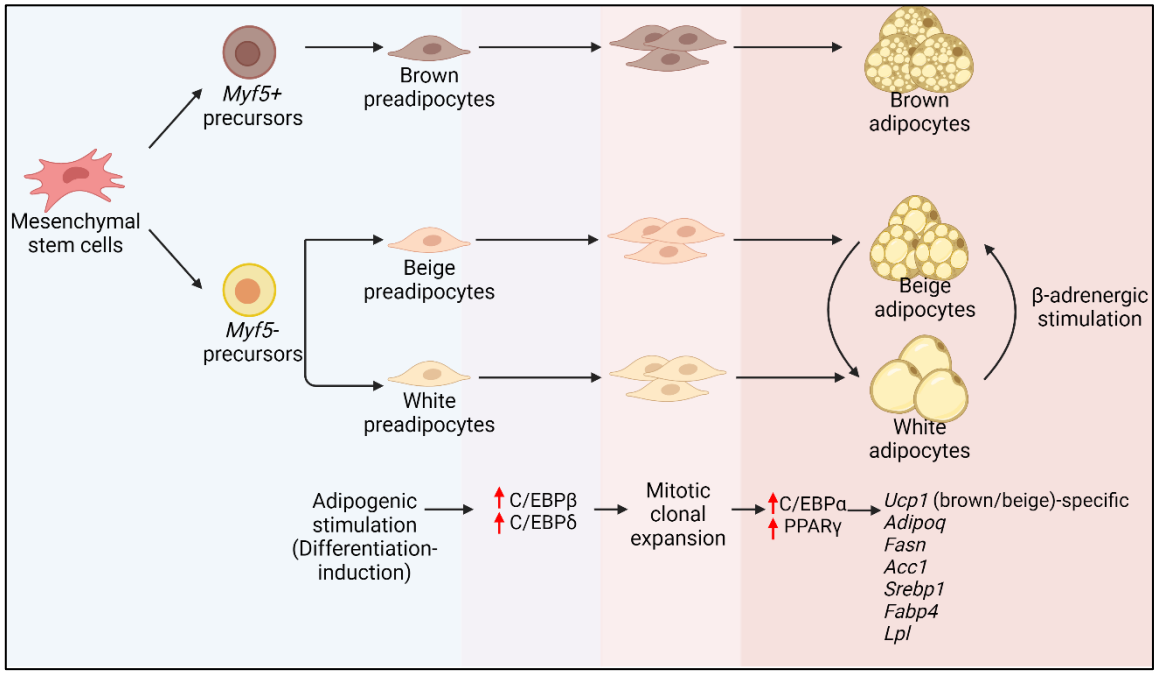

Figure 0-1. The schematic diagram of the process of adipogenesis and related gene expression during adipogenesis

External cues such as cold exposure can trigger non-shivering thermogenesis in BAT and browning of WAT by activating specific signaling cascades within thermogenic adipocytes to increase the rate of heat production [25]. Cold temperatures stimulate the sympathetic nervous system to release norepinephrine, which then binds to β-adrenergic receptors in brown/beige adipocytes and increases intracellular cyclic adenosine monophosphate (cAMP) levels through the activation of adenylyl cyclase [26]. cAMP activates protein kinase A (PKA), and PKA subsequently phosphorylates hormone-sensitive lipase (HSL) and perilipin to release fatty acids from TGs that are both the substrate for thermogenesis

and the regulators of UCP1 activity [12]. Fatty acids produced by lipolysis can undergo β-oxidation to produce reduced electron carriers NADH and FADH, which are then oxidized by the electron transport chain, resulting in the formation of a proton-motive force that will be released by UCP1 as heat [12]. Fatty acids also directly bind UCP1 to assist proton influx into the mitochondrial matrix [12]. β-adrenergic signaling increases glucose uptake to compensate for the loss of mitochondrial ATP production due to uncoupling as well as induces thermogenic gene transcription through activating transcription factor 2/cAMP-responsive element binding protein (ATF2/CREB) transactivation, which subsequently promotes thermogenic gene transcription, including *Ucp1* [33]. Sympathetic activation also results in increased fat mobilization in WAT, and released fatty acids from WAT are used in peripheral tissues, such as thermogenic AT [12]. These series of processes of β-adrenergic stimulation in response to catecholamines, as recapitulated in **Figure 0-2**, induce the thermogenesis and browning of adipocytes to increase their thermogenic capacity. Impairments in these orchestrated processes can affect thermogenic AT function and may lead to metabolic disorders.

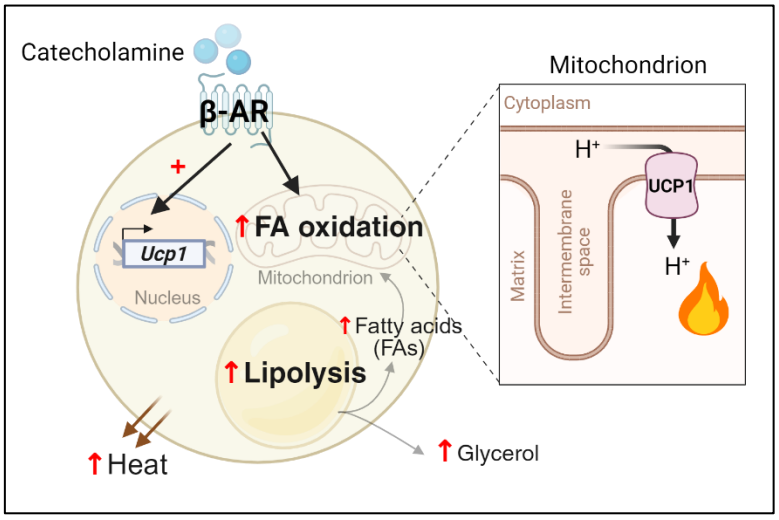

Figure 0-2. The schematic diagram of the mechanism underlying activation of the cold/catecholamine-induced β-adrenergic receptor and its downstream events in thermogenic adipocytes

Adipocyte metabolic dysregulation in obesity

Healthy adipocytes exhibit extensive metabolic flexibility, responding to anabolic and catabolic signals, such as insulin and catecholamines, respectively, to preserve whole-body energy homeostasis. However, in the setting of chronic positive-energy balance, thermogenic adipocytes develop metabolic inflexibility, characterized by a diminished response to signals regulating both the storage and utilization of energy [37]. Hypertrophied adipocytes due to excessive fat storage are accompanied by macrophage recruitment and initiate local inflammation [38,39]. As a result, basal lipolysis is elevated in adipocytes, increasing the leakage of free fatty acids, which can promote inflammation by activating nuclear factor-kappa B (NF-κB) and c-Jun N-terminal kinase (JNK) signaling pathways [40] which has been known to reduce the interaction of insulin receptor substrate 1 (IRS1) with phosphatidylinositol 3-kinase (PI3K), thereby attenuating the cellular response to insulin [41,42]. Activation of NF-κB signaling pathways can also increase the synthesis and secretion of many chemokines, such as interleukin 6 (IL6), tumor necrosis factor alpha (TNFα), interferon gamma (IFNγ), transforming growth factor beta (TGFβ), and monocyte chemotactic protein 1 (MCP1) in adipocytes, resulting in progressive proinflammatory macrophage infiltration [43]. Moreover, the release of fatty acids from insulin-resistant adipocytes results in the accumulation of ectopic fat in peripheral tissues (e.g., liver, muscle) and contributes to obesity-induced metabolic diseases, including T2D [43]. Likewise, failure to proper response to external cues in adipocytes can lead to metabolic dysfunction and pathological conditions, such as T2D and its comorbidities.

Inflammation produces catecholamine resistance in obesity [44]. Catecholamine activates β-adrenergic receptors on adipocytes to increase intracellular levels of cAMP, which causes a kinase cascade resulting in lipolysis and the activation of transcription factors, including ATF2 and ATF4, which promote the expression of genes involved in thermogenesis, such as *Ucp1* [35]. However, chronic inflammation reduces catecholamine responsiveness by attenuating β-adrenergic signaling, which results in a reduction in lipolysis and thermogenesis in response to sympathetic activation in adipocytes

[44]. Although the mechanism underlying catecholamine resistance in adipocytes remains uncertain, several pathways characterized by reduced expression of β-adrenergic receptors, reduced mitochondrial biogenesis, and reduced activity of post-receptor pathways have been implicated [44]. The mechanism that reduces β-adrenergic signaling after long-term TNFα exposure may be involved. For example, TNFα-induced expression of the kinases IκB kinase epsilon (IKKε) and TANK-binding kinase 1 (TBK1) attenuates cAMP signaling by phosphorylating and activating the major adipocyte phosphodiesterase 3B [45]. This reduction in cAMP signaling reduces the expression of several genes involved in lipolysis and thermogenesis, such as *Hsl* and *Ucp1*, thereby diminishing both lipolysis and thermogenesis [46]. Thus, obesity-induced chronic inflammation may contribute to the repression of energy expenditure during obesity; however, the underlying mechanism of chronic inflammation-associated catecholamine resistance in adipocytes is still not understood.

Regulation of lipid metabolism in thermogenic adipocytes: implications for adipocyte thermogenic function

The dysfunction of thermogenic adipocytes has been implicated in aberrant lipid metabolism in thermogenic adipocytes through their regulators. Disruption of adipocyte *de novo* lipogenesis (DNL) by deletion of fatty acid synthase (FAS) in mice induces browning in WAT [47]. Similarly, knockout of *Acc1*, an enzyme catalyzing the carboxylation of acetyl-CoA to malonyl-CoA, induces browning of adipocytes while blocking malonyl-CoA and palmitate synthesis [47]. The previous report indicates that ACC1 and FAS are strong suppressors of adipocyte thermogenic function through promoting lipid synthesis rather than modulating the DNL intermediates, acetyl-CoA or malonyl-CoA [47]. FA activates and fuels UCP1-mediated non-shivering thermogenesis in thermogenic AT. The breakdown of intracellular TGs into FAs is catalyzed by adipose triglyceride lipase (ATGL) in adipocytes. Thermogenic adipocyte-specific loss of ATGL impairs lipolysis in thermogenic adipocytes [48]. Although lipolysis within thermogenic AT itself is not required for thermogenesis, a lack of lipolysis in

thermogenic adipocytes makes them dependent on blood glucose and circulating free FA released from WAT lipolysis for thermogenesis during fasting [48], suggesting that intracellular lipolysis in adipocytes is important for the immediate supply of fuel for thermogenesis in adipocytes. Moreover, thermogenic adipocyte-specific knockout of carnitine palmitoyltransferase 2 (*Cpt2a*$^{-/-}$), an obligate step in mitochondrial long-chain fatty acid oxidation, fails to upregulate thermogenic genes in response to β-adrenergic stimulation, indicating that FA oxidation is required for cold-induced thermogenesis in adipocytes [49]. Taken together, these results suggest that proper regulation of lipid metabolism by its regulators in thermogenic adipocytes is important for exerting their thermogenic function.

The role of the cholesterol biosynthesis pathway in cellular processes, regulation, and its implications in thermogenic adipocyte function

The cholesterol biosynthesis pathway, as shown in **Figure 0-3**, plays an important role in maintaining multiple cellular processes by producing sterol isoprenoids, such as cholesterol, precursor of bile acids, lipoproteins, and steroid hormones, and non-sterol isoprenoids, such as dolichol and heme A [50]. The cholesterol biosynthesis pathway is regulated by HMG-CoA reductase (HMGCR), which is a rate-limiting enzyme of the pathway [50]. Ohashi K, *et al*. have demonstrated that homozygous knockout of HMGCR causes early embryonic lethality in mice; however, heterozygous knockout appears to have no effect on growth and the hepatic cholesterol biosynthesis pathway [51], implying that the cholesterol biosynthesis pathway is essential for maintaining life in mammals and might be robustly regulated. Transcriptional regulation of HMGCR is mediated by two members of the sterol regulatory element binding proteins (SREBP) family, called SREBP1 and SREBP2. In response to intracellular sterol levels, SREBPs regulate the cholesterol biosynthesis

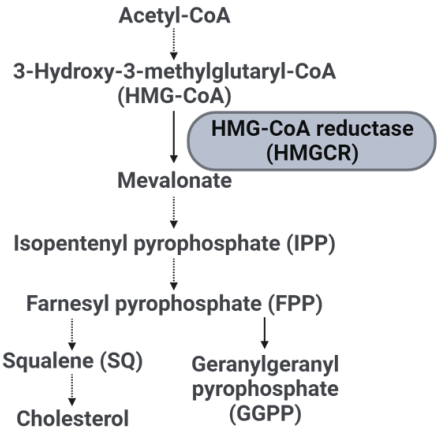

Figure 0-3. Schematic diagram of the cholesterol biosynthesis pathway

pathway [52]. Briefly, when the amount of intracellular sterol increases, the inactive form of SREBPs at the endoplasmic reticulum (ER) binds with SREBP cleavage-activating protein (SCAP) and the insulin-induced gene (INSIG)-1 and -2 [53]. However, in response to sterol deprivation (e.g., when HMGCR activity is inhibited), SREBPs no longer bind SCAP, thus producing a conformational change that triggers the SCAP-SREBP complex dissociation from the INSIGs and translocates from the ER to the Golgi, where SREBPs are cleaved by Golgi-resident proteases [53]. Once released from membranes, transcriptionally active fragments of SREBPs migrate to the nucleus and bind to sterol regulatory elements (SRE) [53]. This initiates the transcription of target genes related to the biosynthesis of cholesterol-derived metabolites and cholesterol uptake to restore intracellular isoprenoid and sterol levels [53].

Statins, competitive inhibitors of HMGCR, are the most widely prescribed for lowering circulating LDL-C levels [53]. Accumulating evidence has indicated that statin has some unexpected effects independent of lowering plasma cholesterol, such as an increased risk of diabetes [54]. The possible mechanism is linked to the inhibition of glucose uptake in adipocytes due to reduced intracellular signaling, which results in insulin resistance in adipocytes [55,56]. Furthermore, adipose-specific ablation of HMG-CoA reductase significantly impaired glucose and insulin tolerance in mice [57], indicating that the adverse effect of statins might be due to inhibition of the cholesterol biosynthesis pathway in AT. Besides, it has been demonstrated that the cholesterol biosynthesis pathway is involved in the determination of lineage into adipocytes or another cell type in some multi-potential cells, which are possibly associated with prenylation [58]. These suggest that metabolites from the cholesterol biosynthesis pathway play multiple roles in cell physiology; however, their physiological role in thermogenic adipocytes has not been fully understood.

Farnesyltransferase and geranylgeranyl transferases are two enzymes that carry out the process of prenylation in the cell, called farnesylation and geranylgeranylation, respectively [59]. This process involves the covalent attachment of hydrophobic molecules (either the C-15 isoprene farnesyl or the C-

20 isoprene geranylgeranyl groups) to the C-terminal end of certain proteins, including the small GTP-binding proteins [59]. This posttranslational modification is essential for the proper function of small GTP-binding proteins that are involved in protein synthesis, intracellular signaling, gene expression, and cell growth [59]. As an example, it has been reported that prenylation of $p21^{ras}$ is important for insulin-stimulated adipogenesis in 3T3-L1 adipocytes by activating MAPK and cyclic AMP response element-binding protein in response to insulin [60], implying the possible role of prenylation in brown adipogenesis.

The relevance of the cholesterol biosynthesis pathway in BAT function has been implicated in several previous reports. SREBPs expression is upregulated in maternally cold-exposed fetal BAT [61]. Moreover, BAT-specific depletion of SREBP prevented the maintenance of body temperature under chronic cold exposure in mice [62], suggesting that the transcriptional activity of SREBPs in BAT is tightly regulated to maintain BAT function. It was found that the cholesterol biosynthesis pathway is essential for recruitment of thermogenic adipocyte in mice as well as in humans, as evidenced by the fact that inhibition of HMGCR with statins strongly suppresses the browning of human white adipocytes *in vitro* and WAT in mice *in vivo* [63], implying the importance of the cholesterol biosynthesis pathway in the regulation of the thermogenic function of adipocytes. However, the role of the cholesterol biosynthesis pathway in thermogenic adipocyte function is not fully understood. Thus, in Chapter 1, the role of the cholesterol biosynthesis pathway in brown adipogenesis and the survival of mature brown adipocytes, which are essential for maintaining the thermogenic function of brown adipocytes, will be investigated.

The role of PPARα, a regulator of fatty acid oxidation, in lipid metabolism and thermogenesis in adipocytes

The peroxisome proliferator-activated receptor α **(**PPARα), a member of the nuclear receptor subfamily, is a ligand-activated transcription factor that forms obligate heterodimers with the retinoid X

receptor (RXR) [64]. Ligand binding results in a conformational change in the receptor, promoting dissociation of repressors, recruitment of co-activators, and subsequent activation of target gene expression [65]. PPARα is highly expressed in tissues with high FA oxidation rates, such as the liver, heart, skeletal muscle, BAT, and kidney [66]. It functions as a nutritional sensor, which allows adaptation of the rates of FA catabolism by controlling the expression of genes involved in peroxisomal β-oxidation, including acyl-CoA oxidase 1 (*Acox1*) and mitochondrial carnitine/acyl carnitine shuttle and β-oxidation, including carnitine palmitoyltransferase 1 (*Cpt1*) and *Cpt2* [65,67]. PPARα-deficient mice develop fatty liver when subjected to a prolonged fast, highlighting the importance of PPARα in managing lipid metabolism [68].

Endogenous PPARα ligands are free FA derivatives formed during FA catabolism, lipogenesis, and lipolysis. Eicosanoid derivatives, including the chemoattractant leukotriene B4 and hydroxyeicosatetraenoic acid eicosanoid, the murine arachidonate 8-lipoxygenase product from arachidonic acid, are thought to be endogenous PPARα agonists [69]. Substrates of ACOX1 are also PPARα agonists, as proven by the disruption of ACOX1 in mice, resulting in elevated PPARα target gene expression [70]. In addition, products of FAS, an enzyme catalyzing the synthesis of FA, -dependent DNL function as PPARα activators. Liver-specific knockout of FAS results in liver steatosis, however, which was reversed by a synthetic PPARα agonist. [71]. ATGL-dependent hydrolysis of intracellular TG also yields lipid PPARα ligands [72]. In line, overexpression of hepatic ATGL triggers PPARα-dependent FA oxidation gene expression and ameliorates hepatic steatosis [72]. Altogether, PPARα plays an important

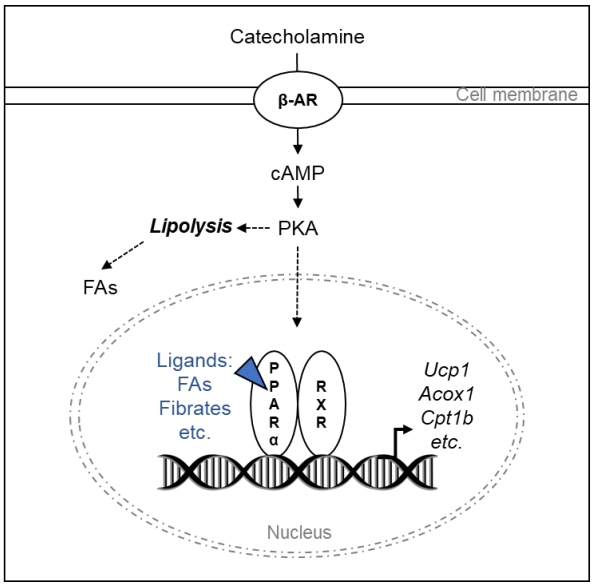

Figure 0-4. Schematic representation of the regulation of cold-induced target gene expressions by PPARα

role in translating products from lipid metabolism into changes in gene expression.

PPARα is highly expressed in thermogenic AT, and it is actually considered a distinctive marker of thermogenic adipocytes [73]. Cold exposure stimulates lipolysis by activation of cyclic AMP-dependent PKA and induces the expression and nuclear translocation of PPARα in thermogenic adipocytes and regulates the gene expression of *Ucp1*, as shown in **Figure 0-4**, by regulating the gene expression of peroxisome proliferator-activated receptor gamma coactivator 1 alpha (PGC1α) and PRDM16, a key protein required for the browning of white adipocytes [73]. PRDM16 co-activates PPARα to activate the expression of PGC1α and thermogenic genes in adipocytes by interacting with PPARα bound to the PPAR-responsive element (PPRE) [73]. Likewise, PPARα functions as a key component of the browning of white adipocytes by regulating thermogenic gene expression in response to cold.

The activation of PPARα by its synthetic agonist (bezafibrate) markedly reduces adiposity and ameliorates insulin resistance in obese mice by stimulating FA oxidation in adipocytes [74]. In line, adipocyte-specific PPARα overexpression protects from obesity-induced insulin resistance in mice [75]. Moreover, PPARα activation has been reported to increase thermogenic potential in adipocytes [76], supporting a role of PPARα in the regulation of adipocyte thermogenic function. Since obesity in mice has been linked to reduced *Ppara* expression levels in WAT as well as reduced thermogenic activity [74,77], decreased expression of *Ppara* may contribute to the reduction in thermogenic capacity in obese WAT. However, the regulatory mechanisms underlying the decreased expression of *Ppara* in obese WAT and its effects on adipocyte thermogenic function are poorly understood.

Objectives of this study

In this study, the roles of the cholesterol biosynthesis pathway and fatty acid oxidation in thermogenic adipocyte function were investigated by focusing on HMGCR and PPARα, a rate-limiting enzyme of the cholesterol biosynthesis pathway and a transcription factor of FA oxidation-related enzymes, respectively. Although HMGCR inhibition has been implicated in lower BAT prevalence in clinical studies, the molecular mechanism underlying it has not been clearly understood. Therefore, Chapter 1 of this study focused on the effects of HMGCR inhibition on brown adipogenesis and survival of mature brown adipocytes, which are important for the maintenance of BAT mass and its function (**Figure 0-5; left**).

Obesity-induced inflammation has been linked to catecholamine resistance, characterized by the reduction in FA oxidation as well as the thermogenic capacity of adipocytes in WAT; however, the mechanistic link between inflammation and catecholamine resistance remains elusive. Chapter 2 of this study focused on the effect of PPARα, not only a transcription factor of FA oxidation-related enzymes but also an important inducer of thermogenic program in adipocytes, on the browning of adipocytes under an inflammatory state (**Figure 0-5; right**). To elucidate the involvement of PPARα in inflammation-induced catecholamine resistance, the effects of inflammation on PPARα expression and also the effects of PPARα expressions on β-adrenergic-stimulated thermogenic gene expression in adipocytes were investigated. Lastly, the molecular mechanism underlying the downregulation of *Ppara* gene expression by inflammation was investigated. Altogether, the findings of the study may contribute to expanding our understanding of the lipid metabolism regulators that control thermogenic adipocyte function, which may lead to new approaches to enhancing the thermogenic activity of AT.

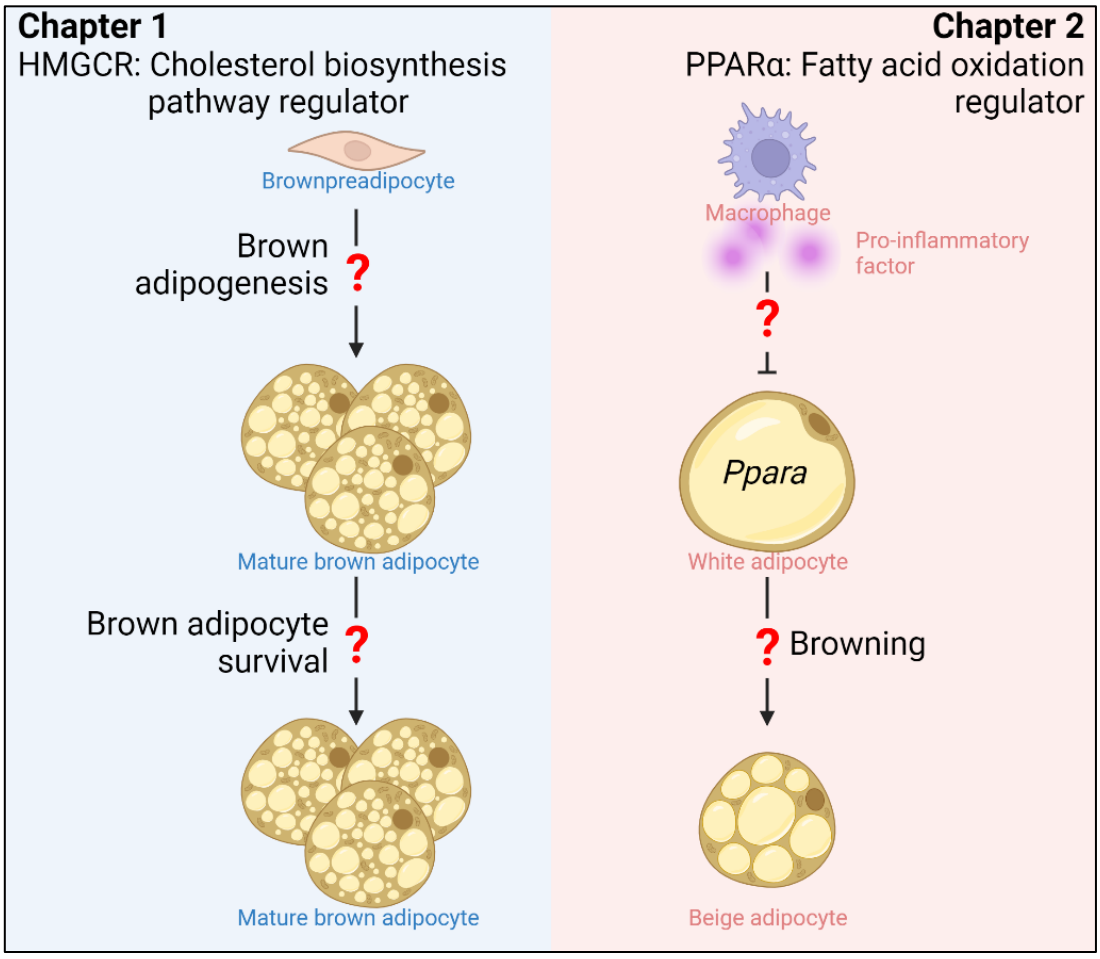

Figure 0-5. The objective of this study is to investigate the role of lipid metabolism regulators HMGCR and PPARα in thermogenic adipocyte function by focusing on: the effect of HMGR inhibition on brown adipogenesis and survival of mature brown adipocytes (Chapter 1); and the effect of *Ppara* downregulation by inflammation on thermogenic adipocyte function (Chapter 2)

Chapter 1

The effect of HMGCR inhibition on brown adipocyte function[1]

Introduction

Obesity is a major risk factor for T2D [2,78] and is characterized by excessive accumulation of adipose tissue, which is composed of WAT and BAT. Unlike WAT, which stores excessive energy in the form of triglycerides, BAT oxidizes energy substrates such as fats, carbohydrates, and branched-chain amino acids to produce heat via mitochondrial UCP1; therefore, BAT is considered a metabolically active tissue [79–82]. Notably, rodent and human studies have shown that BAT activity is inversely correlated with adiposity and insulin resistance [16,20,80]. Moreover, a previous study indicated that individuals with BAT have a significantly lower prevalence of T2D [83]. Thus, increasing the quantity or quality of BAT could be a promising therapeutic strategy for obesity and T2D.

The cholesterol biosynthesis pathway produces both sterols and non-sterols [50]. Among non-sterols, isoprenoids, such as farnesyl pyrophosphate (FPP) and geranylgeranyl pyrophosphate (GGPP), play pivotal roles in the post-translational modification (prenylation) of Ras and Ras-related small GTP-binding proteins and in the formation of biologically important molecules, including coenzyme Q, thereby regulating several cellular processes [50,59]. Statins, which are inhibitors HMGCR, a rate-limiting enzyme in the cholesterol biosynthesis pathway, are widely used for the clinical management of hypercholesterolemia. Along with the low-density lipoprotein cholesterol-lowering effect, statins can exhibit multiple pleiotropic effects that confer protection against cardiovascular diseases [84]. However,

[1] The content described in this chapter was originally published in *iScience*. Kwon J, Yeh YS, Kawarasaki S, Minamino H, Fujita Y, Okamatsu-Ogura Y, Takahashi H, Nomura W, Matsumura S, Yu R, Kimura K, Saito M, Inagaki N, Inoue K, Kawada T, and Goto T. Mevalonate biosynthesis pathway regulates the development and survival of brown adipocytes. *iScience.* (2023) 26(3):106161. doi: 10.1016/j.isci.2023.106161.

statins also exhibit several adverse effects, such as rhabdomyolysis, liver damage, and an increased risk of T2D, which appear to be primarily mediated by the suppression of isoprenoid biosynthesis [85]. Although the mechanisms underlying the adverse effects on skeletal muscle and the liver have been gradually clarified by tissue-specific inhibition of the cholesterol biosynthesis pathway in mice [86–88], the mechanisms underlying the statin-mediated increased risk of T2D remain unclear. A recent study showed an inverse correlation between statin use and active BAT in humans [63]. BAT dysfunction owing to inhibition of the cholesterol biosynthesis pathway could be associated with an increased risk of T2D following statin use.

The number of adipocytes is thought to be defined by the balance between newly differentiated adipocytes from preadipocytes and dead adipocytes. Upon hormonal induction of differentiation, growth-arrested preadipocytes re-enter the cell cycle and undergo several rounds of mitosis, which is referred to as MCE [27,89]. Transcription factors C/EBPβ and C/EBPδ, members of the CCAAT/enhancer-binding protein (C/EBP) family, are involved in the initiation of the clonal expansion phase [30,91]. C/EBPβ and C/EBPδ interact with C/EBP regulatory elements to activate the transcription of adipocyte-specific genes, including peroxisome proliferator-activated receptor gamma (*Pparg*) and *Cebpa*, which are master transcription factors of adipogenesis [30,31]. Differentiated adipocytes meet their fate via apoptosis, where activated caspase 3 induces cell death [92]. Under normal physiological conditions, adipocyte number seems constant, and approximately 10% of fat cells undergo annual turnover in adults [93]. Conditions such as intake of a high-fat diet and PPARγ agonist treatment, which are known to increase adipogenesis, have been found to be associated with increased adipocyte death [94,95]. These studies indicate that adipogenesis and adipocyte death are mutually controlled and are crucial regulatory events for maintaining adipose tissue mass. Dysregulation of either brown adipogenesis or brown adipocyte death can lead to abnormal regulation of BAT mass [96–98]. BAT atrophy leads to impaired thermogenesis and glucose intolerance [99,100].

These findings indicate that brown adipogenesis and brown adipocyte death play pivotal roles

in maintaining BAT mass and function. Although the essential role of the cholesterol biosynthesis pathway in adipocyte browning, which is a process converting white adipocytes to thermogenic adipocytes, has been reported [63], the detailed physiological roles of the cholesterol biosynthesis pathway in brown adipogenesis and brown adipocyte survival and their underlying mechanisms remain largely unknown.

In Chapter 1, we investigated the role of the cholesterol biosynthesis pathway in the regulation of brown adipocyte functions using cell culture and mouse models. The inhibition of HMGCR, the rate-limiting enzyme in the cholesterol biosynthesis pathway and the molecular target of statins, suppressed MCE process and brown adipocyte differentiation via protein geranylgeranylation-mediated suppression of the retinoblastoma protein (RB)- C/EBPβ pathway. The development of BAT in neonatal mice exposed to an HMGCR inhibitor during the fetal period was severely impaired. Moreover, statin treatment-induced GGPP deficiency led to the apoptosis of mature brown adipocytes. Brown adipocyte-specific *Hmgcr* knockout mice displayed BAT atrophy and disrupted thermoregulation during cold exposure. Importantly, both the induction of *Hmgcr* knockout and statin treatment in adult mice induced morphological changes in BAT via the induction of apoptosis. Together, these findings show that the cholesterol biosynthesis pathway-generated GGPP plays an indispensable role in maintaining BAT mass, which subsequently impacts BAT function.

Materials and Methods

Mice

All animal experiments were performed according to protocols approved by the Animal Research Committee of Kyoto University, Kyoto, Japan (permission number: R2-50). All mice were housed at 24 ± 1°C and maintained under a 12 h light/dark cycle. During all experiments, mice were fed a normal chow diet (MF, Oriental Yeast Co., Japan). To achieve LVS-induced pharmacological inhibition

of the cholesterol biosynthesis pathway in the fetus, male UCP1-mRFP1 BAC Tg mice [101] were mated with C57BL/6N-albino female mice (B6N-Tyr$^{c\text{-}Brd}$/BrdCrCrl, Charles River Laboratories). Female mice with confirmed virginal plug the day after mating were subcutaneously administered 10 mg/kg/day of lovastatin (LVS; Tokyo Chemical Industry, Cat. No. L0214) from embryonic day 8.5 (E8.5) to 18.5 (E18.5) (11 days in total). The mRFP1-positive offspring were identified by genotyping and analyzed on postnatal day 0.5 (P0.5). BAT-specific *Hmgcr* KO mice were generated by crossing *Hmgcr*$^{flox/flox}$ mice [57] with *Ucp1-Cre* mice (B6.FVB-Tg [Ucp1-cre] 1Evdr/J, The Jackson Laboratory) to generate *Hmgcr*$^{flox/+}$*Ucp1-Cre* progeny. The progeny was then backcrossed with *Hmgcr*$^{flox/flox}$ mice, and their *Hmgcr*$^{flox/flox}$*Ucp1-Cre* progeny were backcrossed with *Hmgcr*$^{flox/flox}$ mice to yield *Hmgcr*$^{flox/flox}$ and *Hmgcr*$^{flox/flox}$*Ucp1-Cre* progeny. *Hmgcr*$^{flox/flox}$ mice were used as the controls. To generate tamoxifen-inducible adipocyte-specific *Hmgcr* knockout (aiKO) mice, *Hmgcr*$^{flox/flox}$ mice were mated with *Adipoq-Cre*ER^{T2} mice (C57BL/6-Tg [Adipoq-cre/ERT2] 1Soff/J, The Jackson Laboratory). The progeny of *Hmgcr*$^{flox/flox}$*Adipoq-Cre*ER^{T2} mice were obtained in the same manner as *Hmgcr*$^{flox/flox}$*Ucp1-Cre* mice. 13-week-old male *Hmgcr*$^{flox/flox}$*Adipoq-Cre*ER^{T2} mice were intraperitoneally injected with tamoxifen (100 mg/kg/day, Tokyo Chemical Industry, Cat. No. T2510) or corn oil (Nacalai Tesque, Cat. No. 25606-65) for 5 consecutive days. Twenty days after the tamoxifen injection, the mice were sacrificed with isoflurane for further investigation.

HB2 cells

HB2 preadipocytes from the interscapular fat of p53-KO mice were cultured as described previously [102] with some modifications. Briefly, HB2 cells were maintained in Dulbecco's modified Eagle medium (Nacalai Tesque, Cat. No. 08458-16) with 10% fetal bovine serum (Gibco, Cat. No. 10270106) and 100 U/mL penicillin and 100 μg/mL streptomycin (Nacalai Tesque, Cat. No. 26253-84) at 37°C in 5% CO_2. Post-confluent HB2 cells were incubated in a differentiation medium containing 1 μM dexamethasone (DEX; Nacalai Tesque, Cat. No. 11107-64) and 0.5 mM 3-isobutyl-1-

methylxanthine (IBMX; Nacalai Tesque, Cat. No. NU03039) in the growth medium. After 48 h, the cell culture medium was replaced with a post-differentiation medium containing 10 μg/mL insulin (Wako Pure Chemical, Cat. No. 093-06476) and 50 nM 3,3,5-triiodothyronine (T_3; Sigma-Aldrich, Cat. No. T6397) in the growth medium, and the medium was changed every two days. To determine the effect of the cholesterol biosynthesis pathway on brown adipocyte differentiation, post-confluent HB2 brown preadipocytes were treated with LVS (Tokyo Chemical Industry, Cat. No. L0214), atorvastatin (ATR; Tokyo Chemical Industry, Cat. No. A2476), LVS in combination with metabolites from the cholesterol biosynthesis pathway, including mevalonate (MVA; Sigma-Aldrich, Cat. No. 44714), farnesyl pyrophosphate (FPP; Sigma-Aldrich, Cat. No. F6892), geranylgeranyl pyrophosphate (GGPP; Sigma-Aldrich, Cat. No. G6025), and squalene (SQ; Nacalai Tesque, Cat. No. 32115-62), zoledronate (Zol; Sigma-Aldrich, Cat. No. SML0223), Zol in combination with GGPP, LVS in combination with coenzyme Q_{10} (Ubiquinone, Tokyo Chemical Industry, Cat. No. C1971; Ubiquinol, Toronto Research Chemicals, Cat. No. U700500), GGTI-286 (Cayman Chemical, Cat. No. 22756), or GGTI-286 in combination with GGPP until day 2 after the induction of differentiation. On day 4, the HB2 cells were harvested for subsequent experiments. For DNA and intracellular lipid staining, brown adipocytes were double-stained with 5 μg/mL Nile red (Tokyo Chemical Industry, Cat. No. N0659) and 5 μg/mL Hoechst 33342 (Nacalai Tesque, Cat. No. 19172-51). The cells treated with Nile red and Hoechst 33342 were observed under a fluorescence microscope (Olympus IX83; Olympus), and images were captured with a DP71 CCD camera (Olympus). Fluorescence images were collected and merged by using DP-BSW software (Olympus). The fluorescence intensities were measured (Nile red, 485 nm/535 nm; Hoechst 33342, 360 nm/465 nm) by an Infinite® 200 apparatus (Tecan) and analyzed using i-control™ Microplate Reader Software (Tecan). For the LVS treatment experiment with mature brown adipocytes, differentiation-induced mature HB2 cells were treated with LVS, LVS in combination with metabolites from the cholesterol biosynthesis pathway, Zol, Zol in combination with GGPP, coenzyme Q_{10}, or GGTI-286 from day 4 to day 8. On day 8, the HB2 cells were harvested for subsequent experiments. For the

isoproterenol (ISO) treatment experiments, differentiation-induced HB2 cells or immortalized primary brown adipocytes were stimulated with 1 μM ISO (Sigma-Aldrich, Cat. No. I6504) for the indicated time durations, as described in **Figures 1-1F** and harvested for further analysis. Apoptotic cells were detected by using the Annexin V-FITC Apoptosis Detection Kit (Nacalai Tesque, Cat. No. 15342-54) according to the manufacturer's instructions, and cells stained by both Annexin V-FITC and PI were observed under a fluorescence microscope (Olympus IX83, Olympus). Fluorescence images were captured, collected, and merged as mentioned above. Cell viability was measured by using CellTiter-96® Aqueous One Cell Proliferation Assay (MTS assay; Promega, Cat. No. G3581) in accordance with the manufacturer's instructions.

Immortalized brown preadipocytes from interscapular BAT of UCP1-mRFP1 mice

Immortalized brown preadipocytes from interscapular BAT of UCP1-mRFP1 transgenic mice were cultured as described previously [103]. Briefly, post-confluent immortalized primary cells were incubated in a differentiation medium containing 0.25 μM DEX (Nacalai Tesque, Cat. No. 11107-64), 0.5 mM IBMX (Nacalai Tesque, Cat. No. NU03039), 1 nM T_3 (Sigma-Aldrich, Cat. No. T6397), 10 μg/mL insulin (Wako Pure Chemical, Cat. No. 093-06476), 125 μM indomethacin (Wako Pure Chemical, Cat. No. 095-02472), and 0.5 μM rosiglitazone (LKT Laboratories, Cat. No. R5773) in the growth medium. After 48 h, the cell culture medium was replaced with a post-differentiation medium containing 5 μg/mL insulin (Wako Pure Chemical), 1 nM T3 (Sigma-Aldrich), and 0.5 μM rosiglitazone (LKT Laboratories, Cat. No. R5773) in the growth medium, and the medium was changed every two days. For the ISO treatment experiments, differentiation-induced brown adipocytes were stimulated with 1 μM ISO (Sigma-Aldrich, Cat. No. I6504) for the indicated time durations, as described in **Figure S1-1A and S1-1C** and harvested for further analysis.

RNA preparation and quantification of gene expression

Total RNA was extracted using the QIAzol Lysis reagent (QIAGEN, Cat. No. 79306) or Sepasol Super-I (Nacalai Tesque, Cat. No. 09379-84), and 2 μg of total RNA samples was reverse-transcribed using Moloney murine leukemia virus reverse transcriptase (Promega, Cat. No. M170B), according to the manufacturer's instructions, in a thermal cycler. To quantify mRNA expression levels, quantitative reverse transcription-polymerase chain reaction was performed using a Light Cycler 480 II System (Roche) with THUNDERBIRD® SYBR® qPCR Mix (Toyobo, Cat. No. QPS-201). All measured mRNA expression levels were normalized to ribosomal protein lateral stalk subunit P0 (*Rplp0*) expression levels. The primer sequences are provided in **Table S1-2**.

Protein extraction

For whole cell lysates, the cells were washed twice with ice-cold PBS, and lysed in ice-cold lysis buffer (50 mM Tris-HCl pH 7.4, 150 mM NaCl, 1% Triton X-100 [*v/v*], 0.25% deoxycholate [*w/v*], 0.1% sodium dodecyl sulfate [SDS; *w/v*], and 1 mM EDTA) supplemented with 1% protease inhibitor cocktail (Nacalai Tesque, Cat. No. 03969-21) and 1% phosphatase inhibitor cocktail (Nacalai Tesque, Cat. No. 07575-51). After centrifugation at 16,700 ×*g* for 10 min at 4°C, the resulting supernatant was quantified using a DC protein assay Kit (Bio-Rad, Cat. No. 5000112) according to the manufacturer's instructions. Samples were denatured by boiling for 5 min in Laemmli sample buffer and used for western blotting analysis. For BAT lysates, BAT was homogenized and lysed in ice-cold lysis buffer (78 mM Tris-HCl pH 6.8, 6.25% sucrose [*w/v*], and 2% SDS [*w/v*]) supplemented with 1% protease inhibitor cocktail (Nacalai Tesque, Cat. No. 03969-21) and PhosSTOP phosphatase inhibitor cocktail (Roche, Cat. No. 4906837001). After centrifugation at 21,500 ×*g* for 30 min at room temperature, the resulting supernatant was quantified and denatured as mentioned above.

Subcellular fractionation

Cells were washed twice with ice-cold PBS, harvested, and lysed in ice-cold lysis buffer (10

mM HEPES pH 7.9, 10 mM KCl, 1.5 mM $MgCl_2$, 0.1% Triton X-100 [*v/v*], 0.1 mM EDTA and 1 mM dithiothreitol) supplemented with 1% protease inhibitor cocktail (Nacalai Tesque, Cat. No. 03969-21) and PhosSTOP phosphatase inhibitor cocktail (Roche, Cat. No. 4906837001) and incubated on ice for 15 min. The lysates were centrifuged at 860 ×*g* for 5 min at 4°C to isolate nuclei. The cytoplasm-containing supernatants were transferred to new tubes and centrifuged at 13,800 ×*g* for 1 h at 4°C to remove any contaminating nuclei. The supernatants were collected as cytoplasmic fractions. The nuclei pellets were resuspended in high salt buffer (20 mM HEPES pH 7.9, 400 mM KCl, 1.5 mM $MgCl_2$, 1% nonidet P-40 [*v/v*], 0.1 mM EDTA, 10% glycerol [*v/v*] and 1 mM dithiothreitol) supplemented with protease inhibitor and phosphatase inhibitor as mentioned above, followed by sonication with a Bioruptor UCD-300 (Cosmo Bio). The suspension was centrifuged at 16,200 ×*g* for 5 min at 4°C and supernatants were collected as nuclear fractions. Protein quantification was performed using a DC protein assay Kit (Bio-Rad, Cat. No. 5000112) according to the manufacturer's instructions. Samples were denatured by boiling for 5 min in Laemmli sample buffer, and used for western blotting analysis.

Western blotting

Protein samples were separated by SDS-PAGE and transferred to an Immobilon-P polyvinylidene fluoride transfer membrane (Millipore, Cat. No. IPVH00010). After blocking, the membrane was incubated with a primary antibody overnight at 4°C, followed by incubation with the horseradish peroxidase-conjugated secondary antibody (HRP-conjugated goat anti-mouse IgG, Santa Cruz Biotechnology, Cat. No. sc-2005; HRP-conjugated goat anti-rabbit IgG, Novus Biologicals, Cat. No. NBP1-75297). Primary antibodies used in this study were anti-UCP1 (an antiserum from a rabbit immunized with the rat UCP1 purified from BAT in cold-exposed rats, as described previously [108]), anti-β-Actin (Cell Signaling, Cat. No. 4967), anti-HMGCR (Abcam, Cat. No. ab174830), anti-RB (Abcam, Cat. No. ab181616), anti-C/EBPβ (Santa Cruz Biotechnology, Cat. No. sc-150), anti-C/EBPδ (Santa Cruz Biotechnology, Cat. No. sc-636), anti-α-Tubulin (Cell Signaling, Cat. No. 2144), anti-

Histone H3 (Cell Signaling, Cat. No. 3638), anti-Caspase 3 (GeneTex, Cat. No. GTX110543), and anti-Cleaved Caspase 3 (Asp175) (Cell Signaling, Cat. No. 9661). Proteins were visualized by chemiluminescence using an Immobilon Western Chemiluminescent HRP Substrate (Millipore, Cat. No. WBKLS0500). The chemiluminescent signal was detected using an ImageQuant LAS4000 (GE Healthcare) apparatus. The intensity of Western blot bands was quantified with ImageJ software (National Institutes of Health).

Thermal imaging and in vivo fluorescence imaging of neonates

Neonates (P0.5) were removed from the cage and the warmest spot within a defined region in the upper dorsal area of each neonatal mouse was identified by infrared thermographic camera (T335; Teledyne FLIR) **(Figure 1-5G)**. Fluorescence imaging was performed in the interscapular area using a Lumazone in vivo macro imaging system (Roper Technologies). Bright field and fluorescence imaging (excitation filter, 530–560 nm; emission filter, 590–650 nm) were performed with 0.3 s exposure time (**Figure 1-5E**). Surface plots of the images were acquired using PMCapture Pro 6.0 software (Roper Technologies). The range of the surface plot was 50-180 relative fluorescence units (**Figure 1-5F**). Fluorescence intensity was calculated using the ImageJ software (National Institutes of Health).

Rectal temperature measurement

For cold exposure experiments shown in **Figure 1-1B and 1-1D**, 14-week-old male C57BL/6N mice were housed individually and exposed to 10°C with ad libitum food and water. The mice were anesthetized with isoflurane at the indicated time points and dissected for further analysis. For cold exposure experiments shown in **Figure 1-8G**, 3-h-fasted-11–12-week-old male BAT KO and their littermates (Ctrl) were placed individually in cages and exposed to 4°C with free access to water. The rectal temperature was measured with a thermometer (BAT7001H; Physitemp Instruments Inc.) before exposure to cold and every hour after cold exposure. Infrared thermal images were obtained

before and 3 h after cold exposure at 6°C (**Figure 1-8H**). For the CL316,243 injection experiment (**Figure 1-8I**), 11–12-week-old male BAT KO mice and Ctrl mice were anesthetized with isoflurane at concentrations of 1.5%, were placed on a heat block set at 38.5°C. In addition, mice were subcutaneously administered saline or CL316,243 (1 mg/kg; Sigma-Aldrich, Cat. No. C5976) after a stable rectal temperature was confirmed; then, rectal temperature was monitored every minute using a thermometer (BAT7001H; Physitemp Instruments Inc.).

Hematoxylin and eosin staining of tissue sections

BAT was fixed with Bouin's solution (saturated picric acid : 37% formaldehyde : glacial acetic acid = 15 : 5 : 1) for 3 h, embedded in paraffin, and sectioned at 5 μm thickness using a microtome. The sections were transferred onto silane coated slides, deparaffinized with xylene, and rehydrated with sequential washes with diluted ethanol (100%, 99%, 90%, and 80%) followed by washing with running water. The samples were stained with eosin Y (Nacalai Tesque, Cat. No. 14410-42) and counterstained with Gill's hematoxylin (Merck, Cat. No. 105174).

Immunostaining analysis of BAT

For immunofluorescence staining with monocarboxylate transporter 1 (MCT1) and platelet-derived growth factor receptor alpha (PDGFRα), deparaffinized BAT sections were incubated in 0.3% Triton-X100 (Nacalai Tesque, Cat. No. 35501-02)/phosphate buffered saline (PBS) for 1 h, blocked with Blocking One Histo (Nacalai Tesque, Cat. No. 06349-64) for 10 min, and incubated with the primary antibodies diluted with Blocking One Histo (Nacalai Tesque, Cat. No. 06349-64) overnight at 4°C. After washing three times with PBS, the sections were incubated with fluorescence-conjugated secondary antibodies for 2 h. All sections were mounted with Fluoro-KEEPER Antifade Reagent with DAPI (Nacalai Tesque Cat. No. 12745-74) and observed under a confocal microscope (FluoView FV1000 Olympus IX81; Olympus). Fluorescence images were obtained and merged by using FV10-ASW

software (Olympus). Primary antibodies used for immunofluorescence staining included anti-MCT1 (Sigma-Aldrich, Cat. No. AB1286), anti-PDGFRα (Abcam, Cat. No. ab203491). Secondary antibodies used for immunohistochemical staining were as follows: CF488A-labeled goat anti-chicken IgY (Biotium, Cat. No. 20020), and CF568-labeled donkey anti-rabbit IgG (Biotium, Cat. No. 20098).

TUNEL staining of BAT section

TUNEL staining was performed using the *in situ* Apoptosis Detection Kit (Takara, Cat. No. MK500) following the manufacturer's instructions. Briefly, deparaffinized BAT sections were incubated in proteinase K (Nacalai Tesque, Cat. No. 29442-14) containing solution (50 mM Tris-HCl pH 8.0, 1 mM EDTA, and 20 μg/mL proteinase K) for 10 min, washed with PBS, blocked with Blocking One Histo (Nacalai Tesque, Cat. No. 06349-64) for 10 min, and incubated with anti-Perilipin (Novus Biologicals, Cat. No. NB100-60554) diluted with Blocking One Histo (Nacalai Tesque, Cat. No. 06349-64) overnight at 4°C. After washing three times with PBS, the sections were incubated with CF568-labeled donkey anti-goat IgG (Biotium, Cat. No. 20106) and TUNEL labeling buffer for 90 min at 37°C. After washing three times with PBS, all sections were mounted with Fluoro-KEEPER Antifade Reagent with DAPI (Nacalai Tesque, Cat. No. 12745-74) and observed under a confocal microscope (FluoView FV1000 Olympus IX81; Olympus).

Triglyceride measurement

HB2 cells were washed twice with ice-cold PBS, lysed in 0.5% Triton X-100 (Nacalai Tesque, Cat. No. 35501-02)/PBS, and sonicated by Bioruptor UCD-300 (Cosmo Bio, Japan) at a maximum setting for 30 s, performed four times on ice. The sonicated samples were boiled for 10 min and centrifugated at 16,200 ×*g* for 10 min at 4°C. The supernatant was collected, and the triglyceride concentration was measured using a Triglyceride E-test Kit (Wako Pure Chemical, Cat. No. 290-63701) in accordance with the manufacturer's instructions.

Mouse genotyping

mRFP1-positive mice and BAT-specific *Hmgcr* KO mice were identified by genotyping, as described previous [57]. Briefly, the tail tissues (2–3 mm) of mice or tissues were incubated with a lysis buffer (10 mM Tris-HCl pH 8.0, 25 mM EDTA, 0.5% SDS, and 100 mM NaCl) containing 1 mg/mL proteinase K (Nacalai Tesque, Cat. No. 29442-14) at 50°C overnight. After the samples were dissolved, 200 μL of phenol:chloroform:isoamyl alcohol (25:24:1; Nacalai Tesque, Cat. No. 25970-56) was added, and centrifuged at 13,800 ×*g* for 5 min at 4°C. The supernatant was transferred to a new tube, and 200 μL of chloroform was added. After centrifugation at 14,000 ×*g* for 5 min at 4°C, 160 μL of the supernatant was transferred to new tube containing 16 μL of 3 M Na-acetate and 400 μL of ethanol and centrifuged at 19,000 ×*g* for 20 min at 4°C. The DNA pellet was dissolved in TE buffer (pH 8.0). Genomic DNA was amplified using EmeraldAmp MAX PCR Master Mix (Takara, Cat. No. RR320B) in a thermal cycler and confirmed by agarose gel electrophoresis. Primer sequences used are listed in **Table S1-2**.

Transfer C57BL/6N neonates to ICR mice

On postnatal day 0.5 (P0.5), the neonates from the Veh or LVS (sc., 10 mg/kg/day from embryonic day E8.5 to embryonic day E18.5)-treated C57BL/6N mice (SLC, Japan) were removed from their dams and transferred to lactating ICR mice (SLC, Japan) within 24 h to be fostered. The number of neonates to be fostered per ICR mouse (fostering mouse) was limited to 5–6 to minimize the variability in pup weaning weight. ICR mice were used to foster neonates until weaning. The pups were weaned from the dam at 21 days of age and fed a normal chow diet (MF; Oriental Yeast Co., Japan) throughout the experimental period. Among grown-up mice, 9-weeks-old female mice were used in the experiments.

Quantification and statistical analysis

Data are presented as the mean ± standard error of the mean (SEM). Statistical analysis was performed using unpaired two-tailed Student's *t*-test or one-way analysis of variance (ANOVA) followed by Tukey's *post hoc* test. Correlation was analyzed by Pearson's correlation. Differences were considered statistically significant at $P < 0.05$. Statistical differences are indicated as * $P < 0.05$, ** $P < 0.01$, *** $P < 0.001$. Analyses were performed using SPSS Statistics for Windows, Version 17.0 (IBM).

Results

1-1. *Hmgcr* expression levels are highly correlated with *Ucp1* expression levels in BAT and brown adipocytes

To study the role of HMGCR in the regulation of brown adipocyte function, mRNA and protein expression levels of HMGCR in BAT was investigated. As shown in **Figure 1-1A**, mRNA expression levels of *Hmgcr* were found to be high in the testis and brain, which is consistent with a previous study [105]. *Hmgcr* mRNA expression levels in BAT are similar to those in skeletal muscles, in which HMGCR has been reported to be functional [88]. Because the thermogenic function of BAT is upregulated under cold temperatures, HMGCR expression levels during cold exposure were examined. Interestingly, mRNA and protein expression levels of HMGCR were increased by cold exposure (**Figure 1-1B and 1-1D**). Although mRNA expression of *Hmgcr* was immediately induced (~8 h; **Figure 1-1C**), prolonged cold exposure was required to markedly increase its protein levels (~48 h) (**Figure 1-1D**). Both HMGCR mRNA and protein expression patterns were highly correlated with those of UCP1, the gene responsible for non-shivering thermogenesis in brown adipocytes (**Figure 1-1C and 1-1E**). To investigate whether cold-induced β-adrenergic stimulation was involved in the upregulation of *Hmgcr* mRNA expression in brown adipocytes, the effect of isoproterenol (ISO), a β-adrenergic receptor agonist, on *Hmgcr* expression in HB2 brown adipocytes was examined. Similar to *Ucp1*, *Hmgcr* expression was markedly induced by ISO treatment (**Figure 1-1F and S1-1A**). We confirmed that *Hmgcr* expression was closely associated with the expression of *Ucp1* in brown adipocytes during β-adrenergic stimulation (**Figure 1-1G and S1-1B**). Moreover, HMGCR protein exhibited a similar expression pattern as UCP1 protein, peaking at 12 h in response to ISO stimulation (**Figure S1-1C**), which showed a strong positive correlation (**Figure S1-1D**). These findings indicate that *Hmgcr* expression in brown adipocytes is highly associated with *Ucp1* expression, which raises the possibility that the cholesterol biosynthesis pathway plays an important role in regulating BAT function.

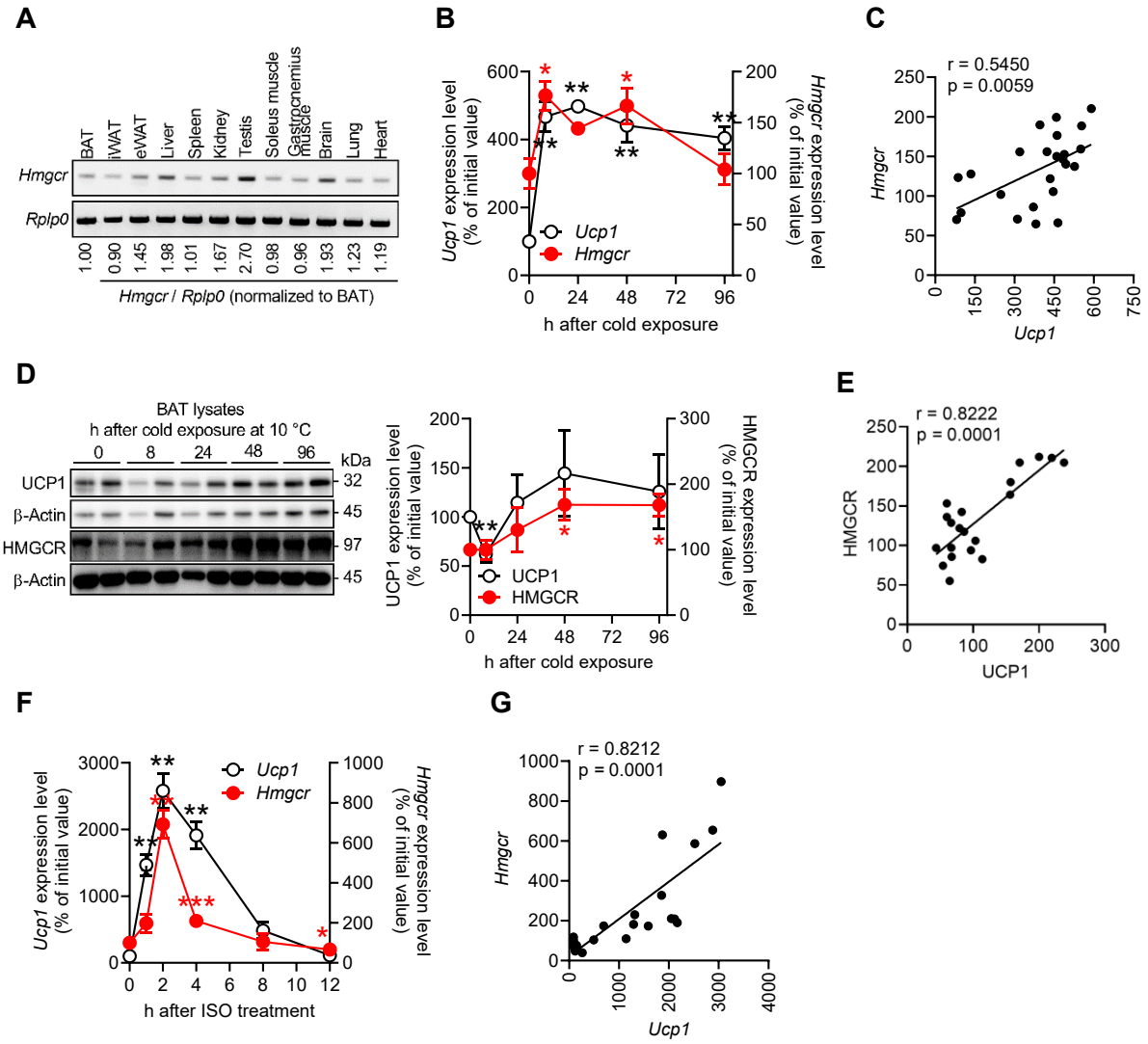

Figure 1-1. *Hmgcr* expression levels highly correlate with *Ucp1* expression levels in BAT and brown adipocytes

(A) *Hmgcr* mRNA levels in various tissues from 8-week-old male C57BL/6J mice (n = 2).

(B) mRNA levels of *Ucp1* and *Hmgcr* in BAT of 14-week-old male C57BL/6N mice exposed to cold at 10°C for an indicated time period (n = 4–8).

(C) Correlation between *Ucp1* and *Hmgcr* analyzed based on data from (B).

(D) Representative immunoblots of UCP1 and HMGCR (left) and relative protein abundance (right; n = 4). Each protein level was normalized to β-Actin.

(E) Correlation between UCP1 and HMGCR analyzed based on data from (D).

(F) mRNA levels of *Ucp1* and *Hmgcr* in HB2 cells after 1 μM isoproterenol (ISO) treatment (n = 3–4).

(G) Correlation between *Ucp1* and *Hmgcr* analyzed based on data from (F).

Data are shown as the mean ± SEM. **P* < 0.05, ***P* < 0.01, ****P* < 0.001 by unpaired two-tailed Student's *t*-test. Correlation was analyzed by Pearson's correlation. Black asterisk: *vs*. initial value of *Ucp1*; Red asterisk: *vs*. initial value of *Hmgcr*.

iWAT, inguinal white adipose tissue; eWAT, epididymal white adipose tissue.

1-2. Inhibition of the cholesterol biosynthesis pathway by statins impairs the differentiation capacity of HB2 brown preadipocytes

First, the mRNA expression level of *Hmgcr* in HB2 cells was determined. *Hmgcr* was highly expressed in HB2 brown preadipocytes and gradually decreased in differentiated HB2 cells, in which adiponectin (*Adipoq*) was highly expressed (**Figure S1-2**). Based on these results, HB2 brown preadipocytes were induced to differentiate in the presence of statins to investigate the potential role of the cholesterol biosynthesis pathway in brown adipocyte differentiation. Treatment with statins (atorvastatin [ATR] and lovastatin [LVS]) in the early stages of brown adipocyte differentiation suppressed lipid accumulation in a dose-dependent manner (**Figure 1-2A and 1-2B**). Moreover, LVS treatment suppressed the expression of adipocyte marker genes, including *Pparg*, fatty acid–binding protein 4 (*Fabp4*), and *Adipoq*, accompanied by marked suppression of *Ucp1* (**Figure 1-2C**). Notably, statin treatment suppressed the adipogenic stimulation-induced increase in DNA content (**Figure 1-2A and 1-2D**), suggesting that HMGCR suppression inhibited MCE during brown adipogenesis. Time-course experiment showed that differentiation induction of brown preadipocytes increased DNA content by almost 2.2 times 48 h after differentiation induction, whereas only 1.6 times increase in DNA content was observed in the presence of LVS (**Figure 1-2E**). These findings indicated that the cholesterol biosynthesis pathway is required for adequate MCE during brown adipocyte differentiation.

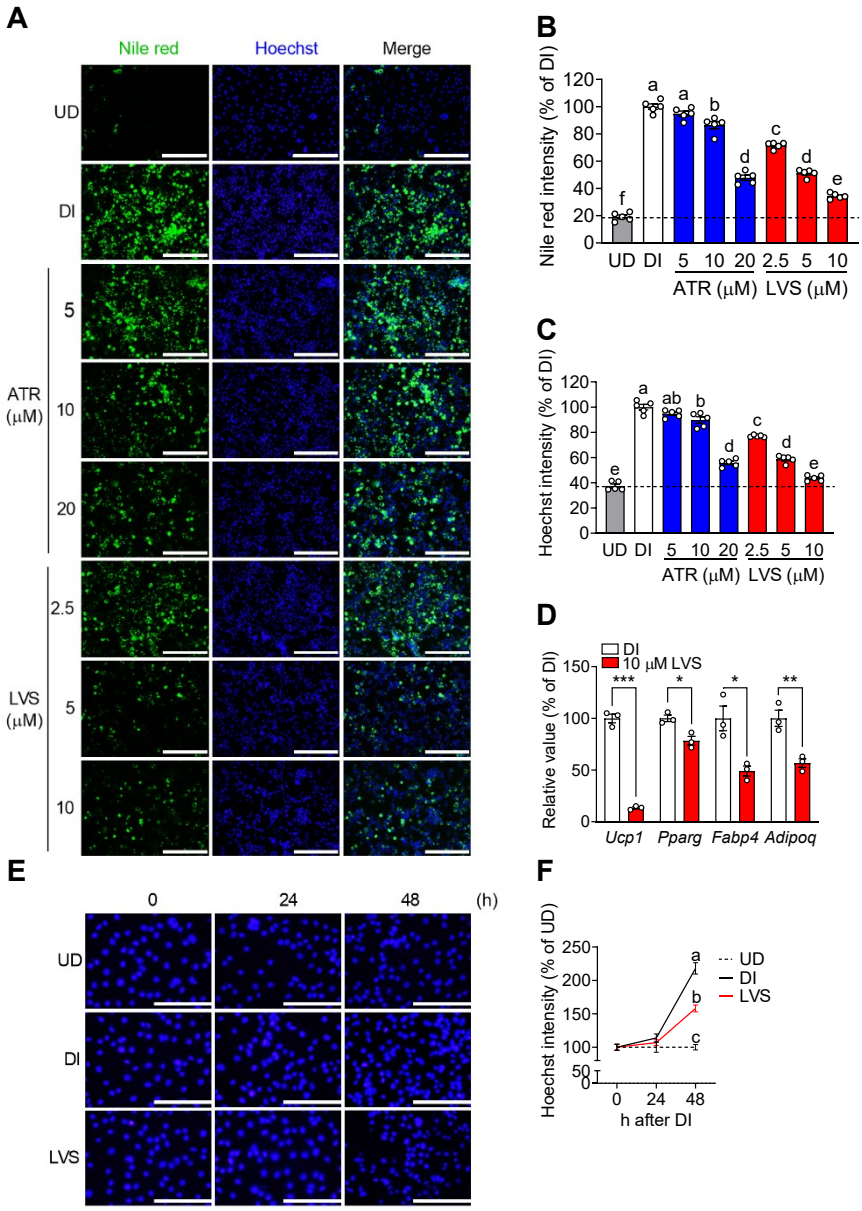

Figure 1-2. Inhibition of the cholesterol biosynthesis pathway by statins impairs the differentiation capacity of HB2 brown preadipocytes

(A) Representative microscopic view of undifferentiated (UD), differentiation-induced (DI), ATR-treated (days 0–2), or LVS-treated (days 0–2) HB2 cells after staining with Nile red (left) and Hoechst (middle) on day 4, respectively. Scale bars, 300 μm.

(B) Relative fluorescence intensity of Nile red (n = 5).

(C) Relative mRNA levels in HB2 cells treated with or without 10μM LVS (days 0–2) on day 4 (n = 3).

(D) Relative fluorescence intensity of Hoechst staining (n = 5).

(E) Representative microscopic view of UD, DI, or 10μM LVS-treated HB2 cells after staining with Hoechst at indicated time points (left) and relative fluorescence intensity of Hoechst (right; n = 5–6). Scale bars, 200 μm.

Data are shown as the mean ± SEM. *$P < 0.05$, **$P < 0.01$, ***$P < 0.001$ by unpaired two-tailed Student's *t*-test for (C). Groups with different letters are significantly different ($P < 0.05$) as determined by one-way ANOVA with Tukey's post-hoc analysis for (B), (D), and (E).

1-3. GGPP recovers the inhibitory effects of lovastatin on HB2 cell differentiation

To determine the metabolites responsible for the regulation of brown adipogenesis in the cholesterol biosynthesis pathway, HB2 cells were treated with LVS in combination with or without mevalonate (MVA), farnesyl pyrophosphate (FPP), geranylgeranyl pyrophosphate (GGPP), or squalene (SQ) (**Figure 1-3A**). It was found that LVS-induced inhibition of brown adipogenesis was largely recovered by MVA or GGPP (**Figure 1-3B**). Analysis of the fluorescence intensity of Nile red–stained cells revealed that the suppressed lipid accumulation by LVS treatment was partially recovered by MVA or FPP and completely recovered by GGPP co-treatment (**Figure 1-3C**). Moreover, LVS-induced suppression of differentiation-induction-activated cell proliferation was completely abolished in the presence of MVA or GGPP but not by FPP or SQ (**Figure 1-3D**). Consistent with the phenotypic results, LVS-induced suppression of the mRNA expression levels of *Ucp1* and adipocyte marker genes, such as *Fabp4* and *Adipoq*, was largely recovered by co-treatment with GGPP in HB2 brown adipocytes (**Figure 1-3E**). The time-course experiment clearly showed that GGPP co-treatment allowed HB2 cells to undergo MCE, as shown by the increase in DNA content to the same extent level as that in differentiation-induced (DI) HB2 cells (**Figure 1-3F**). Because LVS treatment at the concentrations used in this study has been reported to suppress cellular GGPP levels [106,107], these findings clearly indicated that the cholesterol biosynthesis pathway–mediated GGPP production is essential for MCE during brown adipocyte differentiation. To further confirm whether GGPP is the key metabolite for brown adipocyte differentiation, HB2 cells were treated with zoledronate (Zol), a nitrogen-containing bisphosphonate, to inhibit geranylgeranyl pyrophosphate synthase 1, which is required for GGPP biosynthesis [108]. Although Zol treatment at the beginning of brown adipogenesis significantly decreased intracellular lipid accumulation (**Figure 1-3G and 1-3H**) and DNA content (**Figure 1-3G and 1-3I**), these effects were completely reversed by co-treatment with GGPP (**Figure 1-3G–1-3I**). These results indicate that GGPP is required for brown adipogenesis.

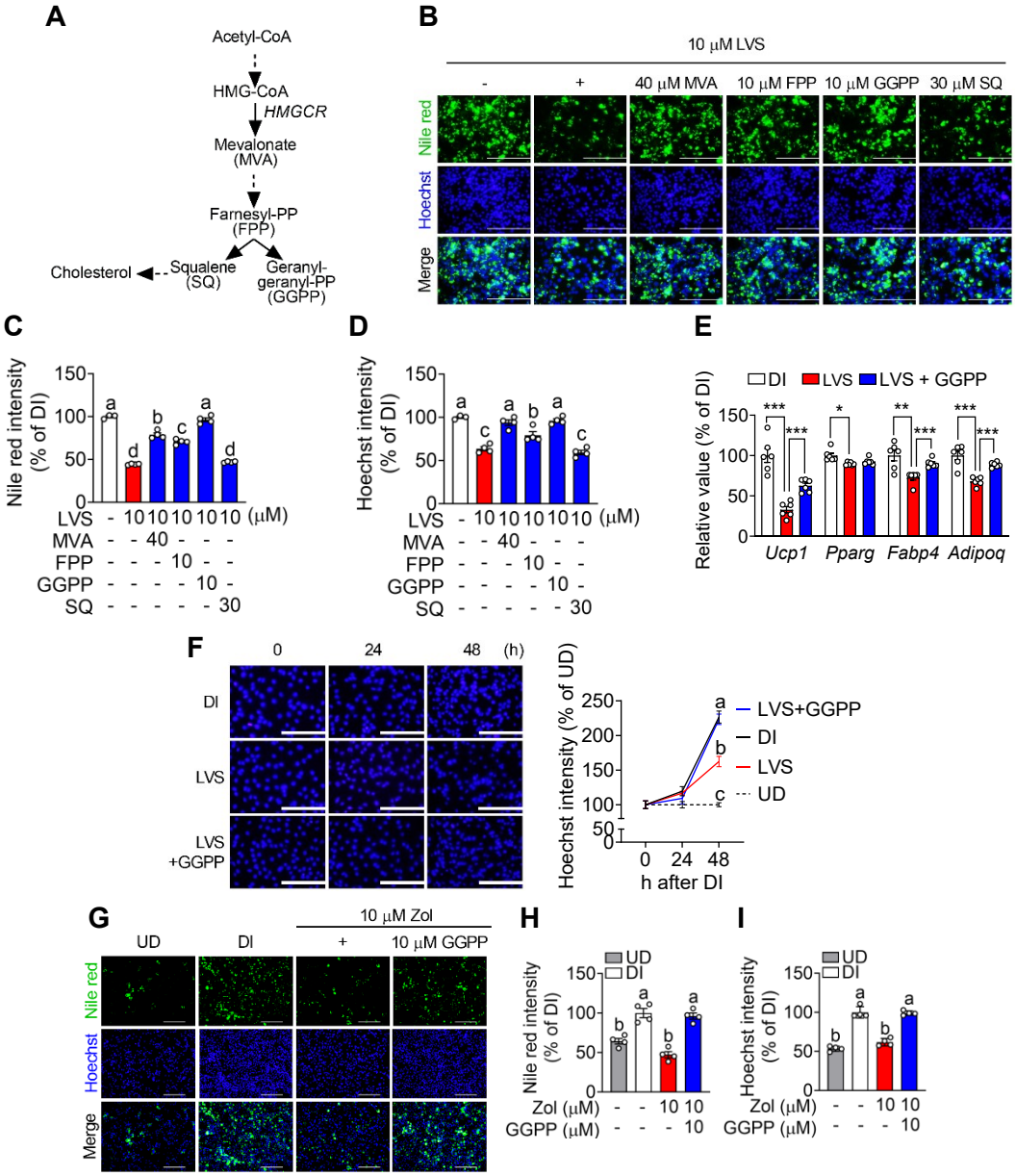

Figure 1-3. GGPP recovers the inhibitory effects of lovastatin on HB2 cell differentiation

(A) Schematic overview of the cholesterol biosynthesis pathway.

(B) Representative microscopic view of DI or LVS-treated HB2 cells with or without MVA, FPP, GGPP, or SQ treatment (days 0–2) after staining with Nile red (top) and Hoechst (middle) on day 4. Scale bars, 200 μm.

(C and D) Relative fluorescence intensities of Nile red (C) and Hoechst (D) staining (n = 3–4).

(E) Relative mRNA levels of DI, 10 μM LVS-treated, or 10 μM LVS plus 10 μM GGPP-treated (days 0–2) HB2 cells on day 4 (n = 6).

(F) Representative microscopic view of UD, DI, 10 μM LVS-treated, or 10 μM LVS plus 10 μM GGPP-treated HB2 cells after staining with Hoechst at the indicated time points (left) and relative fluorescence intensity of Hoechst (right; n = 5–8). Scale bars, 200 μm.

(G) Representative microscopic view of UD, DI, Zol-treated, or Zol plus GGPP-treated (days 0–2) cells after staining with Nile red (top) and Hoechst (middle) on day 4. Scale bars, 200 μm.

(H and I) Relative fluorescence intensities of Nile red (H) and Hoechst (I) staining (n = 4).

Data are shown as the mean ± SEM. *$P < 0.05$, **$P < 0.01$, ***$P < 0.001$ by unpaired two-tailed Student's *t*-test for (E). Groups with different letters are significantly different ($P < 0.05$) as determined by one-way ANOVA with Tukey's post-hoc analysis for (C), (D), (F), (H) and (I).

1-4. Protein geranylgeranylation is required for HB2 cell differentiation

Coenzyme Q_{10}, a product of GGPP, has been shown to be important for BAT function [109]; however, co-treatment with coenzyme Q_{10} (ubiquinol [$CoQH_2$; reduced form] or ubiquinone [CoQ; oxidized form]) could not recover either LVS-induced suppression of lipid accumulation (**Figure 1-4A, 1-4B, S1-3A, and S1-3B**) or LVS-induced suppression of the increase in DNA content (**Figure 1-4C, 1-4D, S1-3A, and S1-3B**), suggesting that LVS-mediated suppression of coenzyme Q_{10} production is not important for the anti-brown adipogenic effects of LVS. The covalent binding of GGPP to a target protein, called protein geranylgeranylation, is catalyzed by geranylgeranyltransferase type 1 (GGTase I) [110]. To investigate the effect of protein geranylgeranylation, GGTI-286, a GGTase I inhibitor, was used at the beginning of brown adipocyte differentiation. Similar to the effects of LVS, treatment with more than 10 μM of GGTI-286 significantly suppressed both lipid accumulation and increased DNA content (**Figure 1-4E and 1-4F**). Although co-treatment with GGPP significantly recovered GGTI-286-induced suppression of lipid accumulation (**Figure 1-4G and 1-4H**) and cell proliferation (**Figure 1-4G and 1-4I**), these recoveries were very limited. These results indicated that GGPP-mediated protein geranylgeranylation is essential for adequate MCE in differentiating brown adipocytes.

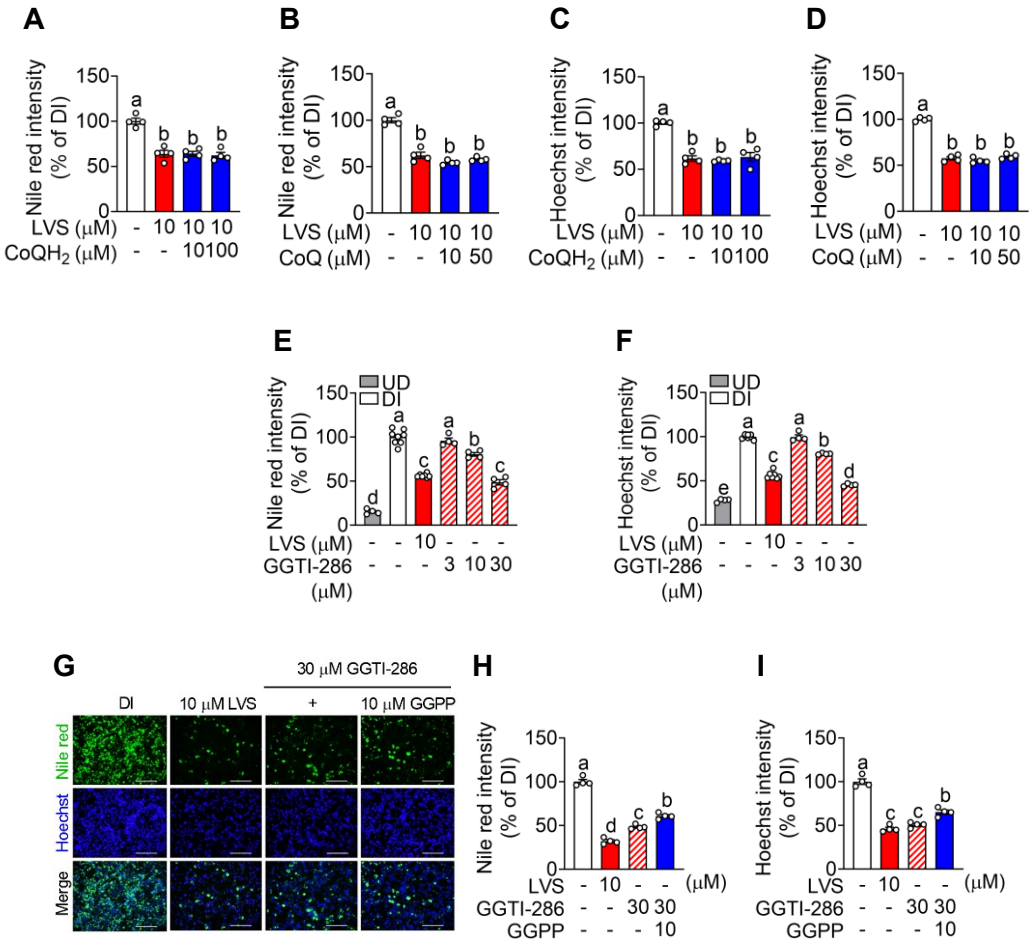

Figure 1-4. Protein geranylgeranylation is required for HB2 cell differentiation

(A and B) Relative fluorescence intensity of Nile red staining of DI or LVS-treated HB2 cells with or without $CoQH_2$ (A; n = 4) or CoQ (B; n = 4) treatment (days 0– 2) on day 4.

(C and D) Relative fluorescence intensity of Hoechst staining of DI or LVS-treated HB2 cells with or without $CoQH_2$ (C; n = 4) or CoQ (D; n = 4) treatment (days 0–2) on day 4.

(E and F) Relative fluorescence intensity of Nile red (E) and Hoechst (F) staining of UD, DI, LVS-treated, or GGTI-286-treated (days 0–2) HB2 cells on day 4 (n = 4–8).

(G) Representative microscopic view of DI, LVS-treated, or GGTI-286-treated HB2 cells with or without GGPP treatment (days 0–2) after staining with Nile red (top) and Hoechst (middle) on day 4. Scale bars, 200 μm.

(H and I) Relative fluorescence intensity of Nile red (H) and Hoechst (I) staining (n = 4).

Data are shown as the mean ± SEM. $*P < 0.05$, $**P < 0.01$, $***P < 0.001$ by unpaired two-tailed Student's *t*-test for (E). Groups with different letters are significantly different ($P < 0.05$) as determined by one-way ANOVA with Tukey's post-hoc analysis for (A–F), (H), and (I).

1-5. Neonates exposed to LVS during the BAT developmental period exhibit BAT atrophy and fail to maintain body temperature

Previous reports have shown that BAT develops from embryonic day 10 (E10) to postnatal day 2 (P2) [111]; thus, pregnant dams were treated with LVS to expose their fetuses to LVS from E8.5 to E18.5, as shown in **Figure 1-5A**. Notably, neonates from the LVS-injected dam showed interscapular BAT atrophy (**Figure 1-5B and 1-5C**). The BAT weight normalized to body weight yielded similar results (**Figure 1-5D**). Experiments using UCP1- monomeric red fluorescent protein 1 (mRFP1) reporter mice [101] showed that LVS exposure during the embryonic period significantly reduced mRFP1-derived fluorescence in the interscapular region, suggesting that UCP1 expression levels in BAT are suppressed by LVS (**Figure 1-5E and 1-5F**). Actually, the surface temperature of neonates exposed to LVS was significantly lower than that of Veh-exposed neonates (**Figure 1-5G**). A histochemical analysis showed that LVS-exposed neonatal BAT barely consisted of adipocytes with lipid droplets compared with Veh-exposed BAT (**Figure 1-5H**). Consistent with this, LVS treatment decreased the number of monocarboxylate transporter isoform 1 (a marker for mature brown adipocytes [112])-positive cells, whereas the number of platelet-derived growth factor alpha (a marker for adipocyte progenitor cells [113])-positive cells increased in LVS-exposed BAT in immunofluorescence analysis (**Figure 1-5I**). Furthermore, both thermogenesis-related genes (*Ucp1*, PPARγ coactivator 1 alpha [*Ppargc1a*], and PR domain containing 16 [*Prdm16*]) and adipocyte marker genes (*Pparg*, *Fabp4*, and *Adipoq*) in BAT were markedly downregulated by LVS treatment (**Figure 1-5J**). Further investigation was performed to determine the effects of fetal LVS exposure on the development of BAT in adult mice, following the schedule shown in **Figure S1-4A**. Fetal LVS exposure did not affect body weight or length, without significant changes in food intake (**Figure S1-4B–S1-4D**). Interestingly, BAT atrophy persisted even after the offspring from the LVS-exposed dam became adults, whereas other tissues and organs showed no apparent differences in weight compared to those of the offspring from the Veh-exposed dam (**Figure S1-4E and S1-4F**). However, obvious histological changes in BAT were not observed in fetal LVS-

exposed BAT (**Figure S1-4G**). Also. There were no significant changes in mRNA expression levels of either thermogenesis-related genes (*Ucp1* and *Ppargc1a*) or adipocyte marker genes (*Pparg*, *Fabp4*, and *Adipoq*) in BAT from a grown-up offspring of the LVS-exposed dam (**Figure S1-4H**). Consistently, no significant differences in UCP1 protein expression levels in BAT were observed between the Veh and LVS groups (**Figure S1-4I**). Taken together, these findings indicate that the cholesterol biosynthesis pathway in the embryonic period not only plays an essential role in the development of BAT in the fetus but also affects BAT mass in adult mice.

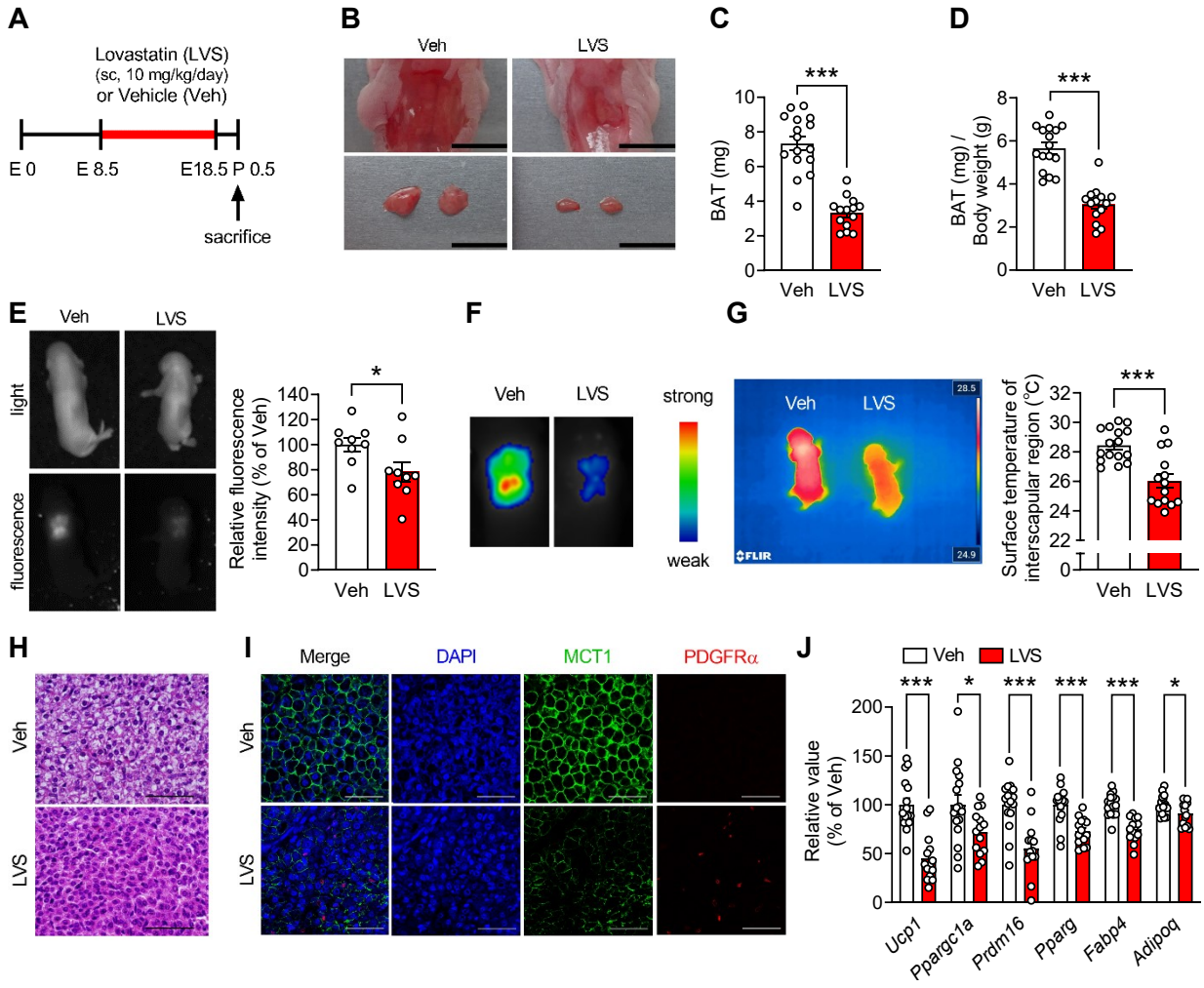

Figure 1-5. Neonates exposed to LVS during the BAT developmental period exhibit BAT atrophy and fail to maintain body temperature

(A) Schematic illustration of the in vivo LVS treatment experiment.

(B) Representative interscapular region (top) and BAT (bottom) images of neonates (P0.5). Scale bars, 1 cm.

(C and D) BAT weight (C) and BAT weight normalized to the body weight (D) of neonates (n = 14–16).

(E) *In vivo* imaging of prone-positioned UCP1-mRFP1 neonates (P0.5) in bright (left top) and fluorescent fields (left bottom) and relative fluorescence intensity around the interscapular area analyzed using ImageJ (right) (n = 9).

(F) Fluorescence intensity of the interscapular area of mice. The range of the surface plot represents 50–180 relative fluorescence units.

(G) Representative image of infrared thermography (left) and surface temperature of the interscapular region of neonates (P0.5) (right; n = 14–16).

(H) Representative images of hematoxylin and eosin (H&E)-stained BAT sections from neonates (P0.5). Scale bars, 50 μm.

(I) Representative immunofluorescence images of BAT isolated from neonates (P0.5). Scale bars, 40 μm.

(J) Relative mRNA levels in BAT isolated from neonates (P0.5) (n = 14–16).

Data are shown as the mean ± SEM. **P* < 0.05, ****P* < 0.001 by unpaired two-tailed Student's *t*-test.

1-6. LVS-mediated suppression of retinoblastoma phosphorylation may be associated with the functional inactivation of C/EBPβ in HB2 cells

C/EBPβ and C/EBPδ are the main MCE regulators [90,91]. Although the mRNA expression of both *Cebpb* and *Cebpd* was induced soon after the induction of differentiation in HB2 brown preadipocytes, LVS treatment did not affect the expression of either gene (**Figure 1-6A and 1-6B**). However, LVS treatment decreased the ratio of nuclear to cytoplasmic C/EBPβ protein levels without affecting nuclear C/EBPδ protein levels (**Figure S1-5**) in differentiating HB2 cells (**Figure 1-6C**), suggesting that LVS treatment decreased the nuclear localization of C/EBPβ protein. Interestingly, total C/EBPβ protein levels were also suppressed by LVS treatment (**Figure 1-6D**), which is consistent with a previous report using white adipocytes [114]. A previous study showed that adipocyte differentiation stimuli-induced hyperphosphorylation of the retinoblastoma (RB) protein is required for the transcriptional activation of C/EBPβ in 3T3-L1 cells [115]. RB phosphorylation was strongly induced within a day by the induction of differentiation in HB2 cells, whereas it was barely detectable in the presence of LVS (**Figure 1-6D**). In fact, LVS treatment suppressed C/EBPβ target genes, which are known to be important transcription factors for terminal differentiation of brown adipocytes, such as *Pparg*, *Cebpa*, and sterol regulatory element binding protein 1c (*Srebp1c*), at 48 h after differentiation induction without affecting *Cebpb* expression levels (**Figure 1-6E–1-6H**). These findings suggest that LVS treatment suppresses RB phosphorylation, which is followed by a change in C/EBPβ nuclear localization and suppression of its transcriptional activation.

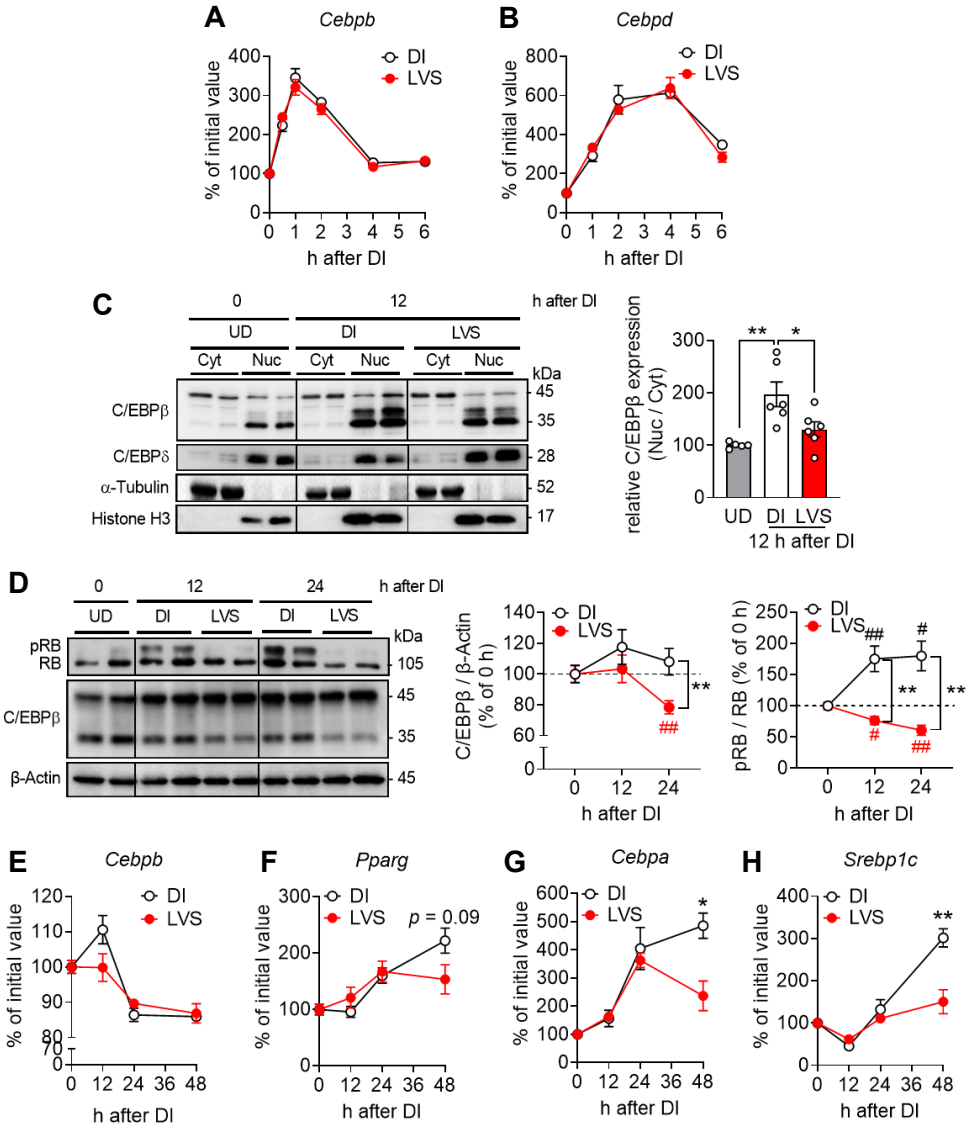

Figure 1-6. LVS-mediated suppression of retinoblastoma phosphorylation may be associated with the functional inactivation of C/EBPβ in HB2 cells

(A and B) Relative mRNA levels of *Cebpb* (A) and *Cebpd* (B) in differentiation-induced HB2 cells with or without 10 μM LVS treatment at the indicated time points (n = 3–8).

(C) Representative immunoblot of subcellular (Cyt, cytoplasm; Nuc, nucleus) expression of C/EBPβ and C/EBPδ in differentiation-induced HB2 cells with or without 10 μM LVS treatment at indicated time points (left). The band intensity of C/EBPβ was quantified using the ImageJ software. Nuclear C/EBPβ levels were normalized to cytoplasmic C/EBPβ levels (Nuc/Cyt) (right; n = 5–6). α-Tubulin, cytoplasmic fraction marker; Histone H3, nuclear fraction marker.

(D) Representative immunoblot of RB and C/EBPβ in differentiation-induced HB2 cells with or without 10 μM LVS treatment at the indicated time points. Phosphorylated RB (pRB) was determined by gel migrational difference (left). The band intensities of total C/EBPβ (middle), pRB, and RB (right) were quantified using the ImageJ software. C/EBPβ or pRB levels were normalized to β-Actin or total RB levels, respectively. C/EBPβ and pRB/RB levels at 0 h were arbitrarily set to 100 (n = 8).

(E–H) Relative mRNA levels of *Cebpb* (E), *Pparg* (F), *Cebpa* (G), and *Srebp1c* (H) in HB2 cells with or without 10 μM LVS treatment at the indicated time points (n = 3–6).

Data are shown as the mean ± SEM. **P* < 0.05, ***P* < 0.01, #*P* < 0.05, ##*P* < 0.01 by unpaired two-tailed Student's *t*-test compared to UD or LVS-treated HB2 cells. Black sharp (#): *vs.* 0 h of DI; red sharp (#): *vs.* 0 h of LVS.

1-7. GGPP recovers LVS-induced cell apoptosis in mature brown adipocytes

Next, the role of the cholesterol biosynthesis pathway in mature brown adipocytes was investigated. Differentiated HB2 brown adipocytes treated with LVS for 96 h showed a decrease in both lipid accumulation (**Figure 1-7A and 1-7B**) and Hoechst-stained nuclei (**Figure 1-7A**). The 3-(4,5-dimethylthiazol-2-yl)-5-(3-carboxymethoxyphenyl)-2-(4-sulfophenyl)-2H-tetrazolium (MTS) assay revealed that LVS treatment reduced the viability of HB2 brown adipocytes (**Figure 1-7C**), suggesting that reduced lipid accumulation and nuclear levels are derived from reduced cell viability. The LVS-induced reduction in lipid accumulation was almost completely recovered by co-treatment with MVA or GGPP (**Figure 1-7B**). FPP co-treatment also partially recovered lipid accumulation, whereas SQ co-treatment showed no recovery effect (**Figure 1-7B**). Consistent with the lipid accumulation levels, co-treatment with MVA or GGPP completely reversed the LVS-induced decrease in cell viability (**Figure 1-7C**). Next, HB2 cells were stained with a fluorescein isothiocyanate (FITC) -conjugated annexin V fluorescent probe and propidium iodide (PI), which stain cells in the early and late stages of apoptosis, respectively. As shown in **Figure 1-7D**, LVS treatment increased the number of both annexin V– and PI-stained HB2 brown adipocytes. The number of apoptotic cells was largely decreased by co-treatment with MVA or GGPP but not by co-treatment with FPP or SQ. Similar results were observed for the expression levels of the Bcl-2-associated X protein (*Bax*) and caspase 3 (*Casp3*), which are pro-apoptotic genes (**Figure 1-7E**). Moreover, cleaved-caspase 3 expression level, which represents the active form of caspase 3, was increased by treatment with LVS, whereas MVA or GGPP co-treatment almost reduced it in HB2 brown adipocytes (**Figure 1-7F**). These findings clearly indicate that the cholesterol biosynthesis pathway in brown adipocytes plays an essential role in survival of brown adipocytes by regulating apoptosis via GGPP production. Moreover, Zol treatment significantly decreased cell viability; however, this effect was almost reversed by co-treatment with GGPP (**Figure 1-7G**). Consistent with this, the increased *Bax* and *Casp3* expression levels after Zol treatment were completely abolished in the presence of GGPP (**Figure 1-7H**). However, co-treatment with coenzyme

Q_{10} hardly prevented the LVS-induced decrease in viability of HB2 cells (**Figure 1-7I and S1-6**). Although 100 μM $CoQH_2$ treatment partially recovered the viability of LVS-treated HB2 cells (**Figure 1-7I**), the expression levels of pro-apoptotic markers remained unchanged (**Figure 1-7J**). To investigate the effect of protein geranylgeranylation, HB2 cells were treated with GGTI-286. It was found that the inhibition of protein geranylgeranylation neither affected cell viability nor increased the expression levels of pro-apoptotic markers in HB2 cells (**Figure 1-7K and 1-7L**). These results indicate that GGPP plays an important role in the regulation of HB2 brown adipocyte survival through mechanisms other than coenzyme Q_{10} production and protein geranylgeranylation.

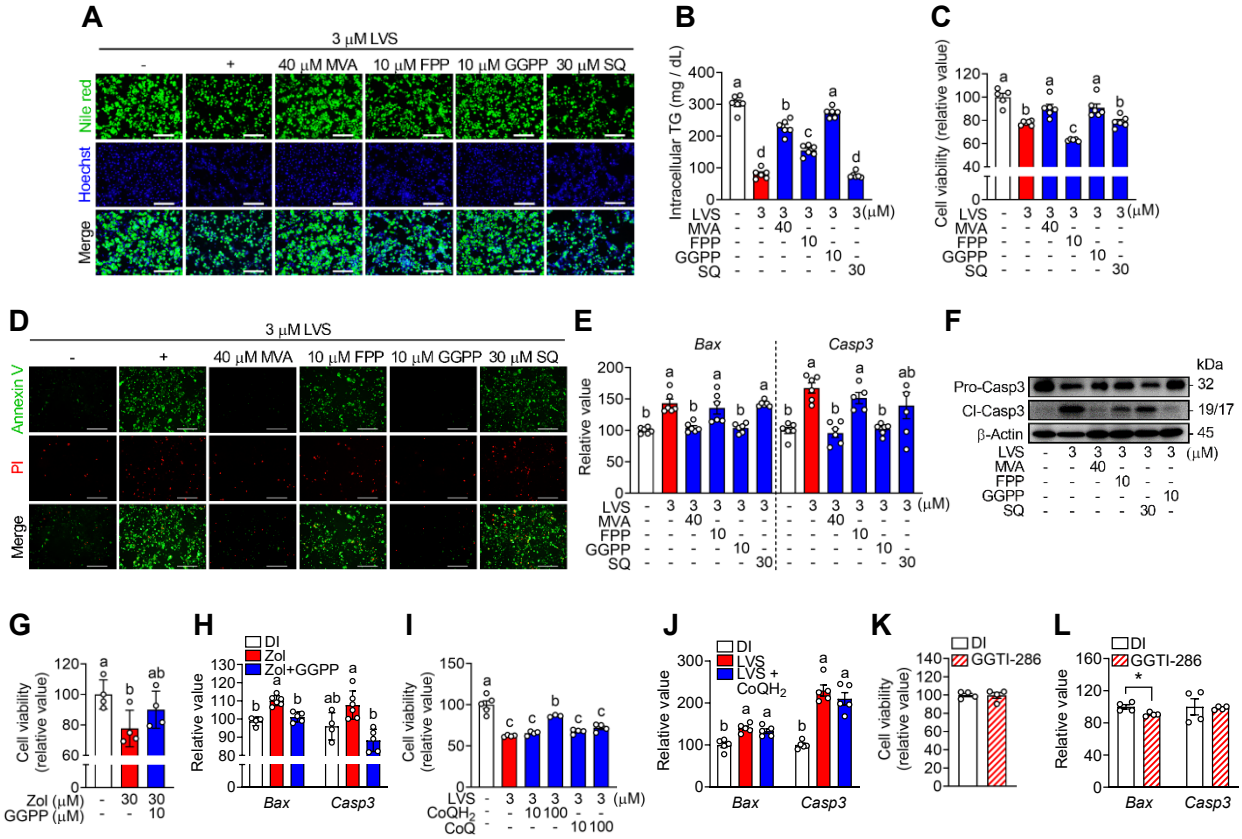

Figure 1-7. GGPP recovers LVS-induced cell apoptosis in mature brown adipocytes.

(A) Representative microscopic view of DI- or LVS-treated HB2 cells with or without MVA, FPP, GGPP, or SQ treatment (days 4–8) after staining with Nile red (top) and Hoechst (middle) on day 8. Scale bars, 200 μm.

(B and C) Quantitative results of accumulated triglycerides (B; n = 6) and MTS assay (C; n = 5–6) in DI- or LVS-treated HB2 cells with or without MVA, FPP, GGPP, or SQ treatment (days 4–8) on day 8.

(D) Representative microscopic view of DI- or LVS-treated HB2 cells with or without MVA, FPP, GGPP, or SQ treatment (days 4–8) after staining with Annexin V (top) and propidium iodide (PI; middle) on day 8. Scale bars, 200 μm.

(E) Relative mRNA levels in DI- or LVS-treated HB2 cells with or without MVA, FPP, GGPP, or SQ treatment (days 4–8) on day 8 (n = 5–6).

(F) Representative immunoblots of pro-caspase 3 (Pro-Casp3) and cleaved caspase 3 (Cl-Casp3) in DI- or LVS-treated HB2 cells with or without MVA, FPP, SQ, or GGPP treatment (days 4–8) on day 8. β-Actin was used as a loading control.

(G and H) Results of MTS assay (G; n = 4) and relative mRNA levels (H; n = 4–6) in DI- or Zol-treated HB2 cells with or without GGPP (days 4–8) on day 8.

(I) MTS assay results of DI- or LVS-treated HB2 cells with or without $CoQH_2$ or CoQ treatment (days 4–8) on day 8 (n = 3–5).

(J) Relative mRNA levels in DI- or LVS-treated HB2 cells with or without $CoQH_2$ treatment (days 4–8) on day 8 (n = 5).

(K and L) Results of MTS assay (K; n = 4) and relative mRNA levels (L; n = 4) in DI- or GGTI-286-treated (days 4–8) HB2 cells on day 8.

Data are shown as the mean ± SEM. *$P < 0.05$, unpaired two-tailed Student's *t*-test for (L). Groups with different letters are significantly different ($P < 0.05$) as determined by one-way ANOVA with Tukey's post-hoc analysis for (B), (C), (E), and (G–J).

1-8. Brown adipocyte–specific *Hmgcr* knockout mice exhibit BAT atrophy and impaired thermoregulation

To validate the role of the cholesterol biosynthesis pathway in *Ucp1*-expressing mature brown adipocytes *in vivo*, *Ucp1-Cre*-driven *Hmgcr* knockout (*Hmgcr*$^{flox/flox}$; *Ucp1-Cre*; BAT KO) mice were generated. The *Hmgcr* knockout allele was observed only in the genomic DNA extracted from BAT but not in other tissues, including WATs, in BAT KO mice (**Figure 1-8A**). BAT KO mice grew normally until adulthood, and the body weight of BAT KO mice did not differ from that of *Hmgcr*$^{flox/flox}$ (control; Ctrl) mice (**Figure 1-8B**). However, the weight of interscapular BAT, unlike other tissues in BAT KO mice, was much lower than that in Ctrl mice, and its weight was only 28.6% of that of Ctrl mice (**Figure 1-8C and 1-8D; Table S1-1**). Histologically, BAT of BAT KO mice exhibited an extensive loss of adipocytes and a relative increase in non-lipid-laden cells (**Figure 1-8E**). It was detected that many cells undergoing apoptosis in BAT of BAT KO mice, as determined by an increase in terminal deoxynucleotidyl transferase–mediated deoxyuridine triphosphate (dUTP) nick end labeling (TUNEL)-positive cells. (**Figure 1-8F**). Histological analysis and TUNEL assay indicated that BAT atrophy observed in BAT KO mice was associated with the loss of cells by apoptosis. In the cold tolerance test, cold exposure at 4°C decreased the rectal temperature of both genotypes, whereas Ctrl mice maintained the rectal temperature even under prolonged cold exposure. The rectal temperature of BAT KO mice gradually decreased and showed a significant decrease compared to that of Ctrl mice after 3 h of cold exposure (**Figure 1-8G**). Infrared thermal images showed that dorsal surface temperatures were drastically reduced in BAT KO mice after cold exposure (**Figure 1-8H**). β_3-adrenergic receptor agonist CL316,243 (CL)-induced BAT thermogenesis was also examined. As shown in **Figure 1-8I**, administration of CL quickly increased the rectal temperature of Ctrl mice but not that of BAT KO mice. To investigate the role of the cholesterol biosynthesis pathway in BAT in adult mice, tamoxifen-inducible adipocyte-specific *Hmgcr* KO (*Hmgcr*$^{flox/flox}$; *Adipoq-CreER*^{T2}; aiKO) mice were generated. Twenty days after KO induction, a loss of lipid-containing adipocytes and the presence of apoptotic cells

were observed in the BAT of tamoxifen-treated aiKO mice (**Figure 1-8J and 1-8K**). These findings clearly show that the cholesterol biosynthesis pathway in mature brown adipocytes is indispensable for maintaining BAT mass and function.

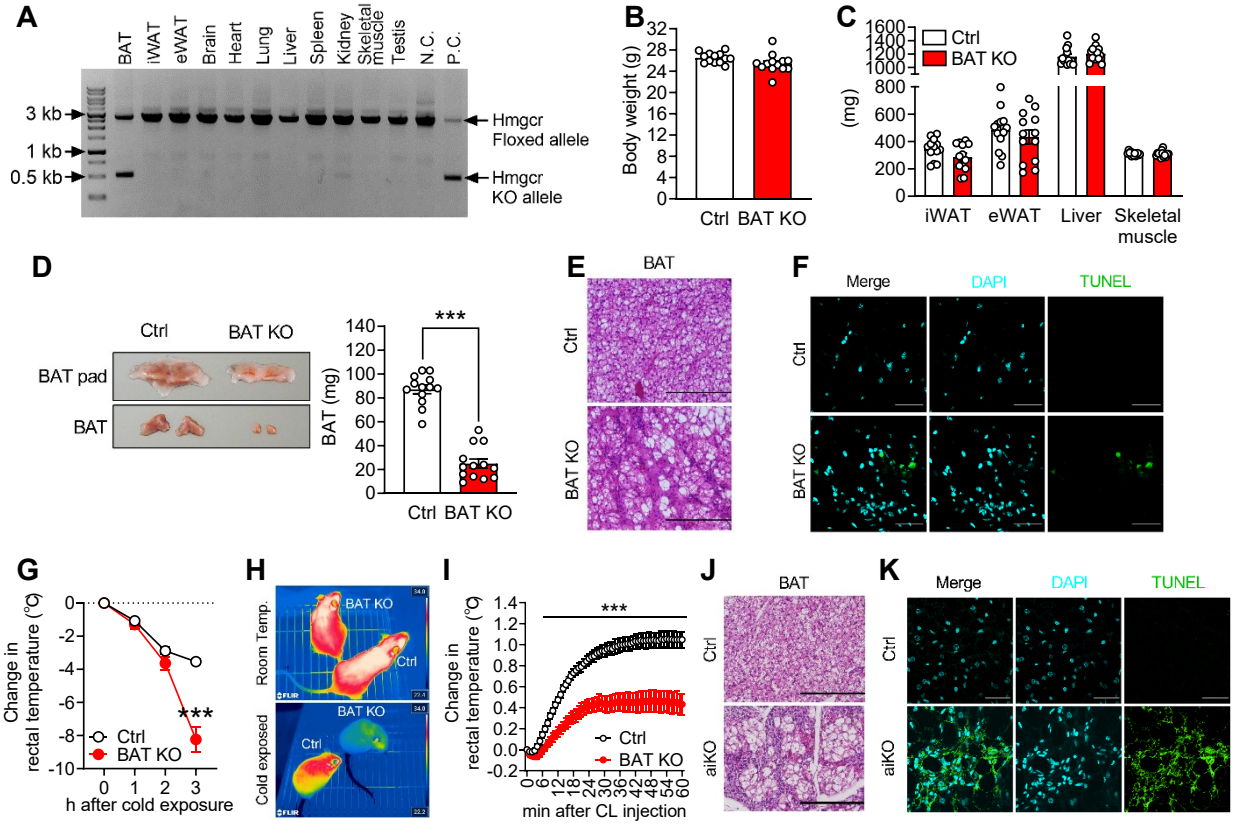

Figure 1-8. Brown adipocyte–specific *Hmgcr* knockout mice exhibit BAT atrophy and impaired thermoregulation

(A) Representative image from genotyping of BAT KO mice (n = 3). Top row, *Hmgcr*-floxed alleles (2757 bp); bottom row, *Hmgcr* knockout alleles (519 bp); N.C., negative control; P.C., positive control.

(B) Body weight of 14- to 15-week-old male Ctrl and BAT KO mice (n = 13).

(C) Weight of inguinal white adipose tissue (iWAT), epididymal white adipose tissue (eWAT), liver, and skeletal muscle (gastrocnemius + soleus) of the aforementioned mice (n = 13).

(D) Representative images (left) and weight of BAT (right; n = 13) from the aforementioned mice.

(E and F) Representative images of H&E-stained BAT section (E; Scale bars, 200 μm) and immunofluorescence images of BAT (F; Scale bars, 30 μm) isolated from 19-week-old male Ctrl and BAT KO mice.

(G) Rectal temperature of 11- to 12-week-old male Ctrl and BAT KO mice exposed to cold at 4°C (n = 10–13).

(H) Infrared thermal images of 11- to 12-week-old male Ctrl and BAT KO mice before and after cold exposure at 6°C for 3 h.

(I) Rectal temperature of 11- to 12-week-old male Ctrl and BAT KO mice exposed to 1 mg/kg CL316,243 (n = 10–13).

(J and K) Representative images of H&E-stained BAT sections (J; Scale bars, 200 μm) and immunofluorescence images of BAT (K; Scale bars, 30 μm) isolated from 16-week-old male Ctrl and aiKO mice.

Data are shown as the mean ± SEM. ***$P < 0.001$ by unpaired two-tailed Student's *t*-test.

Discussion

Increasing BAT thermogenesis, which can be achieved by enhancing BAT activity and mass, could be a promising strategy for treating obesity and obesity-induced T2D. In Chapter 1, cholesterol biosynthesis pathway–generated GGPP was demonstrated to play an indispensable role in retaining the thermogenic capacity of BAT by regulating BAT mass through controlling both brown adipogenesis and apoptosis of brown adipocytes. Notably, it was demonstrated that distinct regulatory mechanisms govern brown adipogenesis and brown adipocyte survival via the cholesterol biosynthesis pathway; the former is partially dependent on geranylgeranylation (**Figure 1-4**), and the latter is independent of geranylgeranylation (**Figure 1-7**), respectively. Recently, Balaz *et al.* [63] reported that HMG-CoA synthase 2 is important for adipocyte browning. The authors showed that the cholesterol biosynthesis pathway–produced GGPP is essential for adipocyte browning by regulating geranylgeranylation-dependent yes-associated protein (YAP) / transcriptional coactivator with PDZ-binding motif (TAZ) signaling. Importantly, findings in the Chapter 1, as well as those of the previous report, could highlight molecular mechanisms underlying a strong negative correlation between statin use and BAT prevalence. Altogether, apart from adipocyte browning, these findings demonstrate that GGPP is the key cholesterol biosynthesis pathway intermediate important for brown adipogenesis and brown adipocyte survival.

Hmgcr expression is regulated by SREBPs, which are transcription factors involved in the expression of key enzymes required for cholesterol, fatty acid, and triglyceride synthesis [116]. SREBP1/2 expression was upregulated in maternal cold-exposed fetal BAT [61]. Moreover, BAT-specific depletion of SREBP prevented the maintenance of body temperature under chronic cold exposure in mice [62]. These results suggest that the transcriptional activity of SREBPs in BAT is tightly regulated to maintain BAT function. In the present study, *Hmgcr* expression levels were altered in cold-innervated BAT and β-adrenergic receptor-activated cultured brown adipocytes, and these changes in expression levels were highly correlated with *Ucp1* expression levels (**Figure 1-1**). Therefore, SREBPs are candidate transcription factors that regulate the cholesterol biosynthesis pathway by modulating

Hmgcr expression in the brown adipocytes.

During early adipocyte differentiation, growth-arrested preadipocytes re-enter the cell cycle, followed by transient mitosis, known as MCE, and subsequently express genes that produce adipocyte-specific phenotypes [27,89]. Forty-eight hours after the induction of differentiation, the DNA content of HB2 brown preadipocytes increased by more than 2-fold; however, the increase in DNA content was suppressed by LVS treatment (**Figure 1-3F**). GGPP supplementation completely recovered LVS-induced suppression of MCE (**Figure 1-3F**), suggesting that the cholesterol biosynthesis pathway plays an essential role in MCE during brown adipogenesis via the production of GGPP. MVA-mediated GGPP production appears to be important for substrate supply, at least partially for protein geranylgeranylation during MCE. Protein geranylgeranylation is especially important for anchoring small GTPases to the plasma membrane for their respective activation. Thus, inactivation of these small GTPases may be involved in inadequate MCE during brown adipogenesis. Geranylgeranylation of small G proteins is important for the proliferation of various cell types [117–119]. These results, as well as those of several previous reports, suggest that GGPP is an important substrate for protein geranylgeranylation, which is essential for adequate MCE during brown adipocyte differentiation.

In this study, it was demonstrated that statin treatment inhibits brown adipogenesis in HB2 cells. Consistently, impaired BAT development was observed in neonates exposed to LVS from E8.5 to E18.5, when differentiation of brown preadipocytes actively occurs [111]. These results suggest that cholesterol biosynthesis pathway–mediated regulation of brown adipocyte differentiation is important for BAT development *in vivo*. Previous studies have shown that Ewing sarcoma, bone-morphogenic protein 7, and homeobox A5 are critical regulators of brown adipogenesis in cultured cells, and its loss of function reduces BAT mass in mice [120–123]. These previous reports clearly indicate that the regulatory mechanisms of brown adipogenesis in cultured cells are closely related to BAT development *in vivo*. Therefore, cholesterol biosynthesis pathway–mediated regulation of brown adipocyte differentiation is thought to be important for BAT development *in vivo*. However, further studies are

needed to investigate the effects of the cholesterol biosynthesis pathway on brown adipogenesis *in vivo*.

Statins inhibit multiple cellular functions of white adipocytes. For example, statin treatment triggers apoptosis in mature white adipocytes; however, this effect is reversed by GGPP treatment [57]. Similarly, it was found that statin treatment induced apoptosis in mature brown adipocytes, which was possibly associated with the lack of downstream products from GGPP. Moreover, statin treatment impairs white adipogenesis by reducing the expression levels of C/EBPβ, C/EBPα, and PPARγ, [114,124,125] which is consistent with the findings of the present study showing reduced adipocyte markers after LVS treatment in differentiating brown adipocytes. In particular, a decrease in nuclear C/EBPβ expression was observed in differentiating brown adipocytes upon LVS treatment. Importantly, C/EBPβ functions not only as a regulator of early adipogenesis [126] but also as a fate switch in thermogenic adipocytes [127,128]. Although most mechanisms underlying statin effects on brown adipocytes and white adipocytes may be similar, further investigation, especially regarding cellular fate, is needed to determine whether statins function as a molecular switch in determining thermogenic adipocyte development.

Although the differentiation of white adipocyte and brown adipocyte is controlled by a similar set of transcription factors, including C/EBPβ, their contribution to the adipocyte differentiation process may differ. The active form of C/EBPβ (LAP) serves as a critical regulator of brown adipogenesis by forming a transcriptional complex with PRDM16, a transcription factor that regulates thermogenic genes in brown adipocytes [128]. One known regulator of C/EBPβ function is RB, which is an important regulator of cell cycle processes and cellular differentiation [129–131]. In 3T3-L1 cells, RB hyperphosphorylation (inactive) induced by adipocyte differentiation stimuli has been implicated in the regulation of adipocyte differentiation via physical interactions with C/EBPβ and in the regulation of its transcriptional activity [115]. RB-deficient mouse embryonic fibroblasts differentiate into adipocytes with a gene expression pattern resembling that of brown adipocytes [132]. It was demonstrated that LVS treatment suppressed the differentiation stimuli-induced inactivation of RB and the simultaneous nuclear

localization of C/EBPβ in HB2 cells, which could be highly informative regarding the essential role of RB in the cholesterol biosynthesis pathway–mediated regulation of brown adipocyte differentiation.

Several studies using tissue-specific *Hmgcr* KO mice have shown that the cholesterol biosynthesis pathway is an important physiological regulator of cell survival by producing non-sterol isoprenoid intermediates in various cells [51,57,86,133]. However, the mechanism by which the cholesterol biosynthesis pathway affects mature brown adipocytes remains unclear. In Chapter 1, it was showed that disruption of the cholesterol biosynthesis pathway led to programmed cell death owing to a lack of GGPP synthesis in mature brown adipocytes. Unlike LVS treatment, treatment with a GGTase I inhibitor did not induce apoptosis in brown adipocytes, suggesting the involvement of mechanisms independent of protein geranylgeranylation. The possible involvement of coenzyme Q_{10} deficiency in statin-induced cell death has been reported in several cell types, such as myotubes and hepatocytes [134,135]. However, in the present study, GGPP deficiency–induced apoptosis was not attributed to a coenzyme Q_{10} deficiency. Therefore, other metabolites derived from GGPP may be involved in statin-induced apoptosis in brown adipocytes. Liver X receptors (LXRs) were shown to regulate statin-induced cell death in 3T3-L1 cells [136]. LXRs suppress proliferation of various cancer cells. For example, Zhang *et al.* [137] showed that treatment with T0901317, a synthetic LXR agonist, suppresses the proliferation of melanoma cells by activating caspase 3, suggesting that LXRs play an important role in cell survival. Interestingly, GGPP has been reported to regulate the function of LXRs by acting as a direct antagonist [138,139]. These reports highlight the possibility that GGPP-mediated LXRs regulation may play an important role in *Hmgcr* deficiency–induced apoptosis in brown adipocytes.

Niemann *et al.* [140] reported that apoptotic brown adipocytes induce *de novo* brown adipogenesis in BAT through the action of inosine to maintain BAT mass. Although brown adipocyte apoptosis occurred in BAT (**Figure 1-8F**), BAT atrophy was observed in BAT KO mice (**Figure 1-8D**), suggesting that the formation of new brown adipocytes in BAT KO mice is very limited. Niemann *et al.* [140] showed that extracellular inosine activates the mammalian target of rapamycin complex 1

(mTORC1) in brown adipocytes, suggesting that mTORC1 may be involved in inosine-induced brown adipogenesis. The importance of mTORC1 signaling in BAT development has been reported by several study groups. For example, mTORC1 inhibition by rapamycin or siRNA decreased the proliferation and differentiation of brown adipocytes [141]. Adipocyte-specific mTORC1 loss in mice completely blocked cold-induced BAT recruitment [142]. Importantly, statin treatment suppresses mTOR signaling [143], suggesting that the cholesterol biosynthesis pathway regulates mTOR signaling. The small GTPase Rac1, a target of GGTase I, regulates mTORC1 activity [144]. In **Figure 1-3H–1-3I**, treatment with a GGTase I inhibitor suppressed brown adipocyte differentiation, suggesting that GGPP depletion by statins might suppress the geranylgeranylated Rac1-mTORC1 axis. This pathway may be involved in the inosine-induced differentiation of brown adipocytes.

It has been reported that the expression levels of geranylgeranyl pyrophosphate synthetase (*Ggps*) are significantly elevated in obese WAT. Moreover, intracellular GGPP levels increase in parallel with adipocyte differentiation (i.e., from ~2 ng/well in white preadipocytes to ~12 ng/well in mature white adipocytes [139]). In contrast to adipocyte differentiation, *Ggps* expression levels are reduced during osteoblast differentiation [58]. Given that adipocytes and osteoblasts share the same mesenchymal precursor, regulation of *Ggps* expression could determine the cell fate toward either adipocyte or osteoblast. The results of previous reports suggest that GGPP may play an important role as an endogenous regulator of brown adipogenesis.

In order for Ras-related GTPases (e.g., RhoA, RhoC, Rac1, Cdc42, Rab, RalA, and RalB) to transduce their signal, they must be anchored to the plasma membrane, which is accomplished by posttranslational modifications that increase their hydrophobicity [59,145]. A key step in this process is catalyzed by geranylgeranyltransferase type 1 (GGTase I), an enzyme that transfers geranylgeranyl from GGPP, a cholesterol biosynthesis intermediate, to the cysteine of the carboxyl terminal CAAX box of proteins (C=cysteine, A=aliphatic amino acid and X=leucine) and the process is called geranylgeranylation [145]. Prenylation of the carboxyl terminal CAAX of Ras-related GTPases is

required for their biological activity. For example, Raf, a serine/threonine kinase, phosphorylates mitogen-activated protein kinase kinase, which in turn activates MAPK by phosphorylating it on threonine and tyrosine. Hyperphosphorylated MAPK translocalizes to the nucleus, where it phosphorylates transcription factors that are involved in the regulation of growth-related genes [146]. GGTI-286 is a cell-permeable peptidomimetic compound resembling the CAAX domain of a protein to be geranylgeranylated and is a competitive inhibitor of protein geranylgeranylation [147]. In culture cells, GGTase I deficiency by 30 μM GGTI-286 treatment dramatically reduced Wnt/β-catenin signaling by reducing the nuclear localization of β-catenin, a target of Rab GTPases, in Chinese hamster ovary cells [148], suggesting that the results obtained using GGTI-286 in this study may not result from off-target effects.

Due to the technical limitations, the changes in GGPP levels in HB2 cells after LVS treatment were not measured in this study. As mentioned in the previous report, it is very difficult to determine the isoprenoid levels in biological samples directly [107]. However, some previous reports determined cellular GGPP levels indirectly by measuring the incorporated GGPP levels into fluorescently-labeled peptides using recombinant GGTase I. A report showed a decrease in the cellular level of GGPP less than 40% and 30% of the initial value following treatment with 1 μM and 10 μM LVS for 24 h, respectively in NIH3T3 cells, a mouse fibroblast line [107]. Another previous report showed a reduction in cellular GGPP level by less than 10% of the initial level in SY5Y-APP695 cells, a human neuroblastoma, after incubation with 5 μM LVS for 24 h [106]. These reports clearly demonstrate that LVS treatment actually decreased cellular GGPP levels, suggesting that the reduction in both adipogenic capacity and cell apoptosis in HB2 brown adipocytes is attributed to the reduced GGPP level caused by HMGCR inhibition.

In conclusion, the cholesterol biosynthesis pathway appears to be critical for maintaining brown adipocyte function by regulating both differentiation and survival of brown adipocytes. GGPP is a pivotal isoprenoid produced by the cholesterol biosynthesis pathway in both processes. The results in

Chapter 1 highlight the importance of the cholesterol biosynthesis pathway in brown adipocytes to identify mechanisms that can be employed to develop therapeutic approaches for lowering statin-induced side effects, such as T2D.

Supplementary Information

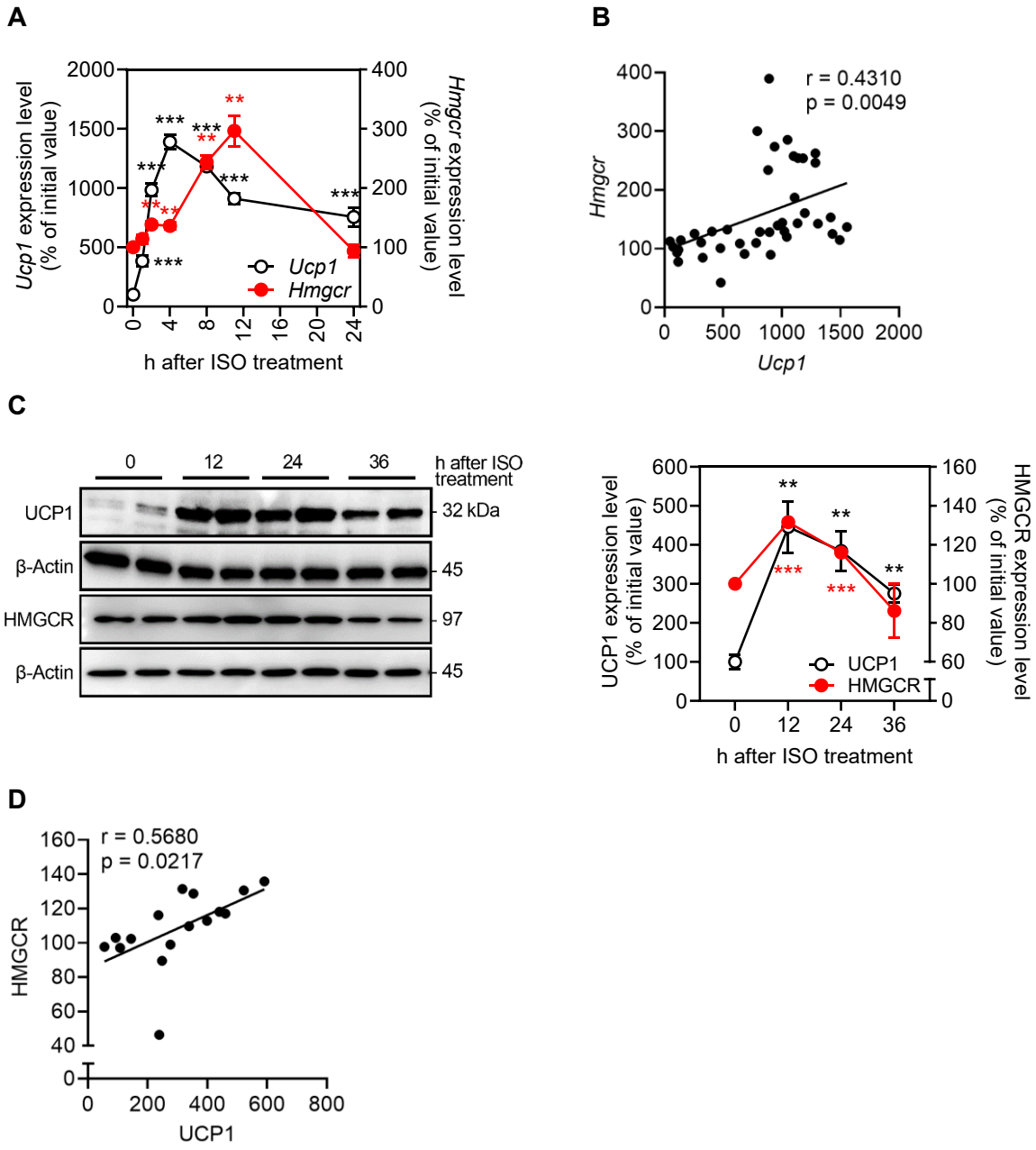

Figure S1-1. Changes in mRNA and protein expression levels of Hmgcr and Ucp1 in ISO-stimulated mature brown adipocytes

(A) mRNA levels of *Ucp1* and *Hmgcr* in differentiation-induced immortalized murine primary brown adipocytes after 1 μM isoproterenol (ISO) treatment on day 6 (n = 5–6).

(B) Correlation between *Ucp1* and *Hmgcr* analyzed based on data from (A).

(C) Representative immunoblots of UCP1 and HMGCR (left) and relative protein abundance (right; n = 4). Each protein level was normalized to β-Actin.

(D) Correlation between UCP1 and HMGCR analyzed based on quantitative data from (C).

Data are shown as mean ± standard error of the mean (SEM). ** $P < 0.01$, *** $P < 0.001$ by unpaired two-tailed Student's *t*-test. Correlation was analyzed by Pearson's correlation. Black asterisk: *vs.* initial value of *Ucp1*; Red asterisk: *vs.* initial value of *Hmgcr*.

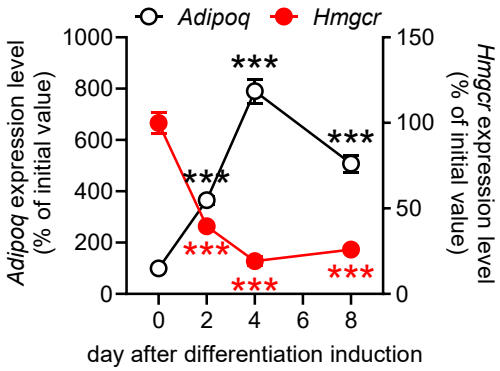

Figure S1-2. mRNA expression levels of *Hmgcr* during brown adipogenesis in HB2 cells
Differentiation-induced HB2 cells were harvested on the indicated time point and mRNA expression levels of HMG-CoA reductase (*Hmgcr*) and adiponectin (*Adipoq*) were measured (n = 5–6).
Data are shown as mean ± standard error of the mean (SEM). *** $P < 0.001$ by unpaired two-tailed Student's *t*-test. Black asterisk: *vs.* initial value of *Adipoq*; Red asterisk: *vs.* initial value of *Hmgcr*.

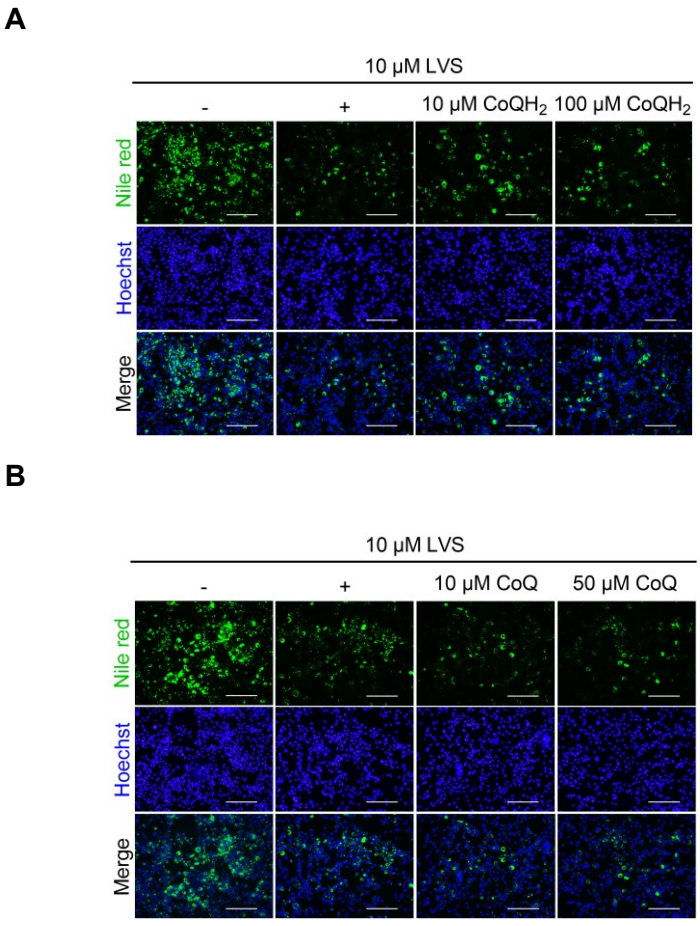

Figure S1-3. Representative microscopic view of HB2 cells
(A–B) Representative microscopic view of differentiation-induced (-) or 10 μM lovastatin (LVS) -treated HB2 cells with or without ubiquinol (A; $CoQH_2$) or ubiquinone (B; CoQ) (days 0–2) after staining with Nile red (top) and Hoechst (middle) on day 4. Scale bar, 200 μm.

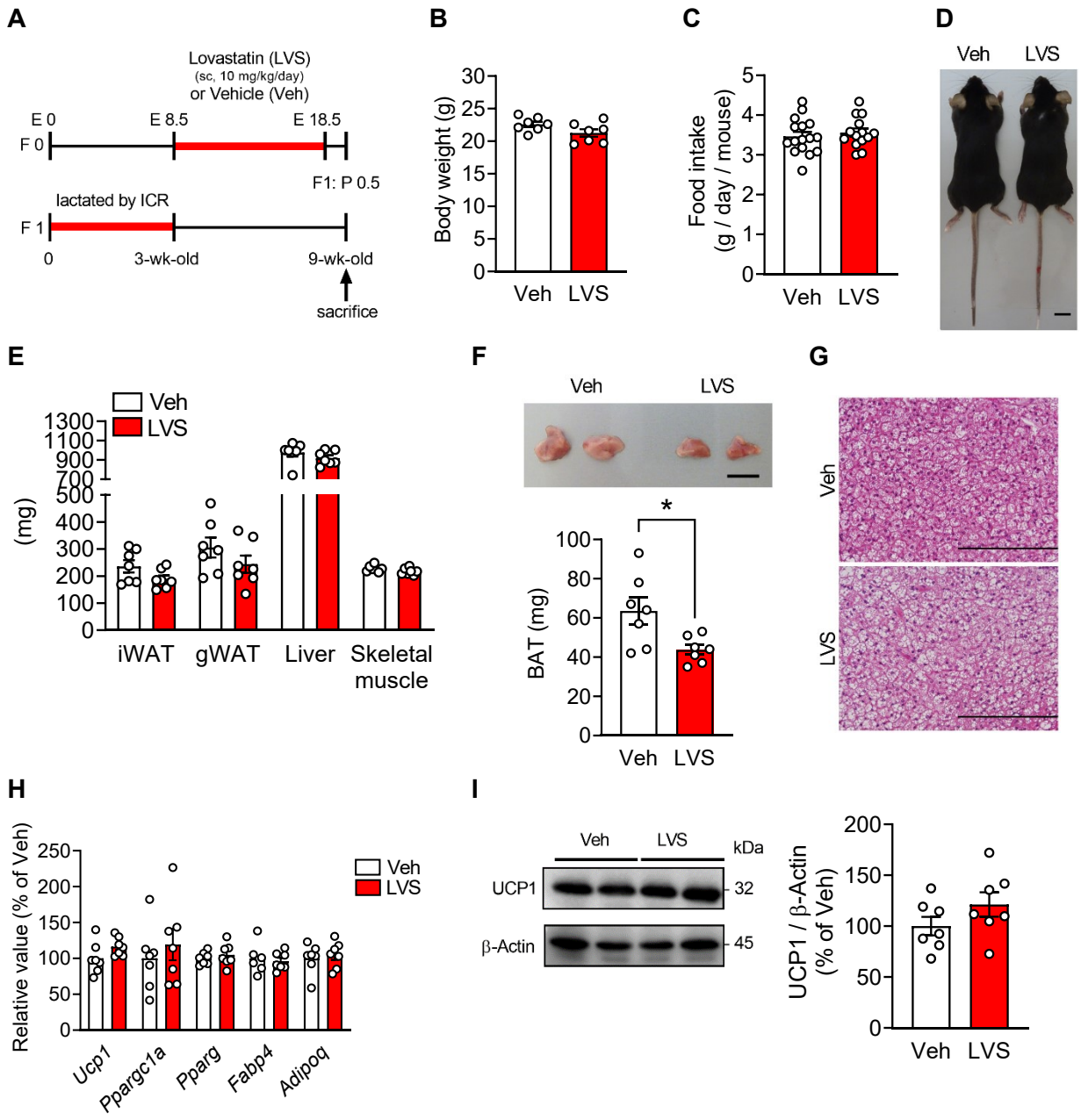

Figure S1-4. Prenatal lovastatin exposure negatively impacts the brown adipose tissue mass of adult female mice

(A) Experimental scheme. (B–C) Body weight (B; n = 7) and food intake (C; n = 14–16) of 9-week-old female mice who had undergone prenatal exposure to vehicle (Veh) or 10 mg/kg/day lovastatin (LVS) from embryonic day 8.5 (E8.5) to embryonic day 18.5 (E18.5). (D–E) Representative body image (D; scale bar, 1 cm) and weight of various tissues (E; n = 7). iWAT: inguinal white adipose tissue; gWAT: gonadal white adipose tissue. (F) Representative gross image (scale bar, 1 cm; Top) and weight of brown adipose tissue (BAT) (n = 7; bottom). (G) H&E staining of BAT sections (scale bar, 200 mm). (H) Relative mRNA expression levels of *Ucp1*, *Ppargc1a*, *Pparg*, *Fabp4*, and *Adipoq* with Veh arbitrarily set to 100 for each gene (n = 6–7). (I) Representative immunoblot of UCP1 of BAT lysates; the band intensity was quantified using ImageJ software (n = 7). β-Actin was used as an internal control to normalize protein expression.

Data are shown as mean ± standard error of the mean (SEM). Significant differences were determined by unpaired two-tailed Student's *t*-test compared to Veh. Statistical differences are indicated as * $P < 0.05$.

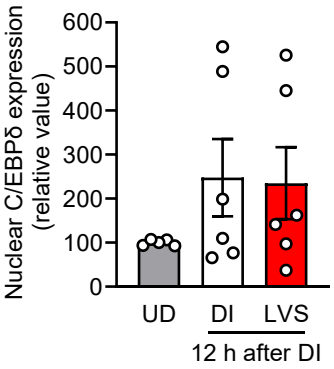

Figure S1-5. C/EBPδ expression levels in HB2 cells

Quantified results of the nuclear expression level of C/EBPδ protein using ImageJ software (n = 5–6). Data are shown as mean ± standard error of the mean (SEM).

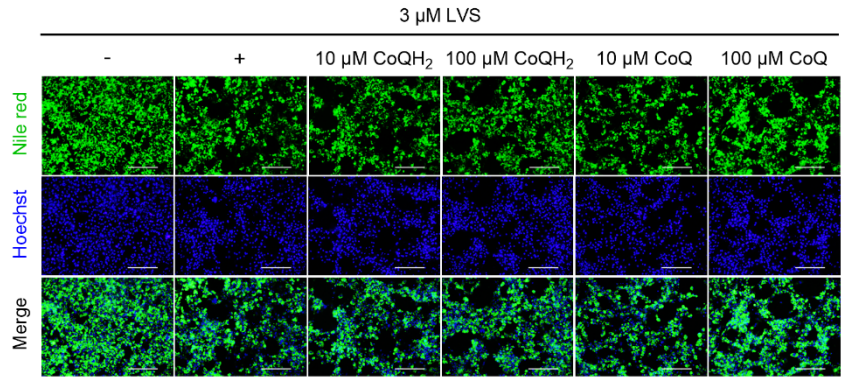

Figure S1-6. Representative microscopic view of HB2 cells

Representative microscopic view of differentiation-induced (-) or 3 μM lovastatin (LVS) -treated HB2 cells with or without ubiquinol ($CoQH_2$) or ubiquinone (CoQ) (days 4–8) after staining with Nile red (top) and Hoechst (middle) on day 8. Scale bar, 200 μm

Table S1-1. Organ and tissue weight of 14–15-week-old male BAT KO mice and their littermates (Ctrl)

	Ctrl	BAT KO
Body weight (g)	26.5 ± 0.3	25.4 ± 0.5
Brown adipose tissue (BAT; mg)	87.1 ± 3.6	24.9 ± 3.9***
Inguinal white adipose tissue (iWAT; mg)	344.4 ± 21.5	285.9 ± 27.5
Epididymal white adipose tissue (eWAT; mg)	482.9 ± 42.2	433.8 ± 50.2
Liver (mg)	1,159.5 ± 37.1	1,204.8 ± 31.3
Skeletal muscle (mg) (Gastrocnemius + Soleus)	311.0 ± 3.6	309.2 ± 5.9

Data are shown as mean ± standard error of the mean (SEM; n = 13). Significant differences were determined by Student's *t*-test compared to Ctrl. *** $P < 0.001$.

Table S1-2. List of PCR primers used in Chapter 1

Oligonucleotides (5′ → 3′)			
mRNA	*Adipoq*	Fw	TACAACCAACAGAATCATTATGACGG
		Rv	GAAAGCCAGTAAATGTAGAGTCGTTGA
	Bax	Fw	GAGCTGCAGAGGATGATTGC
		Rv	CTTGGATCCAGACAAGCAGC
	Casp3	Fw	GGAGCTTGGAACGGTACGC
		Rv	CACATCCGTACCAGAGCGAG
	Cebpa	Fw	TGGACAAGAACAGCAACGAG
		Rv	TCACTGGTCAACTCCAGCAC
	Cebpb	Fw	GCAAGAGCCGCGACAAG
		Rv	GGCTCGGGCAGCTGCTT
	Cebpd	Fw	AGCCCAACTTGGACGCCAG
		Rv	TCGTCGTCGTACATGGCAG
	Fabp4	Fw	AAGACAGCTCCTCCTCGAAGGT
		Rv	TGACCAAATCCCCATTTACGC
	Hmgcr	Fw	TTCAGCAGTGCTTTCTCCGT
		Rv	GGAGGCCTTTGATAGCACCA
	Ppargc1a	Fw	CCCTGCCATTGTTAAGACC
		Rv	TGCTGCTGTTCCTGTTTTC
	Pparg	Fw	GGAGATCTCCAGTGATATCGACCA
		Rv	ACGGCTTCTACGGATCGAAACT
	Prdm16	Fw	CAGCACGGTGAAGCCATTC
		Rv	GCGTGCATCCGCTTGTG
	Rplp0	Fw	TCCTTCTTCCAGGCTTTGGG
		Rv	GACACCCTCCAGAAAGCGAG
	Srebp1c	Fw	GGAGCCATGGATTGCACATT
		Rv	GCCAGAGAAGCAGAAGAGAAG
	Ucp1	Fw	CAAAGTCCGCCTTCAGATCC
		Rv	AGCCGGCTGAGATCTTCTTT
Genotyping	*Hmgcr*	Fw	TTACTGGCTTGCTCAGCTTGCTCCA
		Rv	GACACATGAAGGCATTCTCAGGCAT
	mRfp1	Fw	CATCCCCGACTACTTGAAGC
		Rv	CCATGGTCTTCTTCTGCAT

Chapter 2

The effect of *Ppara* downregulation by inflammation on thermogenic adipocyte function

Introduction[2]

Chronic low-grade adipose tissue inflammation by progressive immune cell infiltration is mechanistically linked to the pathogenesis of obesity-related metabolic diseases [149]. In addition to being the major fat-storing depot, adipose tissue secretes various biologically active molecules, termed adipokines, to maintain energy homeostasis [150]. Normal adipose tissue secretes anti-inflammatory and insulin-sensitizing factors, such as adiponectin [151,152]; however, their expression is reduced in obese adipose tissue which highly expresses pro-inflammatory adipokines, including IL6, TNFα, and MCP1 [38,149]. The elevation of pro-inflammatory cytokines, such as MCP1, promotes macrophage infiltration into the adipose tissue, and the infiltrated macrophages and adipocytes interact in a paracrine manner [153]. For example, TNFα secreted from macrophages inhibits adipocyte insulin signaling and induces lipolysis, further exacerbating the inflammatory phenotype of the macrophages [154]. This paracrine loop contributes to the development of chronic low-grade inflammation and insulin resistance, leading to type 2 diabetes [155]. WAT obtained from patients with insulin resistance and obesity contains more pro-inflammatory macrophages [156] that are strongly correlated with metabolic dysfunction [157,158]. Therefore, the crosstalk between dysfunctional adipocytes and pro-inflammatory macrophages appears to play a crucial role in the pathogenesis of obesity.

---

[2] The content described in this chapter was originally published in *Biochimica et Biophysica Acta (BBA) – Gene Regulatory Mechanisms*. Kwon J, Aoki Y, Takahashi H, Nakata R, Kawarasaki S, Ni Z, Yu R, Inoue H, Inoue K, Kawada T, and Goto T. Inflammation-induced nitric oxide suppresses PPARα expression and function via downregulation of Sp1 transcriptional activity in adipocytes. *Biochim Biophys Acta Gene Regul Mech.* (2023) 1866(4):194987. doi: 10.1016/j.bbagrm.2023.194987.

Peroxisome proliferator-activated receptors (PPARs) are ligand-activated transcription factors belonging to the nuclear hormone receptor superfamily that control genes harboring PPAR-responsive regulatory elements (PPREs) in their promoter by forming complexes with the retinoid X receptors [159]. PPARα, one of these subtypes, is expressed in organs with high rates of FA oxidation and peroxisomal metabolism, such as the liver, heart, and muscle [160]. PPARα plays an important role in controlling the expression of genes involved in lipid oxidation, *Acox1* and *Cpt1*. Ligands such as fibrates are clinically used to treat dyslipidemia because they increase hepatic FA oxidation and decrease triglyceride-rich lipoproteins [161,162].

PPARα is expressed in the adipose tissue of humans and rodents, suggesting that PPARα activation can alter energy metabolism in adipose tissue [163,164]. Previous study shows that the activation of PPARα by its agonist (bezafibrate) markedly reduces adiposity and ameliorates insulin resistance in obese mice by stimulating FA oxidation in adipocytes [74]. Furthermore, adipocyte-specific PPARα over-expression protects from obesity-induced insulin resistance in mice [75]. In contrast, adipocyte-specific *Ppara* knockout male mice have severe adiposity under a high-fat diet (HFD) due to enhanced lipogenesis in adipocytes [165], supporting a function of PPARα in the metabolic regulation of adipose tissue. Moreover, PPARα agonist treatment increases the expression of adiponectin receptor in adipocytes [163]; however, the loss of adipocyte PPARα signaling increases the expression of pro-inflammatory macrophage markers in WAT [165]. Based on these reports, it is suggested that the activation of PPARα signaling in adipocytes has the potential to improve insulin resistance and ameliorate obesity.

Ppara expression levels are reduced in the adipose tissue of obese mice [74], suggesting that decreased expression of *Ppara* in adipose tissue contributes to adipose tissue dysfunction and obesity-related metabolic disorders. However, the regulatory mechanisms underlying the decreased expression of *Ppara* in obese adipose tissue are poorly understood.

Therefore, the present study aimed to elucidate the regulatory mechanisms of *Ppara* expression in the adipose tissue under inflammatory conditions.

First, in Chapter 2, the effect of inflammation on *Ppara* gene expression was investigated. It was observed that *Ppara* gene expression levels were markedly downregulated in WAT of *db/db* mice as well as in 10T1/2 adipocytes cultured with conditioned medium from activated macrophages by lipopolysaccharide (LPS). The loss of *Ppara* gene expression suppressed β-adrenergic stimulation-induced thermogenic gene expression in adipocytes. The reduction in *Ppara* gene expression was, however, partially recovered in the presence of a nitric oxide synthase 2 (NOS2) inhibitor. It was found that endoplasmic reticulum stress mediates the inhibitory action of NO on *Ppara* gene expression. Specifically, NO promotes the release of transcription factor Specificity Protein 1 (Sp1) from its binding motifs at positions -218/-209, -58/-49, and -14/-5 in the *Ppara* promoter region. Moreover, *Ppara* transcript levels were reduced in the WAT of LPS-treated or *db/db* mice; however, this effect was attenuated in the presence of a NOS2 inhibitor. Together, these findings clearly show that inflammation-induced NO suppresses *Ppara* transcription via the inhibition of *Ppara* promoter occupancy by Sp1, which subsequently impacts PPARα function.

Materials and Methods

Chemical reagents

Lipopolysaccharide (LPS; Cat. No. L2630), isoproterenol (ISO; Cat. No. I6504), and GW7647 (GW; Cat. No. G6793) were purchased from Sigma-Aldrich. NOR5 (Cat. No. N448) was from Dojindo. Trimethylamine-*N*-oxide (TMAO; Cat. No. T1362) was from Tokyo chemical industries. SP600125 (Cat. No. BML-EI305-0050) was from Enzo Life Sciences. Mithramycin A (MTA; Cat. No. M3476) was from LKT laboratories. *N*-(3-[aminomethyl]benzyl)acetamidine (1400w; Cat. No. 81520) and *N6*-

(1-iminoethyl)-L-lysine hydrochloride (NIL; Cat. No. 80310) were purchased from Cayman Chemical. Dulbecco's modified Eagle's medium (DMEM; Cat. No. 08458-16)-high glucose, penicillin-streptomycin mixed solution (Cat. No. 26253-84), 3-isobutyl-1-methylxanthine (IBMX; Cat. No. NU03039), dexamethasone (Dex; Cat. No. 11107-64), tunicamycin (Cat. No. 35638-74), and thapsigargin (Cat. No. 33637-31) were purchased from Nacalai Tesque. 4-Phenyl butyric acid sodium (PBA; Cat. No. sc-232961) and 1*H*-[1,2,4]Oxadiazolo[4,3-α]quinoxalin-1-one (ODQ; Cat. No. sc-200325) were purchased from Santa Cruz Biotechnology. Insulin (Cat. No. 093-06476), SB203580 (Cat. No. 195-16553), and *N*-acetyl-$_{L}$-cysteine (NAC; Cat. No. 015-05132) were purchased from Wako Pure Chemical. Fetal bovine serum (FBS) was purchased frum Sigma-Aldrich (Cat. No. 10270106) and BioWest (Cat. No. S1810).

Animal experiments

All experimental procedures were approved by the Animal Research Committee of Kyoto University, Kyoto, Japan (R1-50) or the Animal Care Committee of Nara Women's University, Nara, Japan (17-03). All mice were maintained in a temperature-controlled (23°C±1) facility with a constant 12 h light/dark cycle and free access to food and water. During all experiments, the mice were fed a normal chow diet (MF; Oriental Yeast, Tokyo, Japan). To induce inflammation with LPS, 11-week-old male C57BL/6J mice (SLC, Shizuoka, Japan) were intraperitoneally administered phosphate-buffered saline (PBS) or 200 μg LPS, fasted concomitantly, and sacrificed at the indicated time points (**Figure 2-4A**). For the 1400w treatment experiment, 12-week-old male C57BL6/J mice were intraperitoneally injected with LPS (200 μg) and 1400w (100 mg/kg) and fasted concomitantly. Nine hours after injection, the mice were sacrificed to harvest WAT and blood. The samples were immediately frozen in liquid nitrogen and stored at -80°C until use. To investigate the effect of the NOS2-deriven NO on *Ppara* expression levels in WAT, 7-week-old male C57BL6/J or nitric oxide synthase 2 knockout (*Nos2*$^{-/-}$) mice (B6.129P2-Nos2^{tm1Lau}/J, The Jackson Laboratory, Bar Harbor, ME USA) were intraperitoneally injected

100 μg of LPS and fasted concomitantly. Seven hours after injection, the mice were sacrificed for further investigation. To investigate the effect of obesity-induced inflammation on *Ppara* expression in WAT, 14-week-old male *db/db* (C57BLKS/J Iar-+Lepr^{db}/+Lepr^{db}) mice purchased from the Institute for Animal Reproduction (Ibaraki, Japan) were intraperitoneally injected with vehicle or 1400w (20 mg/kg/day for two consecutive days and 100 mg/kg/day for the third day) for 3 days and sacrificed for further investigation. *m/m* (C57BLKS/J Iar -m^{+}/m^{+}) mice were used as lean controls. The 12-week-old male C57BL6/J (wild-type) or *Ppara*$^{-/-}$ mice (B6;129S4-*Ppara*^{tm1Gonz}/J, The Jackson Laboratory, Bar Harbor, ME USA) were cold exposed at 4°C or at 23°C for 6 h with *ad libitum* food and water and sacrificed for further investigation.

Cell culture

C3H10T1/2 (10T1/2; ATCC, CCL-226) and RAW264.7 macrophages (RAW; RIKEN BioResource Center, Tsukuba, Japan) were cultured in DMEM-high glucose with 10% FBS, 100 U/mL penicillin, and 100 μg/mL streptomycin (P/S) at 37°C under a humidified 5% CO_2 atmosphere. RAW macrophages were cultured in DMEM without or with 0.5 μg/mL LPS for 12 h and then serum-starved in DMEM for 12 h. Both media were collected as control conditioned medium (LPS-CM) and LPS-conditioned medium (LPS+CM), respectively, and stored at -20°C until use. 10T1/2 cells were differentiated by treatment with 0.5 mM IBMX, 0.25 μM DEX, and 10 μg/ml insulin in DMEM containing 10% FBS and 1% P/S for 2 days after the cells reached confluence (day 0). Next, the medium was replaced with DMEM containing 10% FBS, 1% P/S, and 5 μg/ml insulin every 2 days. On day 6, the 10T1/2 adipocytes were treated with conditioned medium (CM) or various compounds at the indicated concentrations for the indicated periods, as shown in the figure legends. To investigate the effects of macrophages on adipocytes, 10T1/2 mature adipocytes were co-cultured with RAW macrophages (inactivated or activated by 0.5μg/mL LPS) in a transwell indirect co-culture system (0.4 μm pore size, Greiner Bio-One, Cat. No. 655640) with or without 200 mM NIL. After 24 hours of co-

culture, 10T1/2 adipocytes were harvested for further investigation. The stromal vascular fraction from WATs of wild-type and *Ppara*$^{-/-}$ mice was isolated as described previously [166]. Post-confluent cells were differentiated in the same manner as 10T1/2 cells. On day 6, adipocytes were stimulated with or without 10 μM ISO for 8 h and harvested for further investigation.

Measurement of the nitric oxide release

The amount of nitric oxide (NO) released was measured using the Griess reagent, as previously described [167]. Briefly, 100 μl of cell culture supernatant was mixed with an equal volume of Griess reagent (final concentration of 0.1% *N*-[1-naphthyl]ethylenediamine dihydrochloride in distilled water and 1% sulfanilamide in 5% phosphoric acid) on a 96-well flat-bottom plate. The absorbance was measured at 550 nm after 10 min using a microplate reader (Bio-Rad). The amount of NO produced was calculated from a standard curve plotted using sodium nitrite. The NO metabolites nitrate (NO_3^-) and nitrite (NO_2^-) in the plasma or adipose tissue were measured using a nitrite/nitrate colorimetric assay kit (Cayman Chemical, Cat. No. 780001) or nitrite/nitrate fluorometric assay kit (Dojindo, Cat. No. 345-08141) following the manufacturer's protocol.

Fatty acid oxidation assay

On day 6, differentiated 10T1/2 adipocytes were treated with CM from macrophages for 16 h or with 0.1 mM NOR5 for 8 h, followed by co-treatment with or without 1 μM GW7647 for 8 h. Adipocytes were then incubated with 2 mL of substrate medium made of DMEM supplemented with [^{14}C] palmitic acid (0.5 μCi/mL; American Radiolabeled Chemicals, Cat. No. ARC-0172A-50), 2.5% fatty acid-free bovine serum albumin, 0.2 mM palmitic acid, and 0.2 mM L-carnitine hydrochloride for 16 h. FA oxidation products were analyzed as previously described [74]. Briefly, the medium sample was collected and centrifuged at 3,000 × *g* for 5 min, and the supernatant was transferred to a 50 mL polypropylene tube containing a piece of filter paper submerged with benzethonium hydroxide (Sigma-

Aldrich, Cat. No. B2156). After the tube was sealed, 200 μL of 70% perchloric acid (Nacalai Tesque, Cat. No. 26503-75) was added to the supernatant to release [^{14}C]CO_2. The tube was then shaken at 37°C for 1 h. A saturated filter paper containing trapped [^{14}C]CO_2 was used to assess radioactivity using a liquid scintillation counter. The acidified supernatant was centrifuged at 10,000 × *g* for 5 min, and the amount of [^{14}C]-labeled acid-soluble metabolites (ASMs) was determined. To normalize the intensity of radioactivity to the protein content in each sample, the adipocytes were washed with cold PBS and collected in 0.1 N NaOH solution. Protein quantification was performed using a DC Protein Assay Kit (Bio-Rad, Cat. No. 5000112) according to the manufacturer's instructions.

Small interfering RNA-mediated Sp1 gene silencing

Differentiated 10T1/2 cells seeded in 12-well plates were washed with PBS, and the growth medium was replaced with OPTI-MEM (Gibco, Cat. No. 31985070). Cells were transfected with Sp1 siRNAs (SASI_Mm01_00145222, SASI_Mm01_00145223, Sigma-Aldrich) or negative control RNA (MISSION siRNA Universal Negative Control, Sigma-Aldrich) at a final concentration of 60 pmol using Lipofectamine 2000 transfection reagent (Invitrogen, Cat. No. 11668019). Twenty-four hours after transfection, cells were harvested for RNA and protein extraction.

Plasmids

To prepare pGL4.14-Ppara-Luc containing a serial deleted 5′ flanking regions of mouse *Ppara* promoter, genomic DNA was amplified by PCR reactions using primers listed in **Table S2-1** and PrimeSTAR MAX DNA Polymerase (Takara Bio, Cat. No. R045A). After digestion of the pGL4.14 vector (Promega, Cat. No. E6691) with *Xho* I, the PCR product was ligated into the pGL4.14 vector with In-Fusion HD enzyme premix (Takara Bio, Cat. No. 639650).

Site-directed mutagenesis

Site-directed mutagenesis of the *Ppara* promoter (-245/+132) was performed by inserting substitutions at positions -215/-213 (GGC to AAA), -184/-182 (GCC to AAA), -99/-97 (GCG to AAA), -82/-80 (CCC to AAA), -51/-49 (GGG to AAA), -42/-40 (GGG to AAA), and -11/-9 (GGC to AAA), which are part of putative Sp1-binding motif, with PCR reactions using the Quick-Change II XL Site-directed mutagenesis kit (Agilent Technologies, Cat. No. 200522) with primer pairs listed in **Table S2-2** and according to the manufacturer's protocol. For site-directed mutagenesis, 12 PCR cycles, consisting of denaturation at 95℃ for 30s, hybridization at 55℃ for 1 min, and final extension at 68℃ for 7 min, were used. The amplified products were treated with *Dpn* I at 37℃ for 1 h, and then used to transform competent XL1-Blue Supercompetent cells.

Luciferase reporter assay

In luciferase assays, reporter plasmids (7 μg/dish) and pRL-CMV (50 ng/dish; Promega, Cat. No. E2231) were transfected into undifferentiated 10T1/2 cells cultured on 10-cm culture dishes using Lipofectamine 2000 reagent (Invitrogen, Cat. No. 11668019), following the manufacturer's instructions. Twenty-four hours after transfection, the cells were cultured in 96-well tissue plates and pretreated with or without 10 mM PBA or 100 mM TMAO for 5 h before co-treatment with or without 0.1 mM NOR5, 5 μM tunicamycin, or 500 nM thapsigargin in serum-free DMEM for 24 h. The cells were lysed for luciferase assays using a Dual-Luciferase Reporter Assay system (Promega, Cat. No. E1910) and a Centro XS3 LB 960 microplate luminometer (Berthold, Bad Wildbad, Germany). The firefly luciferase activity of each reporter plasmid was normalized to Renilla luciferase activity in the transfected cells.

Chromatin immunoprecipitation (ChIP) assay

On day 6, differentiated 10T1/2 adipocytes were treated with or without 0.1 mM NOR5. Twenty-four hours after the treatment, adipocytes were fixed with 1% formaldehyde in PBS (*v/v*) for ChIP assays as previously described [74]. Briefly, the cells were resuspended in lysis buffer (1% SDS,

10 mM EDTA, 50 mM Tris-HCl; pH 8.0, and 1% protease inhibitor cocktail [Nacalai Tesque, Cat. No. 03969-21) and sonicated to shear their DNA. After centrifugation at 21,500 × *g* for 10 min, the supernatant was collected and immunoprecipitated overnight with the antibody against Sp1 (Sigma-Aldrich, Cat. No. 07-645) or rabbit IgG isotype (Novus Biological, Cat. No. NBP1-75297) as a mock control along with protein A/G-Sepharose beads (Santa Cruz Biotechnology, Cat. No. sc-500775A) at 4 °C in a rotary shaker followed by reverse cross-linkage and proteinase K digestion. After purification using phenol/chloroform, the DNA fragments were used as templates for PCR. Oligonucleotide primers comprising the following sequences (upstream and downstream) were used for the PCR: *Ppara*, ACGCTACGGTCCCACGACAG and TTCCTAGCGTGTGCCCTCTC (283 bp).

Western blotting

After washing twice with ice-cold PBS, total cellular proteins were extracted in lysis buffer (50 mM Tris·HCl, 150 mM NaCl, 1% Triton X-100, 0.5% deoxycholate, 0.1% SDS; pH 7.4, and 1% protease inhibitor cocktail [Nacalai Tesque, Cat. No. 03969-21). Protein concentrations of the samples were determined using a DC Protein Assay Kit (Bio-Rad, Cat. No. 5000112) according to the manufacturer's instructions. Protein samples were separated by SDS-PAGE and transferred to Immobilon-P polyvinylidene fluoride membranes (Millipore, Cat. No. PVH00010). After blocking with 5% non-fat dried milk in TBST, the membranes were incubated with anti-Sp1 (Sigma-Aldrich, Cat. No. 07-645) or anti-β-actin (Cell Signaling Technology, Cat. No. 4967) antibodies. Proteins were detected using an ECL Western blotting detection system (GE Healthcare).

RNA preparation and quantification of gene expression

Total RNA was prepared from cultured cells using Sepasol Super-I (Nacalai Tesque, Cat. No. 09379-84) or tissue from QIAzol lysis reagent (Qiagen, Cat. No. 79306), and RNA samples were reverse-transcribed using Moloney murine leukemia virus reverse transcriptase (Promega, Cat. No.

M170B) following the manufacturer's protocol, in a thermal cycler (Takara PCR Thermal Cycler SP). To quantify mRNA expression, real-time qPCR was performed using a LightCycler 480 II System (Roche) with SYBR Green fluorescence signals, as described previously [168]. The primer sequences are provided in **Table S2-3**. All measured mRNA expression levels were normalized to *Rplp0* expression levels.

Statistical analysis

Data were expressed as means ± standard error of the mean (SEM). Statistical significance was evaluated using unpaired Student's *t*-test for the two group or one-way analysis of variance (ANOVA) followed by Tukey's *post hoc* tests. Statistical differences are indicated as * $p < 0.05$, ** $p < 0.01$, *** $p < 0.001$. Correlation was analyzed by Pearson's correlation. Analyses were performed using SPSS Statistics for Windows, Version 17.0 (IBM).

Results

2-1. Reduction in *Ppara* mRNA expression levels was observed in white adipose tissue of *db/db* mice and 10T1/2 cells cultured in conditioned medium derived from activated macrophages

First, the effects of inflammation on *Ppara* gene expression in WAT was investigated. It was found that *db/db* mice, an obese diabetic model, had higher body and adipose tissue weights than lean mice (**Figure 2-1A**–**2-1B**). *Ppara* gene expression levels were significantly downregulated in the WAT of *db/db* mice compared to those of lean mice (**Figure 2-1C**). Next, to examine the expression of *Ppara* in cultured adipocytes under inflammation conditions, differentiated 10T1/2 adipocytes were cultured in conditioned medium (CM) derived from LPS-stimulated RAW 264.7 macrophages (LPS+ CM). Incubation with LPS+ CM significantly reduced mRNA expression levels of *Ppara* in 10T1/2 adipocytes (**Figure 2-1D**). PPARα regulates FA oxidation in many cells [169]. Measurement of FA oxidation using [^{14}C]-labeled palmitic acid revealed that the production of [^{14}C]-labeled CO_2 and acid-soluble metabolites (ASMs), which are the main by-products of β-oxidation, was markedly suppressed in 10T1/2 adipocytes cultured in LPS+ CM compared with those cultured in CM from non-activated macrophages (LPS- CM) (**Figure 2-1E**–**2-1F**). These results suggest that inflammatory factors from activated macrophages downregulate *Ppara* mRNA expression, leading to the suppression of PPARα function in adipocytes.

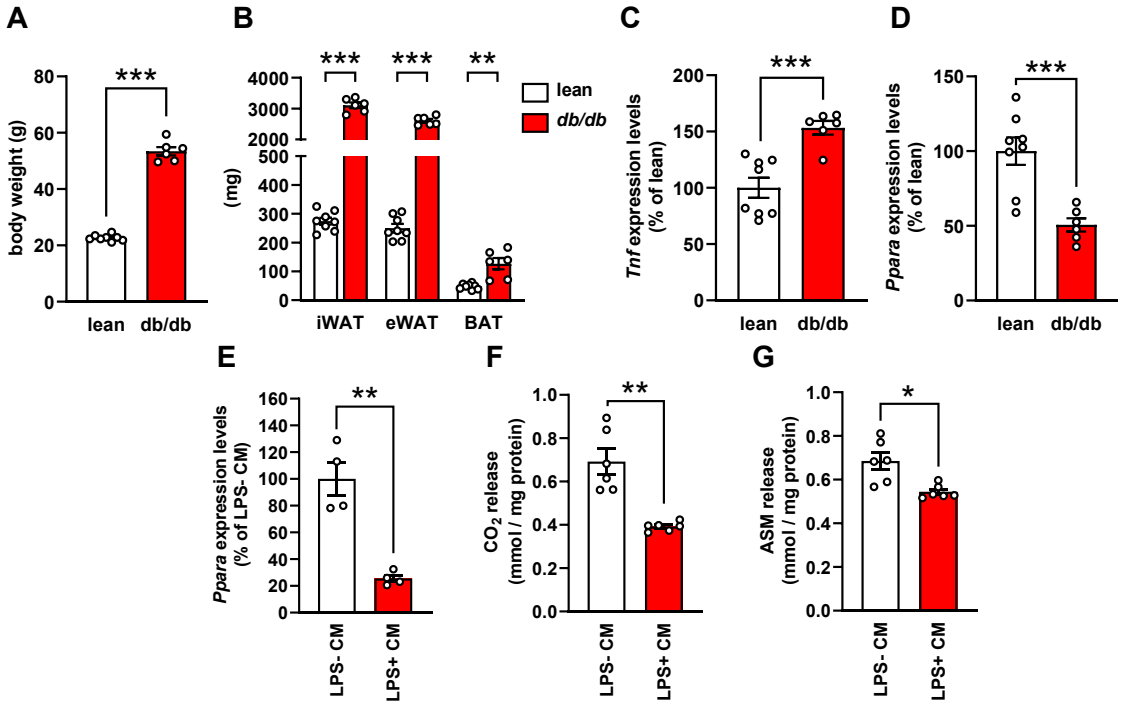

Figure 2-1. Reduction in *Ppara* mRNA expression levels was observed in white adipose tissue of *db/db* mice and 10T1/2 cells cultured in conditioned medium derived from activated macrophages

(A–B) Body weight (A) and weight of inguinal white adipose tissue (iWAT), epididymal white adipose tissue (eWAT), and brown adipose tissue (BAT) of 14-week-old male control (lean) or *db/db* mice (n = 6–8).

(C–D) Tumor necrosis factor alpha (*Tnf*; C) and peroxisome proliferator-activated receptor alpha (*Ppara*; D) mRNA expression levels in WAT of 14-week-old male control (lean) or *db/db* mice (n = 6–8).

(E) mRNA expression levels of *Ppara* in 10T1/2 adipocytes cultured in conditioned medium (CM) from non-activated RAW 264.7 macrophages (LPS- CM) or 500 ng/mL lipopolysaccharide (LPS) -stimulated macrophages (LPS+ CM) for 24 h on day 6 after induction of adipocyte differentiation (n = 4).

(F–G) Oxidation of [^{14}C] palmitic acid to CO_2 (F; n = 6) or acid-soluble metabolites (ASM) (G; n =6) in differentiated 10T1/2 adipocytes cultured in LPS- CM or LPS+ CM for 32 h.

Data are presented as mean ± standard error of the mean (SEM). Statistical analysis was performed using an unpaired Student's *t*-test. * P <0.05, ** P <0.01, *** P < 0.001.

2-2. Impaired *Ppara* gene expression attenuates β-adrenergic stimulation-induced thermogenesis-related gene expression levels in WAT

Inflammation in obese adipose tissue has been reported to be negative regulator of catecholamine signaling-mediated thermogenesis in white adipocytes (browning) [170−173], and PPARα activation increases thermogenic potential in adipocytes [76]. Therefore, to estimate the physiological importance of the downregulation of *Ppara* in catecholamine resistance occurring in obese adipose tissue, the role of PPARα in catecholamine-induced adipocyte browning using *Ppara* KO mice and adipocytes was investigated. Cold exposure, a potent stimulus for β-adrenergic receptors, induced the expression of thermogenic adipocyte-related genes such as *Ucp1, Ppargc1a* and cell-death inducing DNA fragmentation factor alpha subunit-like effector A (*Cidea*), as well as carnitine palmitoyltransferase 1B (*Cpt1b*) in the WAT of WT mice; these inductions were suppressed in the WAT of *Ppara* KO mice **(Figure 2-2A**). Interestingly, *Ppara* mRNA expression in WAT was also induced by cold exposure **(Figure 2-2A**). Furthermore, *Ppara*-deficient adipocytes (differentiated stromal vascular cells from *Ppara* KO mice) exhibited markedly downregulated expression levels of thermogenesis-related genes including *Ucp1, Ppargc1a*, and fibroblast growth factor 21 (*Fgf21*), upon stimulation of β-adrenergic receptors with isoproterenol, compared to control adipocytes **(Figure 2-2B)**. These results indicate that PPARα plays an important role in β-adrenergic stimulation-induced browning of WAT and that inflammation-induced suppression of *Ppara* gene expression in adipocytes may be related to obesity-associated catecholamine resistance in the adipocyte browning process.

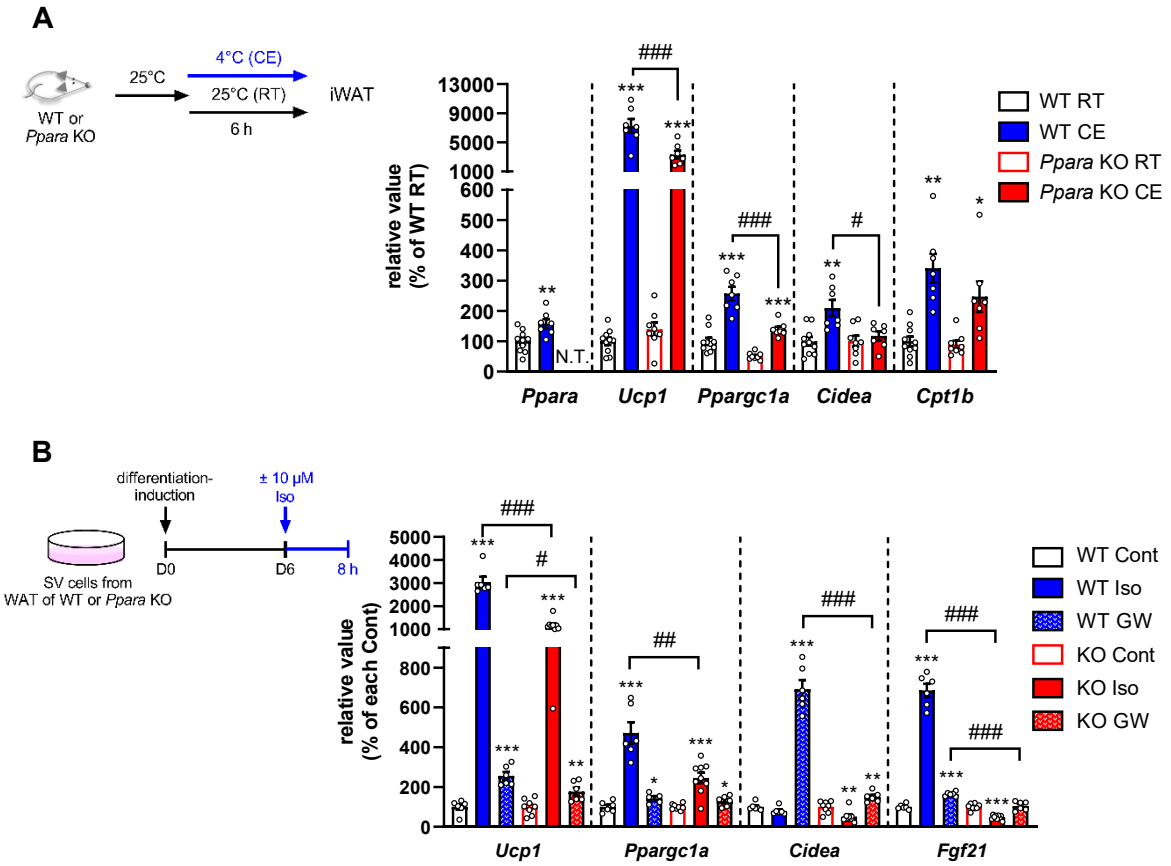

Figure 2-2. Impaired *Ppara* gene expression attenuates β-adrenergic stimulation-induced thermogenesis-related gene expression levels in WAT

(A) mRNA expression levels of *Ppara*, uncoupling protein 1 (*Ucp1*), peroxisome proliferator-activated receptor gamma coactivator 1-alpha (*Ppargc1a*), cell-death inducing DNA fragmentation factor alpha subunit-like effector A (*Cidea*), and carnitine palmitoyltransferase 1B (*Cpt1b*) in WAT of 12-week-old male WT or *Ppara*-knockout (*Ppara* KO) mice exposed to room temperature or cold (4°C) for 6 h (n = 7–10). RT, room temperature-exposed; CE. cold-exposed.

(B) mRNA expression levels of *Ppara*, *Ucp1*, *Ppargc1a*, *Cidea*, and fibroblast growth factor 21 (*Fgf21*) of *Ppara* KO adipocytes stimulated with 10 μM isoproterenol (ISO) for 8 h (n = 6–9).

Data are presented as mean ± standard error of the mean (SEM). Statistical analysis was performed using an unpaired Student's *t*-test or a one-way ANOVA followed by Tukey's test. * P <0.05, ** P < 0.01, *** P < 0.001; # P < 0.05; ## P < 0.01; ### P < 0.001.

2-3. NO suppresses *Ppara* gene expression levels and PPARα ligand-activated fatty acid oxidation in 10T1/2 adipocytes

Next, the factor responsible for downregulated *Ppara* gene expression under inflammation was investigated. It was found LPS treatment increased the mRNA expression of inducible nitric oxide synthase (*Nos2*), which catalyzes the production of nitric oxide from L-arginine, in RAW macrophages (**Figure 2-3A**). In addition, the concentration of nitrite was much higher in the CM from LPS-stimulated macrophages than in the CM from non-stimulated macrophages (**Figure 2-3B**). Co-culture with activated RAW macrophages markedly increased the amount of nitrite in the culture medium in 10T1/2 adipocytes; however, this effect was completely abolished by treatment with NIL, a selective NOS2 inhibitor (**Figure 2-3C**). *Ppara* gene expression in 10T1/2 adipocytes was decreased in co-culture with activated macrophages, whereas treatment with NIL partially but significantly alleviated the suppression of *Ppara* expression (**Figure 2-3D**), suggesting that NO produced by activated macrophages downregulates *Ppara* gene expression levels in adipocytes. Therefore, the effect of NO on *Ppara* gene expression in adipocytes was investigated by treating 10T1/2 adipocytes with NOR5, a spontaneous NO releaser. NOR5 treatment increased the nitrite levels in the culture medium of 10T1/2 adipocytes in a dose-dependent manner (**Figure 2-3E**). Notably, *Ppara* gene expression levels were significantly downregulated by NOR5 treatment, showing an inverse correlation with nitrite concentration in the culture medium (**Figure 2-3E**). To examine whether NO influences PPARα function, 10T1/2 cells were treated with GW7647, a selective PPARα agonist, after treatment with NOR5. Interestingly, although GW7647 treatment enhanced basal FA oxidation, as measured by the production of CO_2 and ASM from [^{14}C]-labeled palmitic acid, NOR5 treatment completely abolished GW7647-induced enhancement of FA oxidation in 10T1/2 adipocytes (**Figure 2-3F–2-3G**). Similarly, NOR5 treatment suppressed the GW7647-induced upregulation of PPARα target gene expressions, such as *Acox1* and *Cpt1b* (**Figure 2-3H–2-3I**). These results suggest that NO suppresses both *Ppara* gene expression and PPARα function in adipocytes.

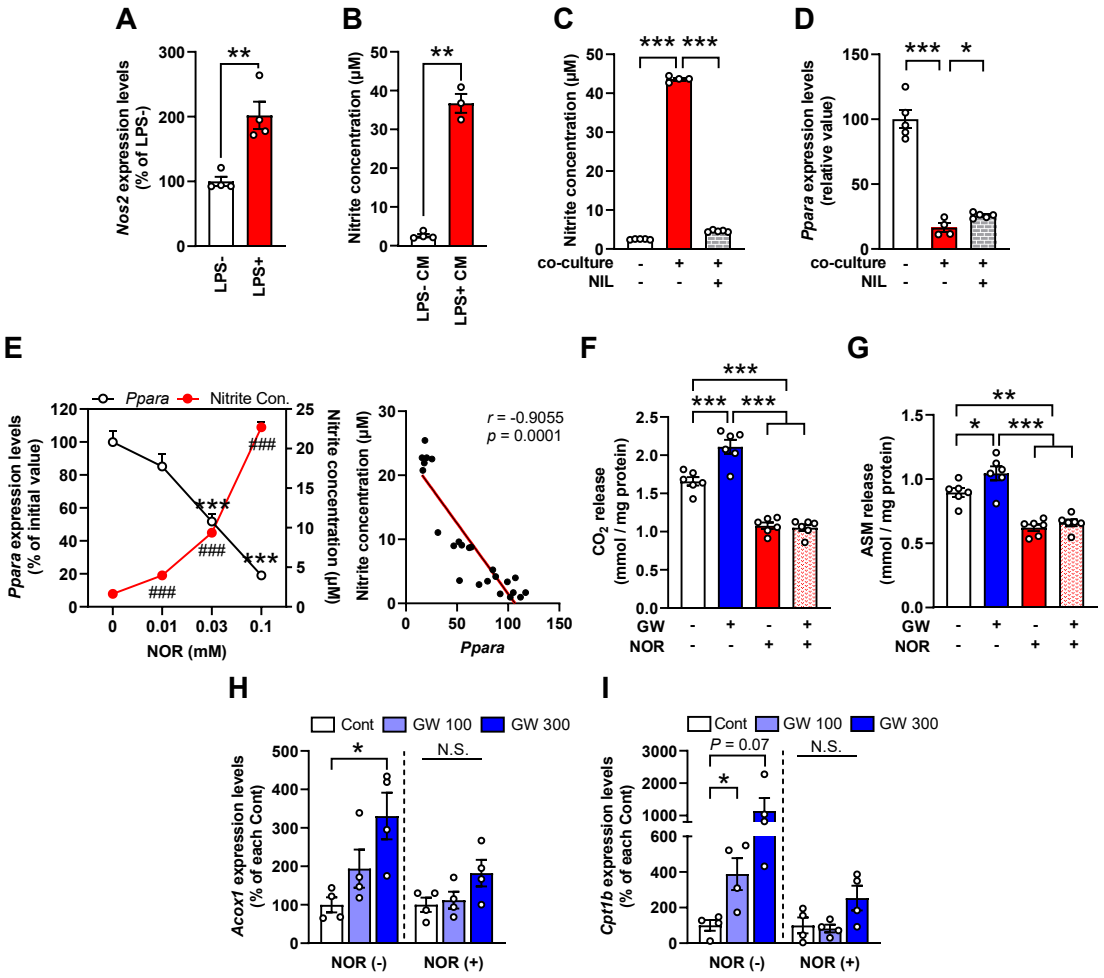

Figure 2-3. NO suppresses *Ppara* gene expression levels and PPARα ligand-activated fatty acid oxidation in 10T1/2 adipocytes

(A–B) mRNA expression levels of inducible nitric oxide synthase (*Nos2*) (A; n = 4) of RAW macrophages incubated with or without LPS (500 ng/mL) for 24 h and nitrite concentration in the culture medium (B; n = 3–4).

(C–D) Nitrite concentration in culture medium (C; n = 4–5) and mRNA expression levels of *Ppara* (D; n = 4–5) in 10T1/2 adipocytes co-cultured with RAW macrophages for 24 h with or without 200 μM N^6-(1-Iminoethyl)-L-lysine (NIL).

(E) Nitrite concentration in culture medium and the mRNA expression levels of *Ppara* in 10T1/2 adipocytes incubated with or without NOR5 at indicated concentrations for 24 h (left; n = 6 per each concentration). Correlation between the amount of nitrite in culture medium and the mRNA expression levels of *Ppara* in 10T1/2 adipocytes (right). *** P <0.001, ### P < 0.001 *vs.* initial value.

(F–G) Oxidation of [^{14}C] palmitic acid to CO_2 (F; n = 6) and to acid-soluble metabolites (ASM; G; n = 6) in 10T1/2 adipocytes co-incubated with or without GW7647 (1 μM) for 24 h following treatment with or without 0.1 mM NOR5 for 8 h.

(H–I) mRNA expression levels of PPARα target genes which are involved in fatty acid oxidation such as acyl-CoA oxidase 1 (*Acox1*; H; n = 4) and carnitine palmitoyltransferase 1B (*Cpt1b*; I; n = 4) of 10T1/2 adipocytes co-incubated with or without 0.1 mM NOR5 for 12 h following treatment with GW7647 (GW) at the indicated concentrations (nM) for 12 h.

Data are presented as mean ± standard error of the mean (SEM). Statistical analysis was performed using an unpaired Student's *t*-test or a one-way analysis of variance (ANOVA) followed by Tukey's test. Correlation was analyzed by Pearson's correlation. * P < 0.05, ** P < 0.01, *** P <0.001. Con., Concentration.

2-4. NO is involved in the inflammation-induced suppression of *Ppara* gene expression in white adipose tissue of mice

To investigate the effect of inflammation on *Ppara* gene expression in adipose tissue, C57BL/6 mice were administered LPS to induce acute systemic inflammation. Following LPS treatment, the plasma concentrations of nitrogen oxides (NOx), markedly increased until 24 h (**Figure S2-1A**). It was found that *Nos2* mRNA levels in WAT peaked at 6 h. In contrast, a gradual decrease in *Ppara* mRNA expression levels was observed until 12 h after LPS treatment (**Figure 2-4A**), suggesting that *Ppara* mRNA expression in the WAT of mice is suppressed under inflammatory conditions. To examine the effect of NO on the inflammation-induced suppression of *Ppara* mRNA expression in WAT, C57BL/6 mice were simultaneously administered LPS only or LPS and 1400w, a selective NOS2 inhibitor. Nine hours after LPS administration, NOx levels in both plasma and WAT increased; however, this increase was suppressed in the presence of 1400w (**Figure 2-4B**–**2-4C**). Although *Nos2* expression levels in the WAT tended to increase with LPS treatment, they did not change in the presence of the NOS2 inhibitor (**Figure S2-1B**). The mRNA expression levels of *Ppara* in WAT were significantly decreased by LPS treatment; however, the suppression was partially but significantly recovered by 1400w treatment (**Figure 2-4D**). To clarify the relevance of NO in the inflammation-induced dysregulation of *Ppara* mRNA expression in WAT, LPS to *Nos2* was administered to KO mice. Plasma NOx levels increased in wild-type (WT) mice injected with LPS, but not in KO mice (**Figure 2-4E**). It was found that LPS-induced suppression of *Ppara* mRNA expression levels by LPS treatment in the WAT of WT mice was partially recovered by knockout of *Nos2* (**Figure 2-4F**), suggesting that NOS2-derived NO inhibits *Ppara* expression levels in WAT. Next, we investigated the effect of NO on *Ppara* mRNA expression in WAT during obesity-induced inflammation as shown in **Figure 2-4G**. Obese and diabetic *db/db* mice showed higher plasma NOx levels than lean mice; however, this effect was suppressed by 1400w treatment (**Figure 2-4H**). Furthermore, *Ppara* mRNA levels were significantly lower in the WAT of *db/db* mice than in lean mice (**Figure 2-4I**). Notably, the suppressed *Ppara* gene expression recovered after 1400w treatment, suggesting that NO is involved in the suppression of *Ppara* gene expression in

the WAT of obese mice (**Figure 2-4I**). Altogether, these findings suggest that NO is involved in the inflammation-induced suppression of *Ppara* gene expression in mouse WAT.

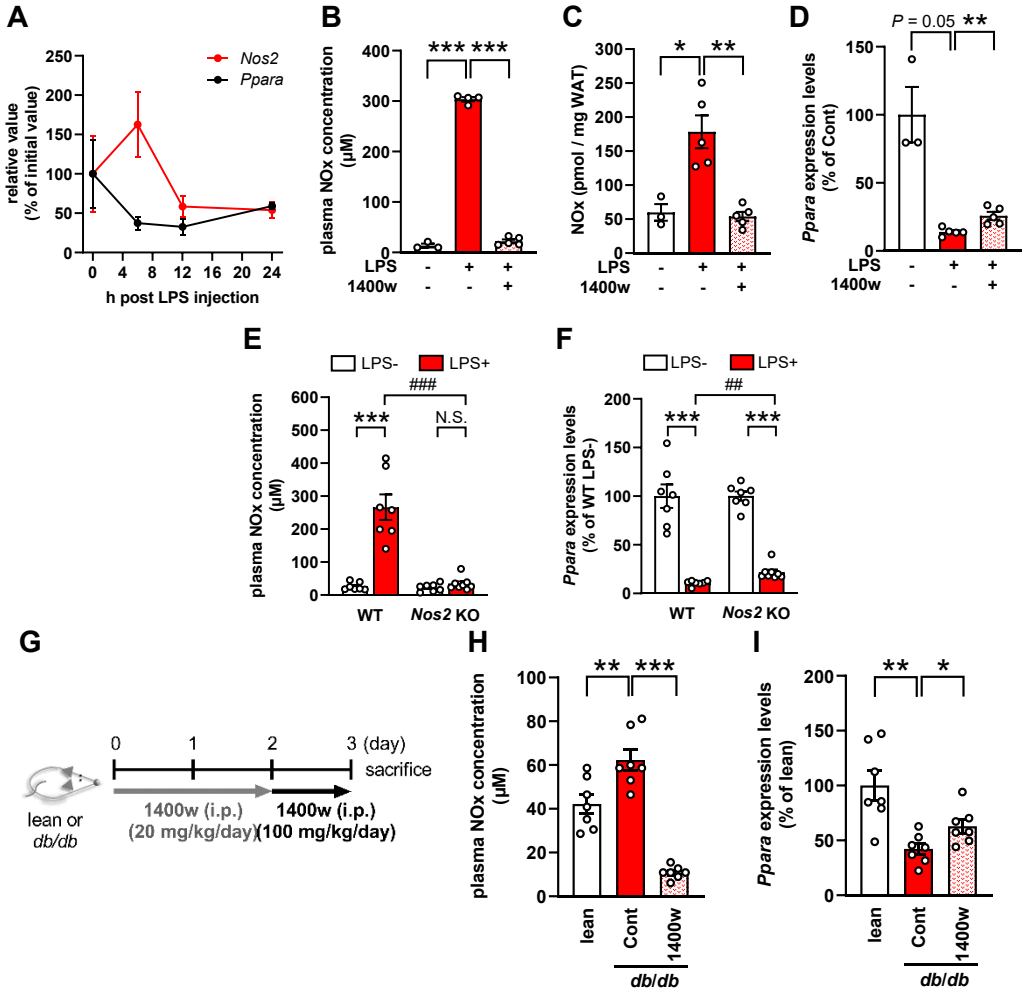

Figure 2-4. NO is involved in the inflammation-induced suppression of *Ppara* gene expression in white adipose tissue of mice

(A) mRNA expression levels of *Nos2* and *Ppara* in WAT of 11–12-week-old male C57BL/6J mice intraperitoneally injected with 200 μg LPS (n = 3–4).

(B–D) Plasma NOx (B; n = 3–5), WAT NOx (C; n = 3–5), and mRNA expression levels of *Ppara* in WAT (D; n = 3–5) of 12-week-old male C57BL/6J mice intraperitoneally injected with LPS with or without 1400w (100 mg/kg).

(E–F) Plasma NOx (E; n = 7–8) and mRNA expression levels of *Ppara* in WAT (F; n = 7–8) of wild-type (WT) or *Nos2*-knockout male mice intraperitoneally injected with PBS or LPS.

(G) Experimental study design. 14-week-old male *db/db* mice were injected intraperitoneally (i.p.) PBS or 1400w (20 mg/kg/day for 1st and 2nd day, followed by 100 mg/kg/day for 3rd day). One hour after the last administration, mice were sacrificed and their plasma and WATs were collected for further investigation. *m/m* mice were used as a lean control.

(H–I) Plasma NOx (H; n = 7) and mRNA expression levels of *Ppara* in WAT (I; n = 7–8) of 14-week-old male lean or *db/db* mice intraperitoneally injected with or without 1400w.

Data are presented as mean ± standard error of the mean (SEM). Statistical analysis was performed using an unpaired Student's *t*-test or a one-way ANOVA followed by Tukey's test. * P <0.05, ** P < 0.01, *** P < 0.001; ## P < 0.01, ### P < 0.001.

2-5. Endoplasmic reticulum stress mediates NO-induced downregulation of *Ppara* gene expression in 10T1/2 adipocytes

NO exerts various physiological effects through the phosphorylation of mitogen-activated protein kinases (MAPKs), activation of protein kinase G (PKG), production of reactive oxygen species (ROS), and induction of endoplasmic reticulum (ER) stress [174-178]. To investigate the signaling pathways responsible for NO-mediated dysregulation of *Ppara* expression, 10T1/2 adipocytes were treated with MAPK (p38 or c-Jun N-terminal kinase [JNK]) or guanylyl cyclase inhibitor, or ROS scavenger; however, NOR5-induced suppression of *Ppara* gene expression was not recovered by these treatments (**Figure S2-2A–S2-2D**). The NO-induced ER stress pathway is involved in the pathogenesis of various diseases [179]. NOR5 treatment significantly increased the expression of ER stress-related genes, including the binding immunoglobulin protein (*Bip*) and CCAAT-enhancer-binding protein homologous protein (*Chop*) in 10T1/2 adipocytes (**Figure 2-5A**). Treatment with tunicamycin or thapsigargin, an ER stress inducer, decreased *Ppara* gene expression in adipocytes (**Figure 2-5B**). To investigate whether ER stress mediates NO-induced downregulation of *Ppara* expression, 10T1/2 adipocytes were treated with NOR5 in the presence of an ER stress inhibitor, trimethylamine N-oxide (TMAO), a chemical chaperone. The upregulated mRNA levels of *Bip* and *Chop* after NOR5 treatment were ameliorated in the presence of TMAO (**Figure 2-5C**). Notably, the NOR5-induced suppression of *Ppara* gene expression was partially recovered in the presence of TMAO (**Figure 2-5D**). These findings suggest that NO suppresses *Ppara* expression in adipocytes, at least in part, by inducing ER stress.

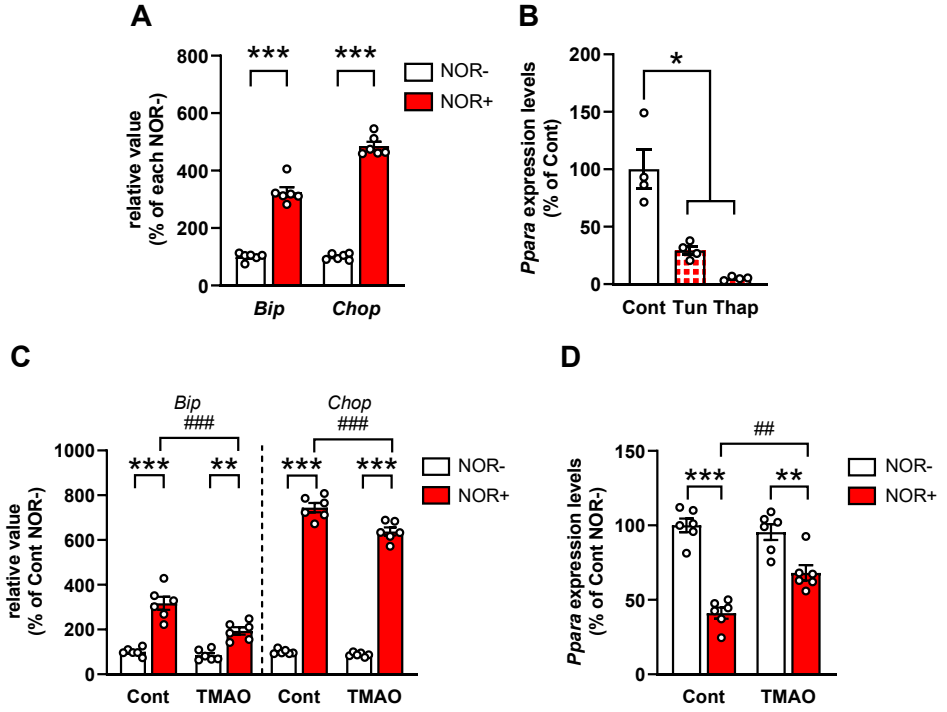

Figure 2-5. Endoplasmic reticulum stress mediates NO-induced downregulation of Ppara gene expression in 10T1/2 adipocytes

(A) mRNA expression levels of binding immunoglobulin protein (*Bip*) and CCAAT-enhancer-binding protein homologous protein (*Chop*) (n = 6) in 10T1/2 adipocytes incubated with or without 0.1 mM NOR5 for 24 h.

(B) mRNA expression levels of *Ppara* (n = 4) in 10T1/2 adipocytes incubated with or without tunicamycin (5 μM) or thapsigargin (500 nM) for 24 h.

(C–D) mRNA expression levels of *Bip*, *Chop* (C; n = 6) and *Ppara* (D; n = 6) in 10T1/2 adipocytes incubated with or without 100 mM trimethylamine-N-oxide (TMAO) for 12 h, followed by co-treatment with or without 0.1 mM NOR5 for 24 h.

Data are presented as mean ± standard error of the mean (SEM). Statistical analysis was performed using an unpaired Student's *t*-test or a one-way ANOVA followed by Tukey's test. * P <0.05, ** P < 0.01, *** P < 0.001; ## P < 0.01, ### P < 0.001.

2-6. NO suppresses *Ppara* promoter activity via the suppression of Sp1 transcriptional activity

To investigate the mechanisms underlying the regulation of the *Ppara* gene by NO, the effect of NO on *Ppara* promoter activity was investigated. To achieve this, 10T1/2 cells were transfected with plasmid encoding luciferase driven by a 3.0-kb 5′-flanking region of the mouse *Ppara* promoter (-3,014/+132). As a result, treatment with either NOR5 or ER stress inducers suppressed *Ppara* promoter activity; however, this effect was reversed by co-incubation with the ER stress inhibitors TMAO or PBA (**Figure 2-6A**). To identify the potential regulatory element in the *Ppara* promoter region responsible

for NO action, the luciferase activity driven by a series of 5′- deletion constructs of the mouse *Ppara* promoter was determined. All deleted constructs showed significantly low promoter activity after NOR5 treatment; however, this was recovered by co-treatment with PBA (**Figure 2-6B**), suggesting that NO suppresses *Ppara* promoter activity via the induction of ER stress. Because none of the deleted constructs abolished the repressive effect of NOR5 (**Figure 2-6B**), it was assumed that the proximal promoter region of up to -245 bp was involved in the NO-induced downregulation of *Ppara* promoter activity. In this region, seven putative binding motifs for the specificity protein 1 (Sp1) were identified. Therefore, seven mutant vectors that disrupted each putative Sp1-binding site was generated based on the reporter vector containing the *Ppara* promoter region (-245/+132) (**Figures 2-6C and S2-3A–S2-3B**). As shown in **Figure 2-6C**, among the seven putative Sp1-binding sites in the *Ppara* promoter, a significant loss of inhibitory effects of NOR5 on *Ppara* promoter activity was obtained in the sequence mutated between -218/-209 (Δ1), -58/-49 (Δ5), or -14/-5 (Δ7). Moreover, the triple mutation of these Sp1 binding sites in the *Ppara* proximal promoter (the Δ1,5,7 construct) alleviated the NOR5-induced suppression of *Ppara* promoter activity (**Figure 2-6D**), suggesting the functional relevance of Sp1-binding sites located between -218/-209, -58/-49, and -14/-5 in the NO-induced dysregulation of mouse *Ppara* promoter activity. Importantly, these Sp1-binding sites are conserved in humans (**Figure 2-6D**). To confirm whether Sp1 occupies the endogenous *Ppara* promoter region (-245/+38) and whether NO interferes with promoter occupancy by Sp1 in 10T1/2 adipocytes, chromatin immunoprecipitation assays was performed. The occupancy by Sp1 of the endogenous *Ppara* proximal promotor region was confirmed, although it was inhibited by NOR5 treatment (**Figure 2-6E**). To further investigate the potential mechanism involved in NO-induced suppression of the occupancy of *Ppara* promoter region by Sp1, if NOR5 treatment inhibits the expression levels of *Sp1* was investigated. NOR5 suppressed *Sp1* mRNA expression in 10T1/2 cells (**Figure 2-6F**), suggesting that the inhibition of Sp1 recruitment to the *Ppara* promoter by NO likely occurred at least partially through an inhibition of *Sp1* expression. Small interfering RNA-mediated suppression of *Sp1* expression led to a significant decrease in *Ppara*

mRNA expression levels (**Figure 2-6H**) and mRNA expression levels of *Ppara* target genes, such as *Acox1* and *Cpt1b* (**Figure 2-6I**). Finally, treatment with mithramycin A (MTA), an Sp1 inhibitor, markedly suppressed the expression of *Ppara* and its target genes (*Acox1* and *Cpt1b*) in 10T1/2 adipocytes (**Figure 2-6J**). Importantly, in the presence of MTA, upregulated expression of target genes by ligand-activated PPARα was completely abolished (**Figure 2-6J**), suggesting that functional Sp1 is essential for proper PPAR*a* activity. These data indicate that NO represses *Ppara* expression by inhibiting Sp1-dependent transcription of *Ppara.*

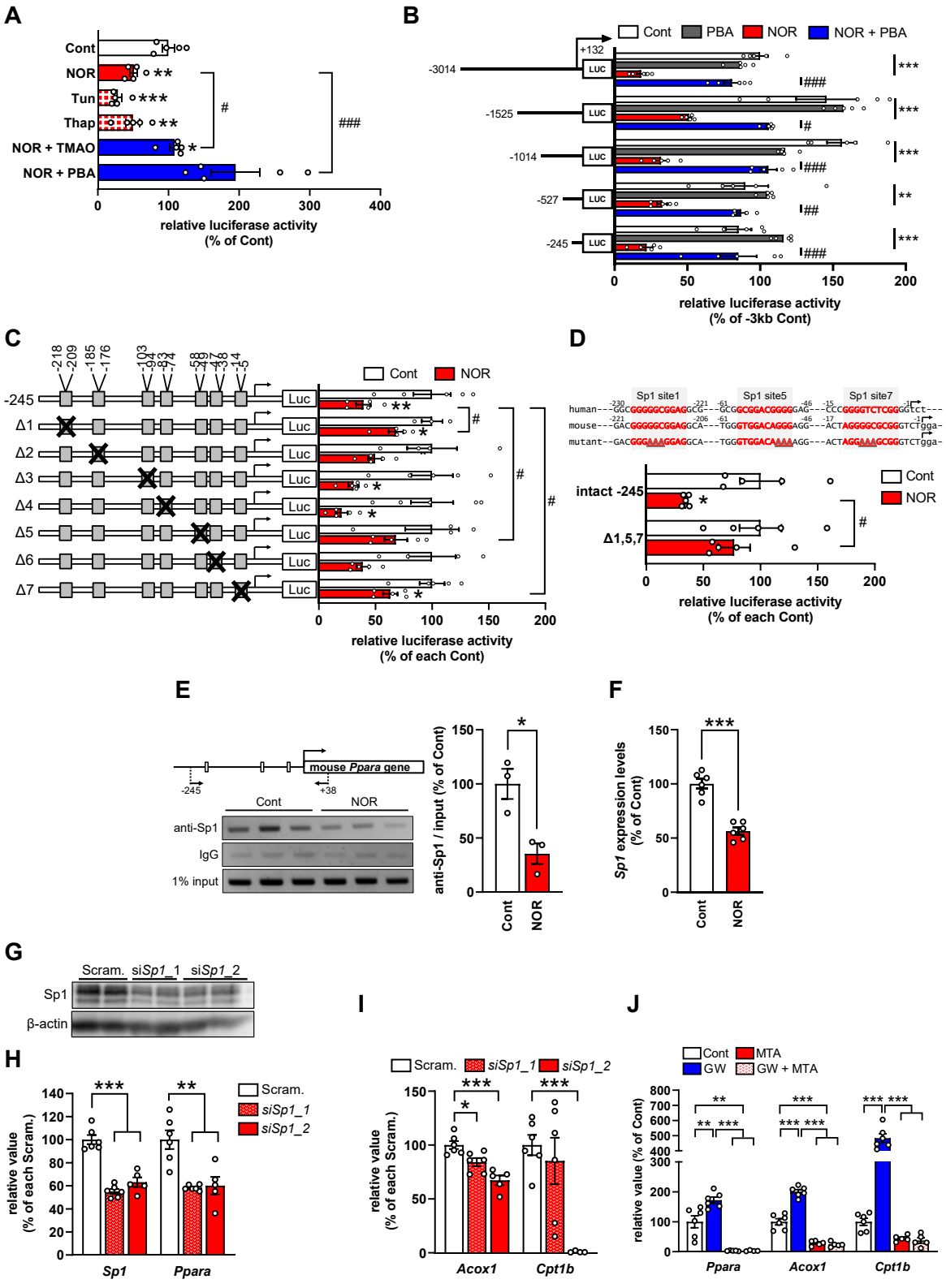
A
Cont
NOR
Tun
Thap
NOR + TMAO
NOR + PBA
relative luciferase activity
(% of Cont)
B
Cont
PBA
NOR
NOR + PBA
-3014
-1525
-1014
-527
-245
relative luciferase activity
(% of -3kb Cont)
C
Cont
NOR
Δ1
Δ2
Δ3
Δ4
Δ5
Δ6
Δ7
relative luciferase activity
(% of each Cont)
D
Sp1 site1
Sp1 site5
Sp1 site7
human
mouse
mutant
intact -245
Δ1,5,7
relative luciferase activity
(% of each Cont)
E
mouse Ppara gene
anti-Sp1
IgG
1% input
anti-Sp1 / input (% of Cont)
F
Sp1 expression levels
(% of Cont)
G
Scram.
siSp1_1
siSp1_2
Sp1
β-actin
H
relative value
(% of each Scram.)
Sp1
Ppara
I
Acox1
Cpt1b
J
MTA
GW
GW + MTA
Ppara
Acox1
Cpt1b

Figure 2-6. NO suppresses *Ppara* promoter activity via the suppression of Sp1 transcriptional activity
(A) Luciferase activities driven by mouse *Ppara* promoter region (-3,014/+132) in 10T1/2 cells treated with or without 0.1 mM NOR5 (NOR) in combination with or without 100 mM TMAO or 10 mM 4-phenylbutyric acid sodium (PBA), 5 μM tunicamycin, or 500 nM thapsigargin for 24 h (n = 5).
(B) Luciferase activities driven by a series of deletion construct of 5′-flanking region of mouse *Ppara* promoter in 10T1/2 cells treated with or without 0.1 mM NOR5 in combination with or without 10 mM PBA for 24 h (n = 5).
(C) Luciferase activities driven by a series of mutated construct of mouse *Ppara* promoter region (-245/+132) in 10T1/2 cells treated with or without 0.1 mM NOR5 for 24 h (n = 3–5).
(D) Luciferase activities driven by triple-mutated construct (Δ1, Δ5, Δ7) of mouse *Ppara* promoter region (-245/+132) in 10T1/2 cells treated with or without 0.1 mM NOR5 for 24 h (n = 5).
(E) Chromatin immunoprecipitation assay performed with the *Ppara* promoter region (-245/+38) of 10T1/2 adipocytes treated with or without 0.1 mM NOR5 for 24 h (n = 3). Band intensities were measured by ImageJ software.
(F) mRNA expression levels of *Sp1* in 10T1/2 adipocytes treated with or without 0.1 mM NOR5 for 24 h (n = 6).
(G) Immunoblots for specificity protein 1 (Sp1) after transfection with control siRNA (scramble) or *Sp1* siRNA for 24 h in 10T1/2 adipocytes. β-actin, a loading control.
(H) mRNA expression levels of *Sp1* and *Ppara* in 10T1/2 adipocytes transfected with scramble or *Sp1* siRNAs (n = 5–6).
(I) mRNA expression levels of *Acox1* and *Cpt1b* in 10T1/2 adipocytes transfected with scramble or Sp1 siRNAs (n = 4–6).
(J) mRNA expression levels of *Ppara*, *Acox1*, and *Cpt1b* in 10T1/2 adipocytes treated with or without 300 nM GW7647 and/or 3 μM mithramycin A (MTA) (n = 4–6).
Data are presented as mean ± standard error of the mean (SEM). Statistical analysis was performed using an unpaired Student's *t*-test or a one-way ANOVA followed by Tukey's test. * P <0.05, ** P < 0.01, *** P < 0.001; # P < 0.05, ## P < 0.01, ### P < 0.001.

Discussion

WAT browning, a process of the WAT acquiring the thermogenic function, is mainly controlled by the sympathetic nervous system; therefore, stimuli like cold exposure result in the activation of sympathetic neurons and the release of catecholamines to activate the thermogenic gene program in adipocytes [180]. Inflammation has been reported to attenuate WAT browning by altering catecholamine signal transduction [46,170]. Results in **Figure 2-2**, suggest that PPARα plays an important role in regulating β-adrenergic receptor-induced adipocyte browning. Additionally, it was found that inflammatory cytokines, including NO, downregulated *Ppara* expression, followed by decreased PPARα function. These findings suggest that inflammation-induced suppression of *Ppara* gene expression in adipocytes may be related to obesity-associated catecholamine resistance in adipocyte browning. Adipocyte-specific *Nos2* deletion has been reported to enhance *Ucp1* expression levels in the thermogenic adipose tissue of obese mice [181]. Therefore, inflammatory factors from macrophages and adipocytes might be related to inflammation-induced catecholamine resistance via the regulation of *Ppara*.

Results in Chapter 2 demonstrated that NO plays an important role in regulating *Ppara* gene expression and PPARα-mediated FA oxidation in adipocytes. *Ppara* expression is downregulated in the WAT of obese mice [74,182,183]. However, the signaling machinery linking obesity, a state of chronic inflammation, to the downregulation of *Ppara* expression in WAT remains unknown. It was found that inflammation (acute and chronic inflammation caused by LPS and obesity, respectively) -induced NOS2-driven NO production suppressed *Ppara* gene transcription via an Sp1-mediated mechanism. Specifically, NO-induced ER stress reduced the occupancy of the transcription factor Sp1 in its binding sites, which is highly conserved between mice and humans, in the *Ppara* proximal promoter region (**Figure 2-6D**). Excessive inflammation and ER stress in subcutaneous WAT of patients with severe obesity were attenuated after bariatric surgery, accompanied by metabolic changes including enhanced FA oxidation, which seems to be related to changes in PPARs expression [184,185]. These studies

indicated that the transcriptional regulation of *Ppara* by Sp1 in response to NO-mediated ER stress could occur in humans.

The proximal promoter region of *Ppara* is responsible for NO-mediated downregulation of *Ppara* expression in adipocytes. Besides Sp1, putative binding motifs of several transcription factors, including nuclear factor erythroid 2-related factor 1 (NRF1) and early growth response protein 1 (EGR1), could be identified in this region. NRF1 and EGR1 are important transcriptional factors to regulate energy and lipid metabolism, such as adipocyte browning [186−189], and their transcriptional activities seem to be closely related to obesogenic conditions, including inflammation and ER stress [190,191]. Therefore, transcription factors other than Sp1, such as NRF1 and EGR1, might participate in the NO-induced *Ppara* downregulation via direct binding to its proximal promoter region. Other factors may also be involved in regulating transcriptional activity of the *Ppara* proximal promoter region by regulating Sp1 function. Histone deacetylase 1 (HDAC1) allows Sp1 to act as a transcriptional repressor by binding to Sp1 [192]. HDAC1 expression is upregulated by ER stress [193], suggesting that NO-induced ER stress may decrease Sp1 transcriptional activity via HDAC1. Cyclin A-cyclin-dependent kinase 2 (CDK2) complex can affect Sp1 transcriptional activity by enhancing Sp1-DNA binding affinity by phosphorylating Ser61 at the Sp1 [194]; however, NO has been reported to suppress the CDK2 activity by repressing cyclin A gene expression [195]. *O*-linked *N*-acetylglucosaminylation (*O*-GlcNAcylation) of Sp1 by *O*-GlcNAc transferase is elevated in the adipose tissue of diabetic mice [196] and the altered *O*-GlcNAcylation of Sp1 is associated with altered transcription activation of its target genes [197,198], implying that inflammatory cytokines affect the transcriptional activity of Sp1. Therefore, NO-ER stress-induced changes in these factors might affect Sp1 transcriptional activity, and they might be co-recruited to its binding site in the *Ppara* promoter region.

The reduction in the expression levels of *Ppara* in adipocytes co-cultured with activated-macrophages and in the WAT of *db/db* mice was recovered by treatment with NOS2 inhibitors; however, these recoveries were only partial, even though NO production was largely inhibited, suggesting that

other inflammatory factors may be involved in the reduced *Ppara* expression. Ye *et al*. reported that LPS diminishes Sp1 activity by degrading the Sp1 protein via nuclear factor kappa B (NF-κB) in the lungs of mice [199]. TNFα activates NF-κB signaling in adipocytes [200], and most TNFα inflammatory signals are delivered by the TNF receptor (TNFR1) [201]. TNFR1 knockout mice are protected from diet-induced obesity and show upregulated thermogenic gene expression in adipose tissue [202]. Because PPARα in adipocytes is important for protecting against diet-induced obesity and maintaining thermogenesis [165], the activated TNFR1-NF-κB-Sp1 axis in adipocytes may be an additional negative regulator of *Ppara* expression in adipocytes. Moreover, nucleotides released into the extracellular space due to plasma membrane damage or cell death under pathophysiological conditions, including inflammation [203,204] may be related. Treatment of adipocytes with an agonist of the purinergic receptor type 6 (P2Y6R), which is activated by uridine diphosphate, decreases *Ppara* mRNA levels in adipocytes, suggesting that inflammation-induced activation of the P2Y6R pathway downregulates *Ppara* mRNA expression levels [205]. Plasma levels of TNFα and uridine are elevated in patients with diabetes [206,207]. Although further investigation is required to confirm the contribution of other inflammatory factors to the suppression of *Ppara* expression levels in adipocytes, these previous reports suggest that, besides NO, TNFα, and uridine diphosphate are related to the downregulation of *Ppara* expression in obese adipose tissue.

NO plays a pivotal role in numerous biological processes via multiple mechanisms, including activation of the MAPK and cGMP/PKG pathways, ROS production, and protein modification [208]. The mRNA expression levels of *Ppara* were suppressed by the addition of the NO donor; however, this was not restored by co-treatment with MAPK inhibitors, a guanylyl cyclase inhibitor, or a ROS scavenger, suggesting that the reduced *Ppara* expression levels are independent of NO-induced MAPK activation, cGMP/PKG activation, or ROS production (**Figure S2-2A–S2-2D**). However, the downregulated *Ppara* expression levels were restored in the presence of an ER stress inhibitor (**Figure 2-6A**), suggesting that NO decreases the mRNA expression of *Ppara* by suppressing its promoter

activity through the enhancement of ER stress. ER stress affects the DNA binding property of Sp1 on the promoter region of its target genes [209,210]. Abdelrahim et al. have shown that ER stress recruits Sp1 to the promoter of GRP78/Bip (an ER stress response gene) in pancreatic cancer cells [209]. In contrast, Donati et al. reported that Sp1 recruitment induced by ER stress varies depending on the genes, and Sp1 recruitment levels on the promoter regions of several ER stress-related genes are decreased [210]. These findings indicate that ER stress in adipocytes induces changes in Sp1 occupancy on the promoter regions of its target genes, and results in Chapter 2 suggest that Sp1 occupancy of the *Ppara* promoter decreases under ER stress, leading to the downregulation of PPARα.

Activation of PPARα in adipose tissue leads to enhanced FA oxidation and the prevention of adipocyte hypertrophy, which is strongly linked to metabolic diseases [211]. Therefore, preventing the decrease in *Ppara* expression in obese adipose tissue can prevent and attenuate obesity-associated metabolic abnormalities. NO-induced ER stress, which was suggested to contribute to reducing *Ppara* expression in adipocytes, is expected to be a novel therapeutic target for obesity and obesity-related metabolic disorders.

Supplementary Information

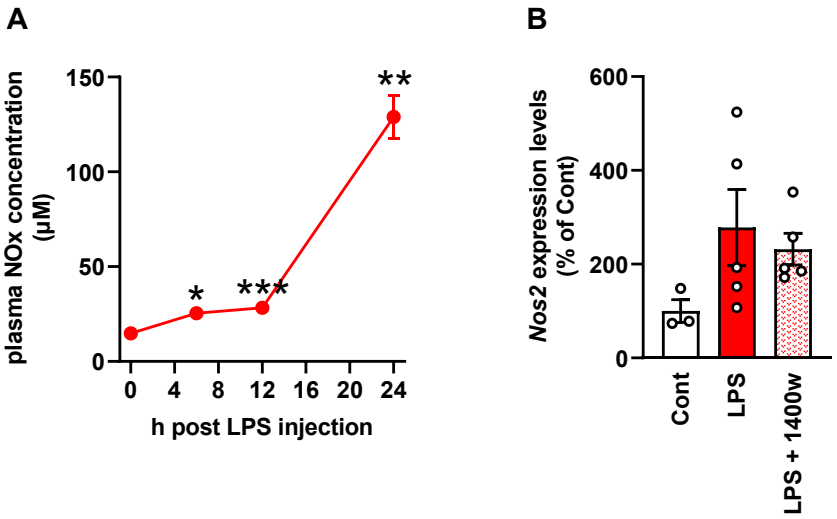

Figure S2-1. NO is involved in the inflammation-induced suppression of *Ppara* gene expression in inguinal white adipose tissue of mice.

(A) 11-week-old male C57BL/6J mice were intraperitoneally injected with 200 μg of LPS and sacrificed at indicated time points. After that, plasma NOx was measured (n = 4) (B) 12-week-old male C57BL/6J mice were intraperitoneally injected with 200 μg of LPS and fasted at the same time. The mice were then injected with vehicle or 1400w (100 mg/kg/9 h) by dividing three times. Nine hours after initial injection, mRNA expression levels of *Nos2* (n = 3–5) were measured.

Data are presented as the mean ± standard error of the mean (SEM). Statistical analysis was performed using unpaired Student's *t*-test. * P <0.05, ** P < 0.01 *vs.* initial value.

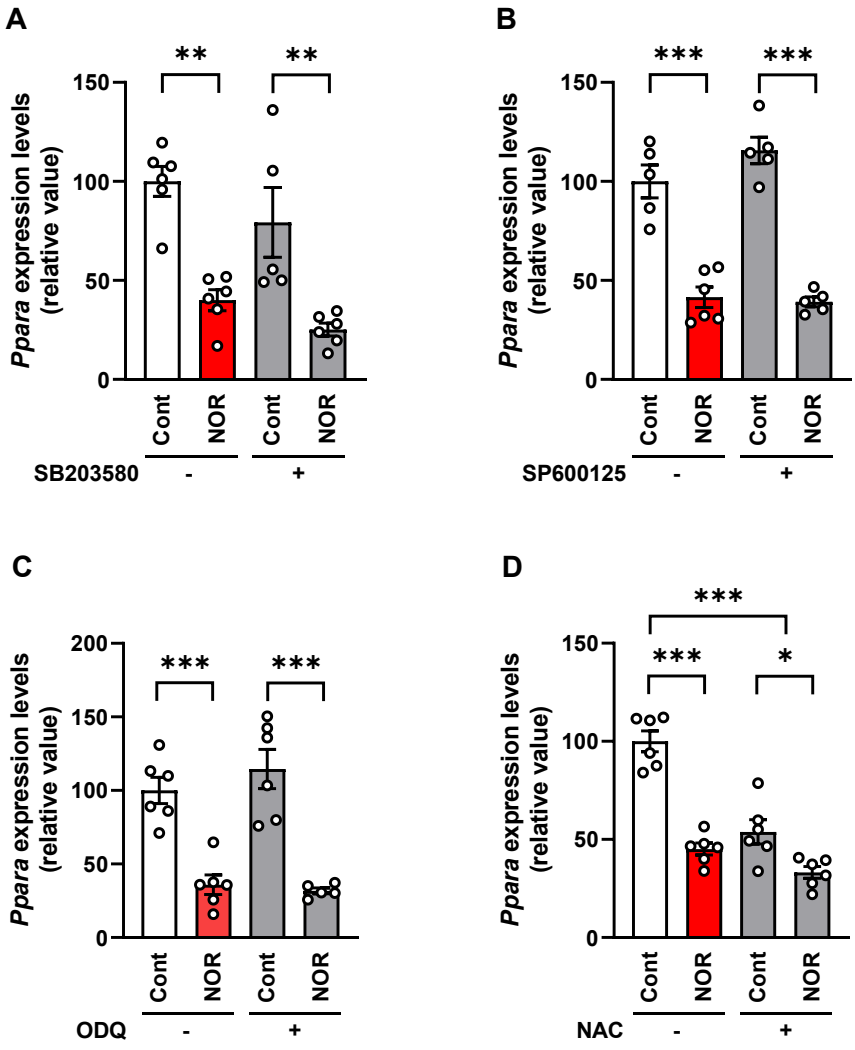

Figure S2-2. Effect of inhibitors of downstream pathway of NO signal on *Ppara* mRNA expression levels in 10T1/2 adipocytes.

(A–D) Six days after differentiation induction, 10T1/2 adipocytes were incubated with (A) 20 μM SB203580 (p38 inhibitor), (B) 20 μM SP600125 (JNK inhibitor), (C) 25 μM ODQ (PKG inhibitor), or (D) 10 mM NAC (ROS scavenger) for an hour, followed by treatment with or without 0.1 mM NOR5 for 24 h. The *Ppara* mRNA expression levels were quantified by real-time qPCR (n = 5–6).

Data are presented as the mean ± standard error of the mean (SEM). Statistical analysis was performed using one-way ANOVA followed by Tukey's test. * $P < 0.05$, ** $P < 0.01$, *** $P < 0.001$.

A

Intact

-245

ACGCTACGGTCCCACGACAGGGGTGACGGGGGCGGAGGCAGCCGCTTACGCCCCTCCTGGCGCC

TCCTCCTGGGCGCGCTTGGCCCTGCGGACCCGCAGGCGGAGTGCAGCCTCAGGTGCCCAGGGGC

TGGAGGGCACGCGCGAGGGCGGGGAGCCAGGCGTCCCCTGTCCCGGGACAGTGAGGTGGGTGG

ACAGGGAGGGGAGGGGCTCGGTGGCGCATGCGCGCGGACTAGGGGCGCGGGTCTGGAGACCCA

CAGCCACTGGAGAGGGCACACGCTAGGAAGGGCACACGCGTGCGAGTTTTCAGGGCCCGCGGAA

CTGTCCGCCACTTCGAGTCCCCTGGAGCGCCGTGCGCCGGCTCCGAACATTGGTGTTCG

+132

B

Mutant

-245

Δ1

ACGCTACGGTCCCACGACAGGGGTGACGGGAAAGGAGGCAGCCGCTTACGCCCCTCCTGGCAAA

Δ2

TCCTCCTGGGCGCGCTTGGCCCTGCGGACCCGCAGGCGGAGTGCAGCCTCAGGTGCCCAGGGGC

Δ3 Δ4

TGGAGGGCACGCGCGAGGAAAGGGAGCCAGGCGTCAAATGTCCCGGGACAGTGAGGTGGGTGG

Δ5 Δ6 Δ7

ACAAAAAGGGGAAAAGCTCGGTGGCGCATGCGCGCGGACTAGGAAAGCGGGTCTGGAGACCCA

CAGCCACTGGAGAGGGCACACGCTAGGAAGGGCACACGCGTGCGAGTTTTCAGGGCCCGCGGAA

CTGTCCGCCACTTCGAGTCCCCTGGAGCGCCGTGCGCCGGCTCCGAACATTGGTGTTCG

+132

Figure S2-3. DNA sequence alignment of intact and mutant site in *Ppara* promoter region (-245/+132).
(A) DNA sequence alignment of intact and (B) mutant in which guanine or cytosine was replaced by adenine of putative Sp1-binding sites in *Ppara* promoter region. Sequence in yellow box indicates the putative Sp1-binding site, underlined red font with bold indicates mutated base sites.

Table S2-1

List of PCR primers for 5′-flanking deletion of *Ppara* promoter construct

Deletion construct		Primer sequence for 5′-flanking deletion construct (5′ → 3′)
-3014/+132	Fw	GCTCGCTAGCCTCGATTCCACCACCTGATTGAAG
	Rv	TCTTGATATCCTCGACGAACACCAATGTTCGGAG
-1525/+132	Fw	GCTCGCTAGCCTCGAATCTCCAGGGTCTCAGTTTTGCA
	Rv	TCTTGATATCCTCGACGAACACCAATGTTCGGAG
-1014/+132	Fw	GCTCGCTAGCCTCGAAGTGCCTGAGCTGGACACAGTCA
	Rv	TCTTGATATCCTCGACGAACACCAATGTTCGGAG
-527/+132	Fw	GCTCGCTAGCCTCGAGCCTCAGTTTACCAACGGATGC
	Rv	TCTTGATATCCTCGACGAACACCAATGTTCGGAG
-245/+132	Fw	GCTCGCTAGCCTCGAACGCTACGGTCCCACGACAG
	Rv	TCTTGATATCCTCGACGAACACCAATGTTCGGAG

Table S2-2

List of PCR primers for site-directed mutation of *Ppara* promoter region (-245/+132)

Mutation No.			Primer sequence for site-directed mutation (5′ → 3′)	
Δ1	Fw	-230	- GACAGGGGTGACGGG**AAA**GGAGGCAGCCGCTTA -	-198
	Rv	-198	- TAAGCGGCTGCCTCC**TTT**CCCGTCACCCCTGTC -	-230
Δ2	Fw	-198	- ACGCCCCTCCTGGC**AAA**TCCTCCTGGGCGCG -	-168
	Rv	-168	- CGCGCCCAGGAGGA**TTT**GCCAGGAGGGGCGT -	-198
Δ3	Fw	-113	- GGGCACGCGCGAGG**AAA**GGGAGCCAGGCGTC -	-83
	Rv	-83	- GACGCCTGGCTCCC**TTT**CCTCGCGCGTGCCC -	-113
Δ4	Fw	-97	- GGGGAGCCAGGCGTC**AAA**TGTCCCGGGACAGTG -	-65
	Rv	-65	- CACTGTCCCGGGACA**TTT**GACGCCTGGCTCCCC -	-97
Δ5	Fw	-72	- GGACAGTGAGGTGGGTGGACA**AAA**AGGGGAGGGGC -	-38
	Rv	-38	- GCCCCTCCCCT**TTT**TGTCCACCCACCTCACTGTCC -	-72
Δ6	Fw	-58	- GTGGACAGGGAGGGGA**AAA**GCTCGGTGGCGCAT -	-26
	Rv	-26	- ATGCGCCACCGAGC**TTT**TCCCCTCCCTGTCCAC -	-58
Δ7	Fw	-26	- TGCGCGCGGACTAGG**AAA**GCGGGTCTGGAGACC -	+7
	Rv	+7	- GGTCTCCAGACCCGC**TTT**CCTAGTCCGCGCGCA -	-26

Table S2-3

List of PCR primers used in Chapter 2

Oligonucleotides (5′ → 3′)			
mRNA	*Acox1*	Fw	ACCTTCACTTGGGCATGTTC
		Rv	TTCCAAGCCTCGAAGATGAG
	Bip	Fw	GTTTGCTGAGGAAGACAAAAAGCTC
		Rv	CACTTCCATAGAGTTTGCTGAT
	Chop	Fw	GTCCAGCTGGGAGCTGGAAG
		Rv	CTGACTGGAATCTGGAGAG
	Cidea	Fw	ATCACAACTGGCCTGGTTACG
		Rv	TACTACCCGGTGTCCATTTCT
	Cpt1b	Fw	CTGTTAGGCCTCAACACCGAAC
		Rv	CTGTCATGGCTAGGCGGTACAT
	Fgf21	Fw	CACCGCAGTCCAGAAAGTCT
		Rv	ATCCTGGTTTGGGGAGTCCT
	Nos2	Fw	CCAAGCCCTCACCTACTTCC
		Rv	CTCTGAGGGCTGACACAAGG
	Ppara	Fw	TCAGGGTACCACTACGGAGT
		Rv	CTTGGCATTCTTCCAAAGCG
	Ppargc1a	Fw	CCCTGCCATTGTTAAGACC
		Rv	TGCTGCTGTTCCTGTTTTC
	Rplp0	Fw	TCCTTCTTCCAGGCTTTGGG
		Rv	GACACCCTCCAGAAAGCGAG
	Sp1	Fw	GGCTGCCCATTTGTACTCATTTAC
		Rv	CCGAAGGGTGCCTGTTAGG
	Ucp1	Fw	CAAAGTCCGCCTTCAGATCC
		Rv	AGCCGGCTGAGATCTTCTTT

Summary

Chapter 1

In Chapter 1, the role of the cholesterol biosynthesis pathway in the regulation of brown adipocyte function was investigated. The inhibition of HMGCR, the rate-limiting enzyme in the cholesterol biosynthesis pathway, suppressed mitotic clonal expansion of brown preadipocytes and brown adipogenesis via the inhibition of protein geranylgeranylation, at least partially. The development of BAT in neonatal mice exposed to an HMGCR inhibitor during the fetal period was severely impaired. Moreover, it was also demonstrated that GGPP deficiency caused by HMGCR inhibition led to the apoptosis of mature brown adipocytes. Brown adipocyte-specific *Hmgcr* knockout mice showed BAT atrophy and hypothermia during cold exposure. Together, the findings in Chapter 1 indicated that the cholesterol biosynthesis pathway-generated GGPP plays an indispensable role in maintaining BAT mass, which subsequently impacts BAT function.

Chapter 2

In Chapter 2, it was found that *Ppara* gene expression levels were downregulated in obese WAT as well as in adipocytes cultured in conditioned medium from LPS-activated macrophages. The loss of *Ppara* gene expression suppressed β-adrenergic stimulation-induced thermogenic gene expression in adipocytes, suggesting that downregulated *Ppara* gene expression may be responsible for reduced thermogenesis in adipocytes upon catecholamine stimulation under inflammation. It was elucidated that NO downregulated *Ppara* expression and its function, fatty acid oxidation, in adipocytes; however, it was partially recovered in the presence of a NOS2 inhibitor, indicating that NOS2-deriven NO is attributed to the downregulation of *Ppara* expression. Sp1 was identified as a key transcriptional

factor in the NO-mediated downregulation of *Ppara*. It was identified that NO downregulated *Ppara* gene expression by suppressing transcription factor Sp1 occupancy in the proximal promoter regions of *Ppara*. Additionally, treatment of obese mice with a NOS2 inhibitor partially but significantly recovered downregulated *Ppara* expression in their WAT. The findings in Chapter 2 provide a possible mechanism underlying the downregulation of the *Ppara* gene expression in adipocytes of obese WAT, which can affect their thermogenic function. The schematic summary of this study is shown in **Figure 3**.

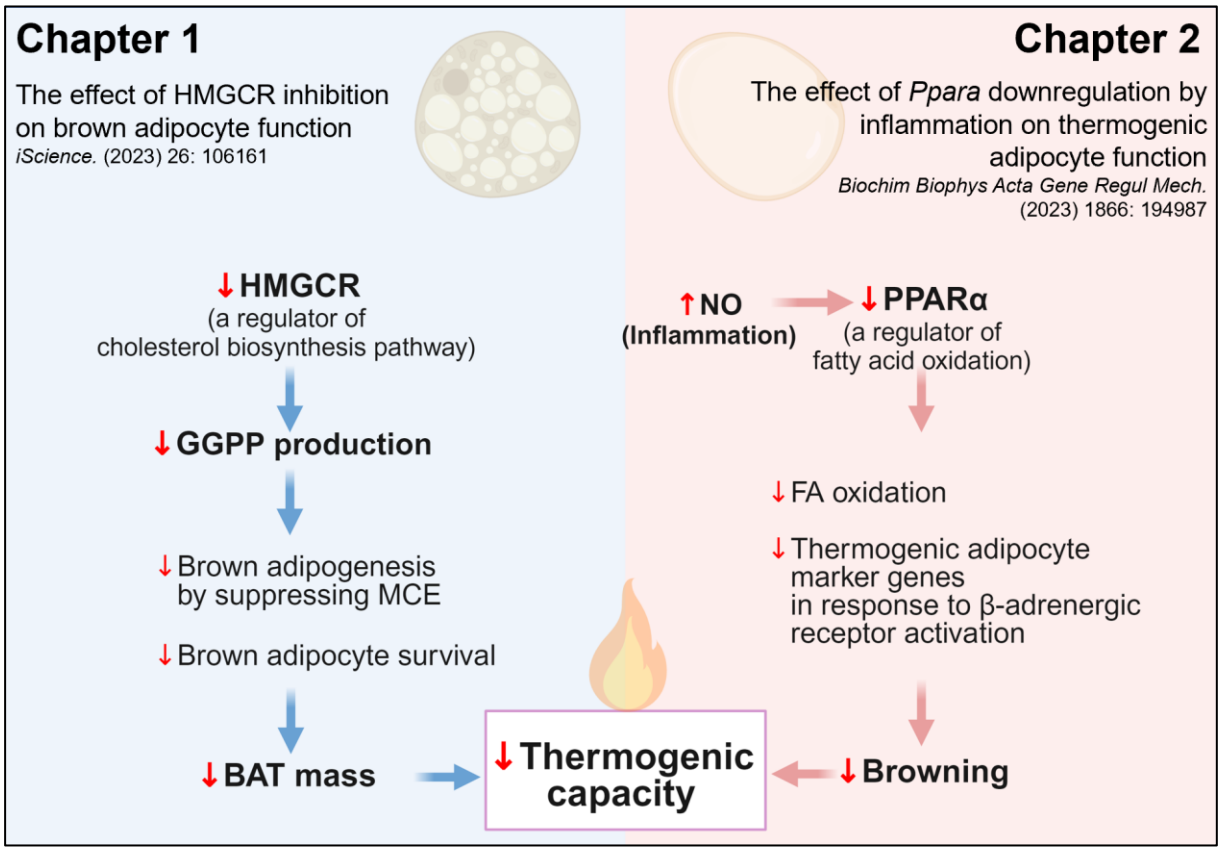

Figure 3. Summary of the findings of the study

References

1. World Obesity Federation, World Obesity Atlas 2023. (2023) p11. Available at: https://data.worldobesity.org/publications/?cat=19. Accessed November 1, 2023.
2. Jung UJ and Choi MS. Obesity and its metabolic complications: the role of adipokines and the relationship between obesity, inflammation, insulin resistance, dyslipidemia and nonalcoholic fatty liver disease. *Int. J. Mol. Sci.* (2014) 15, 6184–6223. doi: 10.3390/ijms15046184.
3. Pi-Sunyer X. The medical risks of obesity. *Postgrad. Med.* (2009) 121, 21–33. doi: 10.3810/pgm.2009.11.2074.
4. Abdelaal M, le Roux CW, and Docherty NG. Morbidity and mortality associated with obesity. *Ann. Transl. Med.* (2017) 5, 161. doi: 10.21037/atm.2017.03.107.
5. World Health Organization (WHO) Physical status: the use and interpretation of anthropometry: report of a WHO Expert Committee. (1995) WHO Technical Report Series 854, p378. Available at https://www.who.int/publications/i/item/9241208546. Accessed November 1, 2023.
6. Schwartz MW, Seeley RJ, Zeltser LM, Drewnowski A, Ravussin E, Redman LM, and Leibel RL. Obesity pathogenesis: an endocrine society scientific statement. *Endocr. Rev.* (2017) 38, 267–296. doi: 10.1210/er.2017-00111.
7. Bays HE, Toth PP, Kris-Etherton PM, Abate N, Aronne LJ, Brown WV, Gonzalez-Campoy JM, Jones SR, Kumar R, La Forge R, et al. Obesity, adiposity, and dyslipidemia: a consensus statement from the National Lipid Association. *J. Clin. Lipidol.* (2013) 7, 304–383. doi: 10.1016/j.jacl.2013.04.001.
8. van Vliet S, Koh HE, Patterson BW, Yoshino M, LaForest R, Gropler RJ, Klein S, and Mittendorfer B. Obesity is associated with increased basal and postprandial β-cell insulin secretion even in the absence of insulin resistance. *Diabetes* (2020) 69, 2112–2119. doi: 10.2337/db20-0377.
9. Arner P and Rydén M. Fatty acids, obesity and insulin resistance. *Obes. Facts.* (2015) 8, 147–155. doi: 10.1159/000381224.
10. Zomer E, Gurusamy K, Leach R, Trimmer C, Lobstein T, Morris S, James WP, and Finer N. Interventions that cause weight loss and the impact on cardiovascular risk factors: a systematic review and meta-analysis. *Obes. Rev.* (2016) 17, 1001–1011. doi: 10.1111/obr.12433.
11. Gesta S, Tseng YH, and Kahn CR. Developmental origin of fat: tracking obesity to its source. *Cell* (2007) 131, 242–256. doi: 10.1016/j.cell.2007.10.004.
12. Cannon B and Nedergaard J. Brown adipose tissue: function and physiological significance. *Physiol. Rev.* (2004) 84, 277–359. doi: 10.1152/physrev.00015.2003.
13. Chen KY, Brychta RJ, Abdul Sater Z, Cassimatis TM, Cero C, Fletcher LA, Israni NS, Johnson JW, Lea HJ, Linderman JD, et al. Opportunities and challenges in the therapeutic activation of human energy expenditure and thermogenesis to manage obesity. *J. Biol. Chem.* (2020) 295, 1926–1942. doi: 10.1074/jbc.REV119.007363.
14. Inokuma K, Okamatsu-Ogura Y, Omachi A, Matsushita Y, Kimura K, Yamashita H, and Saito M. Indispensable role of mitochondrial UCP1 for antiobesity effect of beta3-adrenergic stimulation. *Am. J. Physiol. Endocrinol. Metab.* (2006) 290, E1014–E1021. doi: 10.1152/ajpendo.00105.2005.
15. Barbatelli G, Murano I, Madsen L, Hao Q, Jimenez M, Kristiansen K, Giacobino JP, De Matteis R, and Cinti S. The emergence of cold-induced brown adipocytes in mouse white fat depots is determined predominantly by white to brown adipocyte transdifferentiation. *Am. J. Physiol. Endocrinol. Metab.* (2010) 298, E1244–E1253. doi: 10.1152/ajpendo.00600.2009.
16. Carpentier AC, Blondin DP, Virtanen KA, Richard D, Haman F, and Turcotte ÉE. Brown adipose tissue energy metabolism in humans. *Front. Endocrinol. (Lausanne)* (2018) 9, 447. doi: 10.3389/fendo.2018.00447.

17. Blondin DP, Labbé SM, Noll C, Kunach M, Phoenix S, Guérin B, Turcotte ÉE, Haman F, Richard D, and Carpentier AC. Selective impairment of glucose but not fatty acid or oxidative metabolism in brown adipose tissue of subjects with type 2 diabetes. *Diabetes* (2015) 64, 2388–2397. doi: 10.2337/db14-1651.
18. Koskensalo K, Raiko J, Saari T, Saunavaara V, Eskola O, Nuutila P, Saunavaara J, Parkkola R, and Virtanen KA. Human brown adipose tissue temperature and fat fraction are related to its metabolic activity. *J. Clin. Endocrinol. Metab.* (2017) 102, 1200–1207. doi: 10.1210/jc.2016-3086.
19. Leitner BP, Huang S, Brychta RJ, Duckworth CJ, Baskin AS, McGehee S, Tal I, Dieckmann W, Gupta G, Kolodny GM, et al. Mapping of human brown adipose tissue in lean and obese young men. *Proc. Natl. Acad. Sci. U. S. A.* (2017) 114, 8649–8654. doi: 10.1073/pnas.1705287114.
20. Saito M, Okamatsu-Ogura Y, Matsushita M, Watanabe K, Yoneshiro T, Nio-Kobayashi J, Iwanaga T, Miyagawa M, Kameya T, Nakada K, et al. High incidence of metabolically active brown adipose tissue in healthy adult humans: effects of cold exposure and adiposity. *Diabetes* (2009) 58, 1526–1531. doi: 10.2337/db09-0530.
21. Cypess AM, Lehman S, Williams G, Tal I, Rodman D, Goldfine AB, Kuo FC, Palmer EL, Tseng YH, Doria A, et al. Identification and importance of brown adipose tissue in adult humans. *N. Engl. J. Med.* (2009) 360, 1509–1517. doi: 10.1056/NEJMoa0810780.
22. Raiko J, Holstila M, Virtanen KA, Orava J, Saunavaara V, Niemi T, Laine J, Taittonen M, Borra RJ, Nuutila P, et al. Brown adipose tissue triglyceride content is associated with decreased insulin sensitivity, independently of age and obesity. *Diabetes Obes. Metab.* (2015) 17, 516–519. doi: 10.1111/dom.12433.
23. Hanssen MJ, Hoeks J, Brans B, van der Lans AA, Schaart G, van den Driessche JJ, Jörgensen JA, Boekschoten MV, Hesselink MK, Havekes B, et al. Short-term cold acclimation improves insulin sensitivity in patients with type 2 diabetes mellitus. *Nat. Med.* (2015) 21, 863–865. doi: 10.1038/nm.3891.
24. Chondronikola M, Volpi E, Børsheim E, Porter C, Annamalai P, Enerbäck S, Lidell ME, Saraf MK, Labbe SM, Hurren NM, et al. Brown adipose tissue improves whole-body glucose homeostasis and insulin sensitivity in humans. *Diabetes* (2014) 63, 4089–4099. doi: 10.2337/db14-0746.
25. Lee YH, Petkova AP, Konkar AA, and Granneman JG. Cellular origins of cold-induced brown adipocytes in adult mice. *FASEB J.* (2015) 29, 286–299. doi: 10.1096/fj.14-263038.
26. Wang W and Seale P. Control of brown and beige fat development. *Nat. Rev. Mol. Cell Biol.* (2016) 17, 691–702. doi: 10.1038/nrm.2016.96.
27. Tang, Q-Q, Otto, TC, and Lane, MD. Mitotic clonal expansion: a synchronous process required for adipogenesis. *Proc. Natl. Acad. Sci. U. S. A.* (2003) 100, 44–49. 10.1073/pnas.0137044100.
28. Harms M and Seale P. Brown and beige fat: development, function and therapeutic potential. *Nat. Med.* (2013) 19, 1252–1263. doi: 10.1038/nm.3361.
29. Wu J, Boström P, Sparks LM, Ye L, Choi JH, Giang AH, Khandekar M, Virtanen KA, Nuutila P, Schaart G, et al. Beige adipocytes are a distinct type of thermogenic fat cell in mouse and human. *Cell* (2012) 150, 366–376. doi: 10.1016/j.cell.2012.05.016.
30. Clarke, SL, Robinson, CE, and Gimble, JM. CAAT/enhancer binding proteins directly modulate transcription from the peroxisome proliferator-activated receptor γ2 promoter. *Biochem. Biophys. Res. Commun.* (1997) 240, 99–103. 10.1006/bbrc.1997.7627.
31. Tang, Q-Q, Jiang, M-S, and Lane, MD. Repressive effect of Sp1 on the C/EBPα gene promoter: role in adipocyte differentiation. *Mol. Cell. Biol.* (1999) 19, 4855–4865. 10.1128/MCB.19.7.4855.
32. Mota de Sá P, Richard AJ, Hang H, and Stephens JM. Transcriptional regulation of adipogenesis. *Compr. Physiol.* (2017) 7, 635–674. doi: 10.1002/cphy.c160022.
33. Cao W, Daniel KW, Robidoux J, Puigserver P, Medvedev AV, Bai X, Floering LM, Spiegelman BM, and Collins S. p38 mitogen-activated protein kinase is the central regulator of cyclic AMP-dependent transcription of the brown fat uncoupling protein 1 gene. *Mol. Cell. Biol.* (2004) 24,

3057–3067. doi: 10.1128/MCB.24.7.3057-3067.2004.
34. Wu Z, Rosen ED, Brun R, Hauser S, Adelmant G, Troy AE, McKeon C, Darlington GJ, and Spiegelman BM. Cross-regulation of C/EBP alpha and PPAR gamma controls the transcriptional pathway of adipogenesis and insulin sensitivity. *Mol. Cell* (1999) 3, 151–158. doi: 10.1016/s1097-2765(00)80306-8.
35. Tontonoz P and Spiegelman BM. Fat and beyond: the diverse biology of PPARgamma. *Annu. Rev. Biochem.* (2008) 77, 289–312. doi: 10.1146/annurev.biochem.77.061307.091829.
36. Seale P, Kajimura S, Yang W, Chin S, Rohas LM, Uldry M, Tavernier G, Langin D, and Spiegelman BM. Transcriptional control of brown fat determination by PRDM16. *Cell Metab.* (2007) 6, 38–54. doi: 10.1016/j.cmet.2007.06.001.
37. Sakers A, De Siqueira MK, Seale P, and Villanueva CJ. Adipose-tissue plasticity in health and disease. *Cell* (2022) 185, 419–446. doi: 10.1016/j.cell.2021.12.016.
38. Henninger AM, Eliasson B, Jenndahl LE, and Hammarstedt A. Adipocyte hypertrophy, inflammation and fibrosis characterize subcutaneous adipose tissue of healthy, non-obese subjects predisposed to type 2 diabetes. *PLoS One* (2014) 9, e105262. doi: 10.1371/journal.pone.0105262.
39. Castoldi A, Naffah de Souza C, Câmara NO, and Moraes-Vieira PM. The macrophage switch in obesity development. *Front. Immunol.* (2016) 6, 637. doi: 10.3389/fimmu.2015.00637.
40. Nguyen MT, Favelyukis S, Nguyen AK, Reichart D, Scott PA, Jenn A, Liu-Bryan R, Glass CK, Neels JG, and Olefsky JM. A subpopulation of macrophages infiltrates hypertrophic adipose tissue and is activated by free fatty acids via Toll-like receptors 2 and 4 and JNK-dependent pathways. *J. Biol. Chem.* (2007) 282, 35279–35292. doi: 10.1074/jbc.M706762200.
41. Aguirre V, Werner ED, Giraud J, Lee YH, Shoelson SE, and White MF. Phosphorylation of Ser307 in insulin receptor substrate-1 blocks interactions with the insulin receptor and inhibits insulin action. *J. Biol. Chem.* (2002) 277, 1531–1537. doi: 10.1074/jbc.M101521200.
42. Shoelson SE, Lee J, and Goldfine AB. Inflammation and insulin resistance. *J. Clin. Invest.* (2006) 116, 1793–1801. doi: 10.1172/JCI29069.
43. Cusi K. Role of obesity and lipotoxicity in the development of nonalcoholic steatohepatitis: pathophysiology and clinical implications. *Gastroenterology* (2012) 142, 711–725.e6. doi: 10.1053/j.gastro.2012.02.003.
44. Reilly SM and Saltiel AR. Adapting to obesity with adipose tissue inflammation. *Nat. Rev. Endocrinol.* (2017) 13, 633–643. doi: 10.1038/nrendo.2017.90.
45. Mowers J, Uhm M, Reilly SM, Simon J, Leto D, Chiang SH, Chang L, and Saltiel AR. Inflammation produces catecholamine resistance in obesity via activation of PDE3B by the protein kinases IKKε and TBK1. *Elife* (2013)2, e01119. doi: 10.7554/eLife.01119. PMID: 24368730.
46. Valentine JM, Ahmadian M, Keinan O, Abu-Odeh M, Zhao P, Zhou X, Keller MP, Gao H, Yu RT, Liddle C, et al. β3-Adrenergic receptor downregulation leads to adipocyte catecholamine resistance in obesity. *J. Clin. Invest.* (2022) 132, e153357. doi: 10.1172/JCI153357.
47. Guilherme A, Rowland LA, Wetoska N, Tsagkaraki E, Santos KB, Bedard AH, Henriques F, Kelly M, Munroe S, Pedersen DJ, et al. Acetyl-CoA carboxylase 1 is a suppressor of the adipocyte thermogenic program. *Cell Rep.* (2023) 42, 112488. doi: 10.1016/j.celrep.2023.112488.
48. Schreiber R, Diwoky C, Schoiswohl G, Feiler U, Wongsiriroj N, Abdellatif M, Kolb D, Hoeks J, Kershaw EE, Sedej S, et al. Cold-induced thermogenesis depends on atgl-mediated lipolysis in cardiac muscle, but not brown adipose tissue. *Cell Metab.* (2017) 26, 753–763.e7. doi: 10.1016/j.cmet.2017.09.004.
49. Lee J, Ellis JM, and Wolfgang MJ. Adipose fatty acid oxidation is required for thermogenesis and potentiates oxidative stress-induced inflammation. *Cell Rep.* (2015) 10, 266–279. doi: 10.1016/j.celrep.2014.12.023.
50. Goldstein JL and Brown MS. Regulation of the mevalonate pathway. *Nature* (1990) 343, 425–430. doi: 10.1038/343425a0.

51. Ohashi K, Osuga J, Tozawa R, Kitamine T, Yagyu H, Sekiya M, Tomita S, Okazaki H, Tamura Y, Yahagi N, et al. Early embryonic lethality caused by targeted disruption of the 3-hydroxy-3-methylglutaryl-CoA reductase gene. *J. Biol. Chem.* (2003) 278, 42936–42941. doi: 10.1074/jbc.M307228200.
52. Horton JD, Goldstein JL, and Brown MS. SREBPs: activators of the complete program of cholesterol and fatty acid synthesis in the liver. *J. Clin. Invest.* (2002) 109, 1125–1131. doi: 10.1172/JCI15593.
53. Guerra B, Recio C, Aranda-Tavío H, Guerra-Rodríguez M, García-Castellano JM, and Fernández-Pérez L. The mevalonate pathway, a metabolic target in cancer therapy. *Front. Oncol.* (2021) 1, 626971. doi: 10.3389/fonc.2021.626971.
54. Cederberg H, Stančáková A, Yaluri N, Modi S, Kuusisto J, and Laakso M. Increased risk of diabetes with statin treatment is associated with impaired insulin sensitivity and insulin secretion: a 6 year follow-up study of the METSIM cohort. *Diabetologia* (2015) 58, 1109–1117. doi: 10.1007/s00125-015-3528-5.
55. Takaguri A, Satoh K, Itagaki M, Tokumitsu Y, and Ichihara K. Effects of atorvastatin and pravastatin on signal transduction related to glucose uptake in 3T3L1 adipocytes. *J. Pharmacol. Sci.* (2008) 107, 80–89. doi: 10.1254/jphs.fp0072403.
56. Brault M, Ray J, Gomez YH, Mantzoros CS, and Daskalopoulou SS. Statin treatment and new-onset diabetes: a review of proposed mechanisms. *Metabolism* (2014) 63, 735–745. doi: 10.1016/j.metabol.2014.02.014.
57. Yeh Y-S, Jheng H-F, Iwase M, Kim M, Mohri S, Kwon J, Kawarasaki S, Li Y, Takahashi H, Ara T, et al. The mevalonate pathway is indispensable for adipocyte survival. *iScience* (2018) 9, 175–191. doi: 10.1016/j.isci.2018.10.019.
58. Chiellini C, Cochet O, Negroni L, Samson M, Poggi M, Ailhaud G, Alessi MC, Dani C, and Amri EZ. Characterization of human mesenchymal stem cell secretome at early steps of adipocyte and osteoblast differentiation. *BMC Mol. Biol.* (2008) 9, 26. doi: 10.1186/1471-2199-9-26.
59. Casey, PJ. Biochemistry of protein prenylation. *J. Lipid Res.* (1992) 33, 1731–1740. doi: 10.1016/S0022-227541331-8.
60. Klemm DJ, Leitner JW, Watson P, Nesterova A, Reusch JE, Goalstone ML, and Draznin B. Insulin-induced adipocyte differentiation. Activation of CREB rescues adipogenesis from the arrest caused by inhibition of prenylation. *J. Biol. Chem.* (2001) 276, 28430–28435. doi: 10.1074/jbc.M103382200.
61. Ghosh S, Park CH, Lee J, Lee N, Zhang R, Huesing C, Reijnders D, Sones J, Münzberg H, Redman L, et al. Maternal cold exposure induces distinct transcriptome changes in the placenta and fetal brown adipose tissue in mice. *BMC Genomics* (2021) 22, 500. doi: 10.1186/s12864-021-07825-6.
62. Adlanmerini M, Carpenter BJ, Remsberg JR, Aubert Y, Peed LC, Richter HJ, and Lazar MA. Circadian lipid synthesis in brown fat maintains murine body temperature during chronic cold. *Proc. Natl. Acad. Sci. U. S. A.* (2019) 116, 18691–18699. doi: 10.1073/pnas.1909883116.
63. Balaz M, Becker AS, Balazova L, Straub L, Müller J, Gashi G, Maushart CI, Sun W, Dong H, Moser C, et al. (2019). Inhibition of mevalonate pathway prevents adipocyte browning in mice and men by affecting protein prenylation. *Cell Metab.* 29, 901–916. 10.1016/j.cmet.2018.11.017.
64. Berger J and Moller DE. The mechanisms of action of PPARs. *Annu. Rev. Med.* (2002) 53, 409–435. doi: 10.1146/annurev.med.53.082901.104018.
65. Kroker AJ and Bruning JB. Review of the structural and dynamic mechanisms of PPARγ partial agonism. *PPAR Res.* (2015) 2015, 816856. doi: 10.1155/2015/816856.
66. Forman BM, Chen J, and Evans RM. Hypolipidemic drugs, polyunsaturated fatty acids, and eicosanoids are ligands for peroxisome proliferator-activated receptors alpha and delta. *Proc. Natl. Acad. Sci. U. S. A.* (1997) 94, 4312–4317. doi: 10.1073/pnas.94.9.4312.
67. Todisco S, Santarsiero A, Convertini P, De Stefano G, Gilio M, Iacobazzi V, and Infantino V. Ppar

alpha as a metabolic modulator of the liver: role in the pathogenesis of nonalcoholic steatohepatitis (NASH). *Biology (Basel)* (2022) 11, 792. doi: 10.3390/biology11050792.
68. Kersten S, Seydoux J, Peters JM, Gonzalez FJ, Desvergne B, and Wahli W. Peroxisome proliferator-activated receptor alpha mediates the adaptive response to fasting. *J. Clin. Invest.* (1999) 103, 1489–1498. doi: 10.1172/JCI6223.
69. Yu K, Bayona W, Kallen CB, Harding HP, Ravera CP, McMahon G, Brown M, and Lazar MA. Differential activation of peroxisome proliferator-activated receptors by eicosanoids. *J. Biol. Chem.* (1995) 270, 23975–23983. doi: 10.1074/jbc.270.41.23975.
70. Fan CY, Pan J, Usuda N, Yeldandi AV, Rao MS, and Reddy JK. Steatohepatitis, spontaneous peroxisome proliferation and liver tumors in mice lacking peroxisomal fatty acyl-CoA oxidase. Implications for peroxisome proliferator-activated receptor alpha natural ligand metabolism. *J. Biol. Chem.* (1998) 273, 15639–15645. doi: 10.1074/jbc.273.25.15639.
71. Chakravarthy MV, Pan Z, Zhu Y, Tordjman K, Schneider JG, Coleman T, Turk J, and Semenkovich CF. "New" hepatic fat activates PPARalpha to maintain glucose, lipid, and cholesterol homeostasis. *Cell Metab.* (2005) 1, 309–322. doi: 10.1016/j.cmet.2005.04.002.
72. Pawlak M, Lefebvre P, and Staels B. Molecular mechanism of PPARα action and its impact on lipid metabolism, inflammation and fibrosis in non-alcoholic fatty liver disease. *J. Hepatol.* (2015) 62, 720–733. doi: 10.1016/j.jhep.2014.10.039.
73. Hondares E, Rosell M, Díaz-Delfín J, Olmos Y, Monsalve M, Iglesias R, Villarroya F, and Giralt M. Peroxisome proliferator-activated receptor α (PPARα) induces PPARγ coactivator 1α (PGC-1α) gene expression and contributes to thermogenic activation of brown fat: involvement of PRDM16. *J. Biol. Chem.* (2011) 286, 43112–43122. doi: 10.1074/jbc.M111.252775.
74. Goto T, Lee JY, Teraminami A, Kim YI, Hirai S, Uemura T, Inoue H, Takahashi N, and Kawada T. Activation of peroxisome proliferator-activated receptor-alpha stimulates both differentiation and fatty acid oxidation in adipocytes. *J. Lipid. Res.* (2011) 52, 873–884. doi: 10.1194/jlr.M011320.
75. Takahashi H, Sanada K, Nagai H, Li Y, Aoki Y, Ara T, Seno S, Matsuda H, Yu R, Kawada T, et al. Over-expression of PPARα in obese mice adipose tissue improves insulin sensitivity. *Biochem. Biophys. Res. Commun.* (2017) 493, 108–114. doi: 10.1016/j.bbrc.2017.09.067.
76. Rachid TL, Penna-de-Carvalho A, Bringhenti I, Aguila MB, Mandarim-de-Lacerda CA, and Souza-Mello V. Fenofibrate (PPARalpha agonist) induces beige cell formation in subcutaneous white adipose tissue from diet-induced male obese mice. *Mol. Cell. Endocrinol.* (2015) 402, 86–94. doi: 10.1016/j.mce.2014.12.027.
77. Jung RT, Shetty PS, James WP, Barrand MA, and Callingham BA. Reduced thermogenesis in obesity. *Nature* (1979) 279, 322–323. doi: 10.1038/279322a0.
78. Steinberger J, and Daniels SR. Obesity, insulin resistance, diabetes, and cardiovascular risk in children: an American Heart Association scientific statement from the Atherosclerosis, Hypertension, and Obesity in the Young Committee (Council on Cardiovascular Disease in the Young) and the Diabetes Committee (Council on Nutrition, Physical Activity, and Metabolism). *Circulation* (2003) 107, 1448–1453. doi: 10.1161/01.CIR.0000060923.07573.F2.
79. Bartelt A, Bruns OT, Reimer R, Hohenberg H, Ittrich H, Peldschus K, Kaul MG, Tromsdorf UI, Weller H, Waurisch C, et al. Brown adipose tissue activity controls triglyceride clearance. *Nat. Med.* (2011) 17, 200–205. doi: 10.1038/nm.2297.
80. Chondronikola M, Volpi E, Børsheim E, Porter C, Saraf MK, Annamalai P, Yfanti C, Chao T, Wong D, Shinoda K, et al. Brown adipose tissue activation is linked to distinct systemic effects on lipid metabolism in humans. *Cell Metab.* (2016) 23, 1200–1206. doi: 10.1016/j.cmet.2016.04.029.
81. Stanford KI, Middelbeek RJW, Townsend KL, An D, Nygaard EB, Hitchcox KM, Markan KR, Nakano K, Hirshman MF, Tseng Y-H, et al. Brown adipose tissue regulates glucose homeostasis and insulin sensitivity. *J. Clin. Invest.* (2013) 123, 215–223. doi: 10.1172/JCI62308.
82. Yoneshiro T, Wang Q, Tajima K, Matsushita M, Maki H, Igarashi K, Dai Z, White PJ, McGarrah

RW, Ilkayeva OR, et al. BCAA catabolism in brown fat controls energy homeostasis through SLC25A44. *Nature* (2019) 572, 614–619. doi: 10.1038/s41586-019-1503-x.
83. Vijgen GHEJ, Bouvy ND, Teule GJJ, Brans B, Schrauwen P, and van Marken Lichtenbelt WD. Brown adipose tissue in morbidly obese subjects. *PLoS One* (2011) 6, e17247. doi: 10.1371/journal.pone.0017247.
84. Oesterle A, Laufs U, and Liao JK. Pleiotropic effects of statins on the cardiovascular system. *Circ. Res.* (2017) 120, 229–243. doi: 10.1161/CIRCRESAHA.116.308537.
85. Newman CB, Preiss D, Tobert JA, Jacobson TA, Page RL, Goldstein LB, Chin C, Tannock LR, Miller M, Raghuveer G, et al. Statin safety and associated adverse events: a scientific statement from the American Heart Association. *Arterioscler. Thromb. Vasc. Biol.* (2019) 39, E38–E81. doi: 10.1161/ATV.0000000000000073.
86. de Giorgi M, Jarrett KE, Burton JC, Doerfler AM, Hurley A, Li A, Hsu RH, Furgurson M, Patel KR, Han J, et al. Depletion of essential isoprenoids and ER stress induction following acute liver-specific deletion of HMG-CoA reductase. *J. Lipid Res.* (2020) 61, 1675–1686. doi: 10.1194/jlr.RA120001006.
87. Nagashima S, Yagyu H, Ohashi K, Tazoe F, Takahashi M, Ohshiro T, Bayasgalan T, Okada K, Sekiya M, Osuga J, et al. Liver-specific deletion of 3-hydroxy-3-methylglutaryl coenzyme A reductase causes hepatic steatosis and death. *Arterioscler. Thromb. Vasc. Biol.* (2012) 32, 1824-1831. doi: 10.1161/ATVBAHA.111.240754.
88. Osaki Y, Nakagawa Y, Miyahara S, Iwasaki H, Ishii A, Matsuzaka T, Kobayashi K, Yatoh S, Takahashi A, Yahagi N, et al. Skeletal muscle-specific HMG-CoA reductase knockout mice exhibit rhabdomyolysis: a model for statin-induced myopathy. *Biochem. Biophys. Res. Commun.* (2015) 466, 536–540. doi: 10.1016/j.bbrc.2015.09.065.
89. Rosen ED, Walkey CJ, Puigserver P, and Spiegelman BM. Transcriptional regulation of adipogenesis. *Genes Dev.* (2000) 14, 1293–1307. doi: 10.1101/gad.14.11.1293.
90. Hishida T, Nishizuka M, Osada S, and Imagawa M. The role of C/EBPδ in the early stages of adipogenesis. *Biochimie* (2009) 91, 654–657. doi: 10.1016/j.biochi.2009.02.002.
91. Tang Q-Q, Otto TC, and Lane MD. CCAAT/enhancer-binding protein β is required for mitotic clonal expansion during adipogenesis. *Proc. Natl. Acad. Sci. U. S. A.* (2003) 100, 850–855. doi: 10.1073/pnas.0337434100.
92. Elmore S. Apoptosis: a review of programmed cell death. *Toxicol. Pathol.* (2007) 35, 495–516. doi: 10.1080/01926230701320337.
93. Spalding KL, Arner E, Westermark PO, Bernard S, Buchholz BA, Bergmann O, Blomqvist L, Hoffstedt J, Näslund E, Britton T, et al. Dynamics of fat cell turnover in humans. *Nature* (2008) 453, 783–787. doi: 10.1038/nature06902.
94. Kim SM, Lun M, Wang M, Senyo SE, Guillermier C, Patwari P, and Steinhauser ML. Loss of white adipose hyperplastic potential is associated with enhanced susceptibility to insulin resistance. *Cell Metab.* (2014) 20, 1049–1058. doi: 10.1016/j.cmet.2014.10.010.
95. Yamauchi T, Kamon J, Waki H, Murakami K, Motojima K, Komeda K, Ide T, Kubota N, Terauchi Y, Tobe K, et al. The mechanisms by which both heterozygous peroxisome proliferator-activated receptor γ (PPARγ) deficiency and PPARγ agonist improve insulin resistance. *J. Biol. Chem.* (2001) 276, 41245–41254. doi: 10.1074/jbc.M103241200.
96. He W, Barak Y, Hevener A, Olson P, Liao D, Le J, Nelson M, Ong E, Olefsky JM, and Evans RM. Adipose-specific peroxisome proliferator-activated receptor γ knockout causes insulin resistance in fat and liver but not in muscle. *Proc. Natl. Acad. Sci. U. S. A.* (2003) 100, 15712–15717. doi: 10.1073/pnas.253682810.
97. Lynes MD, Schulz TJ, Pan AJ, and Tseng YH. Disruption of insulin signaling in Myf5-expressing progenitors leads to marked paucity of brown fat but normal muscle development. *Endocrinology* (2015) 156, 1637–1647. doi: 10.1210/en.2014-1773.

98. Zhao J, Yang Q, Zhang L, Liang X, Sun X, Wang B, Chen Y, Zhu M, and Du M. AMPKα1 deficiency suppresses brown adipogenesis in favor of fibrogenesis during brown adipose tissue development. *Biochem. Biophys. Res. Commun.* (2017) 491, 508–514. doi: 10.1016/j.bbrc.2017.06.149.
99. Guerra C, Navarro P, Valverde AM, Arribas M, Brüning J, Kozak LP, Kahn CR, and Benito M. Brown adipose tissue–specific insulin receptor knockout shows diabetic phenotype without insulin resistance. *J. Clin. Invest.* (2001) 108, 1205–1213. doi: 10.1172/JCI13103.
100. Xiong W, Zhao X, Villacorta L, Rom O, Garcia-Barrio MT, Guo Y, Fan Y, Zhu T, Zhang J, Zeng R, et al. Brown adipocyte-specific PPARγ (peroxisome proliferator-activated receptor γ) deletion impairs perivascular adipose tissue development and enhances atherosclerosis in mice. *Arterioscler. Thromb. Vasc. Biol.* (2018) 38, 1738–1747. doi: 10.1161/ATVBAHA.118.311367.
101. Kawarasaki S, Kuwata H, Sawazaki H, Sakamoto T, Nitta T, Kim CS, Jheng H-F, Takahashi H, Nomura W, Ara T, et al. A new mouse model for noninvasive fluorescence-based monitoring of mitochondrial UCP1 expression. *FEBS Lett.* (2019) 593, 1201–1212. doi: 10.1002/1873-3468.13430.
102. Irie Y, Asano A, Cañ X, Nikami H, Aizawa S-I, and Saito M. Immortal brown adipocytes from p53-knockout mice: differentiation and expression of uncoupling proteins. *Biochem. Biophys. Res. Commun.* (1999) 255, 221–225. doi: 10.1006/bbrc.1998.9999.
103. Kenmochi M, Kawarasaki S, Takizawa S, Okamura K, Goto T, and Uchida K. Involvement of mechano-sensitive Piezo1 channel in the differentiation of brown adipocytes. *J. Physiol. Sci.* (2022) 72, 1-15. doi: 10.1186/s12576-022-00837-1.
104. Kawada T, Sakabe S, Aoki N, Watanabe T, Higeta K, Iwai K, and Sugimoto E. Intake of sweeteners and pungent ingredients increases the thermogenin content in brown adipose tissue of rat. *J. Agric. Food Chem.* (1991) 39, 651–654. doi: 10.1021/jf00004a004.
105. Yue F, Cheng Y, Breschi A, Vierstra J, Wu W, Ryba T, Sandstrom R, Ma Z, Davis C, Pope BD, et al. A comparative encyclopedia of DNA elements in the mouse genome. *Nature* (2014) 515, 355–364. doi: 10.1038/nature13992.
106. Hooff GP, Peters I, Wood WG, Müller WE, and Eckert GP. Modulation of cholesterol, farnesylpyrophosphate, and geranylgeranylpyrophosphate in neuroblastoma SH-SY5Y-APP695 cells: impact on amyloid beta-protein production. *Mol. Neurobiol.* (2010) 41, 341–350. doi: 10.1007/s12035-010-8117-5.
107. Tong H, Holstein SA, and Hohl RJ. Simultaneous determination of farnesyl and geranylgeranyl pyrophosphate levels in cultured cells. *Anal. Biochem.* (2005) 336, 51–59. doi: 10.1016/j.ab.2004.09.024.
108. No JH, de Macedo Dossin F, Zhang Y, Liu Y-L, Zhu W, Feng X, Yoo JA, Lee E, Wang K, Hui R, et al. Lipophilic analogs of zoledronate and risedronate inhibit Plasmodium geranylgeranyl diphosphate synthase (GGPPS) and exhibit potent antimalarial activity. *Proc. Natl. Acad. Sci. U. S. A.* (2012) 109, 4058–4063. doi: 10.1073/pnas.1118215109.
109. Anderson CM, Kazantzis M, Wang J, Venkatraman S, Goncalves RLS, Quinlan CL, Ng R, Jastroch M, Benjamin DI, Nie B, et al. Dependence of brown adipose tissue function on CD36-mediated coenzyme Q uptake. *Cell Rep.* (2015) 10, 505–515. doi: 10.1016/j.celrep.2014.12.048.
110. Zhang FL, and Casey PJ. Influence of metal ions on substrate binding and catalytic activity of mammalian protein geranylgeranyltransferase type-I. *Biochem. J.* (1996) 320, 925–932. doi: 10.1042/bj3200925.
111. Song A, Dai W, Jang MJ, Medrano L, Li Z, Zhao H, Shao M, Tan J, Li A, Ning T, et al. Low-and high-thermogenic brown adipocyte subpopulations coexist in murine adipose tissue. *J. Clin. Invest.* (2020) 130, 247–257. doi: 10.1172/JCI129167.
112. Fukano K, Okamatsu-Ogura Y, Tsubota A, Nio-Kobayashi J, and Kimura K. Cold exposure induces proliferation of mature brown adipocyte in a β3-adrenergic receptor-mediated pathway. *PLoS One*

(2016) 11, e0166579. doi: 10.1371/journal.pone.0166579.
113. Shin S, Pang Y, Park J, Liu L, Lukas BE, Kim SH, Kim K-W, Xu P, Berry DC, and Jiang Y. Dynamic control of adipose tissue development and adult tissue homeostasis by platelet-derived growth factor receptor alpha. *Elife* (2020) 9, e56189. doi: 10.7554/eLife.56189.
114. Mäuser W, Perwitz N, Meier B, Fasshauer M, and Klein J. Direct adipotropic actions of atorvastatin: differentiation state-dependent induction of apoptosis, modulation of endocrine function, and inhibition of glucose uptake. *Eur. J. Pharmacol.* (2007) 564, 37–46. doi: 10.1016/j.ejphar.2007.02.024.
115. Cole KA, Harmon AW, Harp JB, and Patel YM. Rb regulates C/EBPβ-DNA-binding activity during 3T3-L1 adipogenesis. *Am. J. Physiol. Cell Physiol.* (2004) 286, C349–C354. doi: 10.1152/ajpcell.00255.2003.
116. Eberlé D, Hegarty B, Bossard P, Ferré P, and Foufelle F. SREBP transcription factors: master regulators of lipid homeostasis. *Biochimie* (2004) 86, 839–848. doi: 10.1016/j.biochi.2004.09.018.
117. Chong D, Chen Z, Guan S, Zhang T, Xu N, Zhao Y, and Li C. Geranylgeranyl pyrophosphate-mediated protein geranylgeranylation regulates endothelial cell proliferation and apoptosis during vasculogenesis in mouse embryo. *J. Genet. Genom.* (2021) 48, 300–311. doi: 10.1016/j.jgg.2021.03.009.
118. Khwaja A, Sharpe CC, Noor M, and Hendry BM. The role of geranylgeranylated proteins in human mesangial cell proliferation. *Kidney Int.* (2006) 70, 1296–1304. doi: 10.1038/sj.ki.5001713.
119. Philips MR, and Cox AD. Geranylgeranyltransferase I as a target for anti-cancer drugs. *J. Clin. Invest.* (2007) 117, 1223–1225. doi: 10.1172/JCI32108.
120. Cao W, Huang H, Xia T, Liu C, Muhammad S, and Sun C. Homeobox a5 promotes white adipose tissue browning through inhibition of the tenascin C/toll-like receptor 4/nuclear factor kappa B inflammatory signaling in mice. *Front. Immunol.* (2018) 9, 647. doi: 10.3389/fimmu.2018.006.
121. Holzman MA, Ryckman A, Finkelstein TM, Landry-Truchon K, Schindler KA, Bergmann JM, Jeannotte L, and Mansfield JH. HOXA5 participates in brown adipose tissue and epaxial skeletal muscle patterning and in brown adipocyte differentiation. *Front. Cell Dev. Biol.* (2021) 311. doi: 10.3389/fcell.2021.632303.
122. Park JH, Kang HJ, Kang SI, Lee JE, Hur J, Ge K, Mueller E, Li H, Lee B-C, and Lee SB. A multifunctional protein, EWS, is essential for early brown fat lineage determination. *Dev. Cell* (2013) 26, 393–404. doi: 10.1016/j.devcel.2013.07.002.
123. Tseng Y-H, Kokkotou E, Schulz TJ, Huang TL, Winnay JN, Taniguchi CM, Tran TT, Suzuki R, Espinoza DO, Yamamoto Y, et al. New role of bone morphogenetic protein 7 in brown adipogenesis and energy expenditure. *Nature* (2008) 454, 1000–1004. doi: 10.1038/nature07221.
124. Li X, Cui Q, Kao C, Wang GJ, and Balian G. Lovastatin inhibits adipogenic and stimulates osteogenic differentiation by suppressing PPARγ2 and increasing Cbfa1/Runx2 expression in bone marrow mesenchymal cell cultures. *Bone* (2003) 33, 652–659. doi: 10.1016/S8756-3282(03)00239-4.
125. Nakata M, Nagasaka S, Kusaka I, Matsuoka H, Ishibashi S, and Yada T. Effects of statins on the adipocyte maturation and expression of glucose transporter 4 (SLC2A4): implications in glycaemic control. *Diabetologia* (2006) 49, 1881–1892. doi: 10.1007/s00125-006-0269-5.
126. Guo L, Li X, and Tang QQ. Transcriptional regulation of adipocyte differentiation: a central role for CCAAT/enhancer-binding protein (C/EBP) β. *J. Biol. Chem.* (2015) 290, 755–761. doi: 10.1074/jbc.R114.619957.
127. Fukunaka A, Fukada T, Bhin J, Suzuki L, Tsuzuki T, Takamine Y, Bin B-H, Yoshihara T, Ichinoseki-Sekine N, Naito H, et al. Zinc transporter ZIP13 suppresses beige adipocyte biogenesis and energy expenditure by regulating C/EBP-β expression. *PLoS Genet.* (2017) 13, e1006950. doi: 10.1371/journal.pgen.1006950.
128. Kajimura S, Seale P, Kubota K, Lunsford E, Frangioni JV, Gygi SP, and Spiegelman BM. Initiation

of myoblast to brown fat switch by a PRDM16–C/EBP-β transcriptional complex. *Nature* (2009) 460, 1154–1158. doi: 10.1038/nature08262.
129. Charles A, Tang X, Crouch E, Brody JS, and Xiao ZXJ. Retinoblastoma protein complexes with C/EBP proteins and activates C/EBP-mediated transcription. *J. Cell. Biochem.* (2001) 83, 414–425. doi: 10.1002/jcb.1239.
130. Chen PL, Riley DJ, Chen Y, and Lee WH. Retinoblastoma protein positively regulates terminal adipocyte differentiation through direct interaction with C/EBPs. *Genes Dev.* (1996) 10, 2794–2804. doi: 10.1101/gad.10.21.2794.
131. Khidr L, and Chen PL. RB, the conductor that orchestrates life, death and differentiation. *Oncogene* (2006) 25, 5210–5219. doi: 10.1038/sj.onc.1209612.
132. Hansen JB, Jørgensen C, Petersen RK, Hallenborg P, de Matteis R, Bøye HA, Petrovic N, Enerbäck S, Nedergaard J, Cinti S, et al. Retinoblastoma protein functions as a molecular switch determining white versus brown adipocyte differentiation. *Proc. Natl. Acad. Sci. U. S. A.* (2004) 101, 4112–4117. doi: 10.1073/pnas.0301964101.
133. Lacher SM, Bruttger J, Kalt B, Berthelet J, Rajalingam K, Wörtge S, and Waisman A. HMG-CoA reductase promotes protein prenylation and therefore is indispensible for T-cell survival. *Cell Death Dis.* (2017) 8, e2824. doi: 10.1038/cddis.2017.221.
134. Moschetti A, Dagda RK, and Ryan RO. Coenzyme Q nanodisks counteract the effect of statins on C2C12 myotubes. *Nanomed.: Nanotechnol. Biol. Med.* (2021) 37, 102439. doi: 10.1016/j.nano.2021.102439.
135. Tavintharan S, Ong CN, Jeyaseelan K, Sivakumar M, Lim SC, and Sum CF. Reduced mitochondrial coenzyme Q10 levels in HepG2 cells treated with high-dose simvastatin: A possible role in statin-induced hepatotoxicity? *Toxicol. Appl. Pharmacol.* (2007) 223, 173–179. doi: 10.1016/j.taap.2007.05.013.
136. Madsen L, Petersen RK, Steffensen KR, Pedersen LM, Hallenborg P, Ma T, Frøyland L, Døskeland SO, Gustafsson JÅ, and Kristiansen K. Activation of liver X receptors prevents statin-induced death of 3T3-L1 preadipocytes. *J. Biol. Chem.* (2008) 283, 22723–22736. doi: 10.1074/jbc.M800720200.
137. Zhang W, Jiang H, Zhang J, Zhang Y, Liu A, Zhao Y, Zhu X, Lin Z, and Yuan X. Liver X receptor activation induces apoptosis of melanoma cell through caspase pathway. *Cancer Cell Int.* (2014) 14, 1–6. doi: 10.1186/1475-2867-14-16.
138. Gan X, Kaplan R, Menke JG, MacNaul K, Chen Y, Sparrow CP, Zhou G, Wright SD, and Cai TQ. Dual mechanisms of ABCA1 regulation by geranylgeranyl pyrophosphate. *J. Biol. Chem.* (2001) 276, 48702–48708. doi: 10.1074/jbc.M109402200.
139. Yeh Y-S, Goto T, Takahashi N, Egawa K, Takahashi H, Jheng H-F, Kim Y-I, and Kawada T. Geranylgeranyl pyrophosphate performs as an endogenous regulator of adipocyte function via suppressing the LXR pathway. *Biochem. Biophys. Res. Commun.* (2016) 478, 1317–1322. doi: 10.1016/j.bbrc.2016.08.119.
140. Niemann B, Haufs-Brusberg S, Puetz L, Feickert M, Jaeckstein MY, Hoffmann A, Zurkovic J, Heine M, Trautmann E-M, Müller CE, et al. Apoptotic brown adipocytes enhance energy expenditure via extracellular inosine. *Nature* (2022) 609, 361–368. doi: 10.1038/s41586-022-05041-0.
141. Vila-Bedmar R, Lorenzo M, and Fernandez-Veledo S. Adenosine 5′-monophosphate-activated protein kinase-mammalian target of rapamycin cross talk regulates brown adipocyte differentiation. *Endocrinology* (2010) 151, 980–992. doi: 10.1210/en.2009-0810.
142. Labbé SM, Mouchiroud M, Caron A, Secco B, Freinkman E, Lamoureux G, Gélinas Y, Lecomte R, Bossé Y, Chimin P, et al. mTORC1 is required for brown adipose tissue recruitment and metabolic adaptation to cold. *Sci. Rep.* (2016) 6, 1–17. doi: 10.1038/srep37223.
143. Gong L, Xiao Y, Xia F, Wu P, Zhao T, Xie S, Wang R, Wen Q, Zhou W, Xu H, et al. The mevalonate coordinates energy input and cell proliferation. *Cell Death Dis.* (2019) 10, 327. doi:

10.1038/s41419-019-1544-y.
144. Saci A, Cantley LC, and Carpenter CL. Rac1 regulates the activity of mTORC1 and mTORC2 and controls cellular size. *Mol. Cell* (2011) 42, 50–61. doi: 10.1016/j.molcel.2011.03.017.
145. Vogt A, Qian Y, Blaskovich MA, Fossum RD, Hamilton AD, and Sebti SM. A non-peptide mimetic of Ras-CAAX: selective inhibition of farnesyltransferase and Ras processing. J. Biol. Chem. (1995) 270, 660–664. doi: 10.1074/jbc.270.2.660.
146. Stokoe D, Macdonald, SG, Cadwallader K, Symons, M, and Hancock JF. Activation of Raf as a result of recuitment to the plasma membrane. *Science* (1994) 264, 1463–1467. doi: 10.1126/science.7811320.
147. Watanabe M, Fiji HDG, Guo L, Chan L, Kinderman SS, Salmon DJ, Kwon O, and Tamanoi F. Inhibitors of protein geranylgeranyltransferase I and Rab geranylgeranyltransferase identified from a library of allenoate-derived compounds. J. Biol. Chem. (2008) 283, 9571–9579. doi: S0021-9258(20)57027-0/fulltext.
148. Nishiya N, Oku Y, Kumagai Y, Sato Y, Yamaguchi E, Sasaki A, Shoji M, Ohnishi Y, Okamoto H, and Uehara Y. A zebrafish chemical suppressor screening identifies small molecule inhibitors of the Wnt/β-catenin pathway. *Chem. Biol.* (2014) 21, 530–540. doi: 10.1016/j.chembiol.2014.02.015.
149. Kawai T, Autieri MV, and Scalia R. Adipose tissue inflammation and metabolic dysfunction in obesity. *Am. J. Physiol. Cell. Physiol.* (2021) 320, C375−C391. doi: 10.1152/ajpcell.00379.2020.
150. Choe SS, Huh JY, Hwang IJ, Kim JI, and Kim JB. Adipose tissue remodeling: Its role in energy metabolism and metabolic disorders. *Front. Endocrinol. (Lausanne)* (2016) 7, 30. doi: 10.3389/fendo.2016.00030.
151. Yamauchi T, Kamon J, Minokoshi Y, Ito Y, Waki H, Uchida S, Yamashita S, Noda M, Kita S, Ueki K, et al. Adiponectin stimulates glucose utilization and fatty-acid oxidation by activating AMP-activated protein kinase. *Nat. Med.* (2002) 8, 1288−1295. doi: 10.1038/nm788.
152. Reneau J, Goldblatt M, Gould J, Kindel T, Kastenmeier A, Higgins R, Rengel LR, Schoyer K, James R, et al. Effect of adiposity on tissue-specific adiponectin secretion. *PLoS One* (2018) 13, e0198889. doi: 10.1371/journal.pone.0198889.
153. Bai Y and Sun Q. Macrophage recruitment in obese adipose tissue. *Obes. Rev.* (2015) 16, 127−136. doi: 10.1111/obr.12242.
154. Suganami T, Nishida J, and Ogawa Y. A paracrine loop between adipocytes and macrophages aggravates inflammatory changes. Role of free fatty acids and tumor necrosis factor α *Arterioscler. Thromb. Vasc. Biol.* (2005) 25, 2062−2068. doi: 10.1161/01.ATV.0000183883.72263.13.
155. Oguntibeju OO. Type 2 diabetes mellitus, oxidative stress and inflammation: examining the links. *Int. J. Physiol. Pathophysiol. Pharmacol.* (2019) 11, 45−63. eCollection 2019.
156. Hardy OT, Perugini RA, Nicoloro SM, Gallagher-Dorval K, Puri V, Straubhaar J, and Czech MP. Body mass index-independent inflammation in omental adipose tissue associated with insulin resistance in morbid obesity. *Surg. Obes. Relat. Dis.* (2011) 7, 60−67. doi: 10.1016/j.soard.2010.05.013.
157. Klöting N, Fasshauer M, Dietrich A, Kovacs P, Schön MR, Kern M, Stumvoll M, and Blüher M. Insulin-sensitive obesity. *Am. J. Physiol. Endocrinol. Metab.* (2010) 299, E506−E515. doi: 10.1152/ajpendo.00586.2009.
158. Wentworth JM, Naselli G, Brown WA, Doyle L, Phipson B, Smyth GK, Wabitsch M, O'Brien PE, and Harrison LC. Pro-inflammatory CD11c+CD206+ adipose tissue macrophages are associated with insulin resistance in human obesity. *Diabetes* (2010) 59, 1648−1656. doi: 10.2337/db09-0287.
159. Michalik L and Wahli W. Involvement of PPAR nuclear receptors in tissue injury and wound repair. *J. Clin. Invest.* (2006) 116, 598−606. doi: 10.1172/JCI27958.
160. Kersten S, Desvergne B, and Wahli W. Roles of PPARs in health and disease. *Nature* (2000) 405, 421−424. doi: 10.1038/35013000.
161. Staels B, Dallongeville J, Auwerx J, Schoonjans K, Leitersdorf E, and Fruchart JC. Mechanism of

action of fibrates on lipid and lipoprotein metabolism. *Circulation* (1998) 98, 2088−2093. doi: 10.1161/01.cir.98.19.2088.
162. Derosa G, Sahebkar A, and Maffioli P. The role of various peroxisome proliferator-activated receptors and their ligands in clinical practice. *J. Cell. Physiol.* (2018) 233, 153−161. doi: 10.1002/jcp.25804.
163. Tsuchida A, Yamauchi T, Takekawa S, Hada Y, Ito Y, Maki T, and Kadowaki T. Peroxisome proliferator-activated receptor (PPAR) alpha activation increases adiponectin receptors and reduces obesity-related inflammation in adipose tissue: comparison of activation of PPARalpha, PPARgamma, and their combination. *Diabetes* (2005) 4, 3358−3370. doi: 10.2337/diabetes.54.12.3358.
164. Loviscach M, Rehman N, Carter L, Mudaliar S, Mohadeen P, Ciaraldi TP, Veerkamp JH, and Henry RR. Distribution of peroxisome proliferator-activated receptors (PPARs) in human skeletal muscle and adipose tissue: relation to insulin action. *Diabetologia* (2000) 43, 304−311. doi: 10.1007/s001250050048.
165. Hinds TD Jr, Kipp ZA, Xu M, Yiannikouris FB, Morris AJ, Stec DF, Wahli W, and Stec DE. Adipose-specific PPARα knockout mice have increased lipogenesis by PASK-SREBP1 signaling and a polarity shift to inflammatory macrophages in white adipose tissue. *Cells* (2021) 11, 4. doi: 10.3390/cells11010004.
166. Kawarasaki S, Matsuo K, Kuwata H, Zhou L, Kwon J, Ni Z, Takahashi H, Nomura W, Kenmotsu H, Inoue K, et al. Screening of flavor compounds using Ucp1-luciferase reporter beige adipocytes identified 5-methylquinoxaline as a novel UCP1-inducing compound. *Biosci. Biotechnol. Biochem.* (2022) 86, 380−389. doi: 10.1093/bbb/zbab216.
167. Granger DL, Taintor RR, Boockvar KS, and Hibbs JB Jr. Measurement of nitrate and nitrite in biological samples using nitrate reductase and Griess reaction. *Methods Enzymol.* (1996) 268, 142−151. doi: 10.1016/s0076-6879(96)68016-1.
168. Takahashi N, Kawada T, Yamamoto T, Goto T, Taimatsu A, Aoki N, Kawasaki H, Taira K, Yokoyama KK, Kamei Y, et al. Overexpression and ribozyme-mediated targeting of transcriptional coactivators CREB-binding protein and p300 revealed their indispensable roles in adipocyte differentiation through the regulation of peroxisome proliferator-activated receptor gamma. *J. Biol. Chem.* (2002) 277, 16906−16912. doi: 10.1074/jbc.M200585200.
169. Bougarne N, Weyers B, Desmet SJ, Deckers J, Ray DW, Staels B, and De Bosscher K. Molecular actions of PPARα in lipid metabolism and inflammation. *Endocr. Rev.* (2018) 39, 760−802. doi: 10.1210/er.2018-00064.
170. Sakamoto T, Nitta T, Maruno K, Yeh YS, Kuwata H, Tomita K, Goto T, Takahashi N, and Kawada T. Macrophage infiltration into obese adipose tissues suppresses the induction of UCP1 level in mice. *Am. J. Physiol. Endocrinol. Metab.* (2016) 310, E676−E687. doi: 10.1152/ajpendo.00028.2015.
171. Goto T, Naknukool S, Yoshitake R, Hanafusa Y, Tokiwa S, Li Y, Sakamoto T, Nitta T, Kim M, Takahashi N, et al. Proinflammatory cytokine interleukin-1β suppresses cold-induced thermogenesis in adipocytes. *Cytokine* (2016) 77, 107−114. doi: 10.1016/j.cyto.2015.11.001.
172. Okla M, Wang W, Kang I, Pashaj A, Carr T, and Chung S. Activation of Toll-like receptor 4 (TLR4) attenuates adaptive thermogenesis via endoplasmic reticulum stress. *J. Biol. Chem.* (2015) 290, 26476–26490. doi: 10.1074/jbc.M115.677724.
173. Yuliana A, Daijo A, Jheng HF, Kwon J, Nomura W, Takahashi H, Ara T, Kawada T, and Goto T. Endoplasmic reticulum stress impaired uncoupling protein 1 expression via the suppression of peroxisome proliferator-activated receptor γ binding activity in mice beige adipocytes. *Int. J. Mol. Sci.* (2019) 20, 274. doi: 10.3390/ijms20020274.
174. Lander HM, Jacovina AT, Davis RJ, and Tauras JM. Differential activation of mitogen-activated protein kinases by nitric oxide-related species. *J. Biol. Chem.* (1996) 271, 19705−19709. doi:

10.1074/jbc.271.33.19705.
175. Kim H, Shim J, Han PL, and Choi EJ. Nitric oxide modulates the c-Jun N-terminal kinase/stress-activated protein kinase activity through activating c-Jun N-terminal kinase kinase. *Biochemistry* (1997) 36, 13677−13681. doi: 10.1021/bi970837f.
176. Magenta A, Greco S, Capogrossi MC, Gaetano C, and Martelli F. Nitric oxide, oxidative stress, and p66Shc interplay in diabetic endothelial dysfunction. *Biomed. Res. Int.* (2014) 2014, 193095. doi: 10.1155/2014/193095.
177. Kim SM, Yuen T, Iqbal J, Rubin MR, and Zaidi M. The NO-cGMP-PKG pathway in skeletal remodeling. *Ann. N. Y. Acad. Sci.* (2021) 1487, 21−30. doi: 10.1111/nyas.14486.
178. Oyadomari S, Takeda K, Takiguchi M, Gotoh T, Matsumoto M, Wada I, Akira S, Araki E, and Mori M. Nitric oxide-induced apoptosis in pancreatic beta cells is mediated by the endoplasmic reticulum stress pathway. *Proc. Natl. Acad. Sci. U. S. A.* (2001) 98, 10845−10850. doi: 10.1073/pnas.191207498.
179. Gotoh T and Mori M. Nitric oxide and endoplasmic reticulum stress. *Arterioscler. Thromb. Vasc. Biol.* (2006) 26, 1439−1446. doi: 10.1161/01.ATV.0000223900.67024.15.
180. Fischer K, Ruiz HH, Jhun K, Finan B, Oberlin DJ, van der Heide V, Kalinovich AV, Petrovic N, Wolf Y, Clemmensen C, et al. Alternatively activated macrophages do not synthesize catecholamines or contribute to adipose tissue adaptive thermogenesis. *Nat. Med.* (2017) 23, 623–630. doi: 10.1038/nm.4316.
181. Vilela VR, Samson N, Nachbar R, Perazza LR, Lachance G, Rokatoarivelo V, Centano-Baez C, Zancan P, Sola-Penna M, Bellmann K, et al. Adipocyte-specific Nos2 deletion improves insulin resistance and dyslipidemia through brown fat activation in diet-induced obese mice. *Mol. Metab.* (2022) 57, 101437. doi: 10.1016/j.molmet.2022.101437.
182. Rong JX, Qiu Y, Hansen MK, Zhu L, Zhang V, Xie M, Okamoto Y, Mattie MD, Higashiyama H, Asano S, et al. Adipose mitochondrial biogenesis is suppressed in db/db and high-fat diet-fed mice and improved by rosiglitazone. *Diabetes* (2007) 56, 1751−1760. doi: 10.2337/db06-1135.
183. Sansbury BE, Cummins TD, Tang Y, Hellmann J, Holden CR, Harbeson MA, Chen Y, Patel RP, Spite M, Bhatnagar A, et al. Overexpression of endothelial nitric oxide synthase prevents diet-induced obesity and regulates adipocyte phenotype. *Circ. Res.* (2012) 111, 1176−1189. doi: 10.1161/CIRCRESAHA.112.266395.
184. Ferraz-Bannitz R, Welendorf CR, Coelho PO, Salgado W Jr, Nonino CB, Beraldo RA, and Foss-Freitas MC. Bariatric surgery can acutely modulate ER-stress and inflammation on subcutaneous adipose tissue in non-diabetic patients with obesity. *Diabetol. Metab. Syndr.* (2021) 13, 19. doi: 10.1186/s13098-021-00623-w.
185. Jahansouz C, Xu H, Hertzel AV, Kizy S, Steen KA, Foncea R, Serrot FJ, Kvalheim N, Luthra G, Ewing K, et al. Partitioning of adipose lipid metabolism by altered expression and function of PPAR isoforms after bariatric surgery. *Int. J. Obes. (Lond.)* (2018) 42, 139−146. doi: 10.1038/ijo.2017.197.
186. Bartelt A, Widenmaier SB, Schlein C, Johann K, Goncalves RLS, Eguchi K, Fischer AW, Parlakgül G, Snyder NA, Nguyen TB, et al. Brown adipose tissue thermogenic adaptation requires Nrf1-mediated proteasomal activity. *Nat. Med.* (2018) 24, 292–303. doi: 10.1038/nm.4481.
187. Hou Y, Liu Z, Zuo Z, Gao T, Fu J, Wang H, Xu Y, Liu D, Yamamoto M, Zhu B, et al. Adipocyte-specific deficiency of Nfe2l1 disrupts plasticity of white adipose tissues and metabolic homeostasis in mice. *Biochem. Biophys. Res. Commun.* (2018) 503, 264–270. doi: 10.1016/j.bbrc.2018.06.013.
188. Bléher M, Meshko B, Cacciapuoti I, Gergondey R, Kovacs Y, Duprez D, L'Honoré A, and Havis E. Egr1 loss-of-function promotes beige adipocyte differentiation and activation specifically in inguinal subcutaneous white adipose tissue. *Sci. Rep.* (2020) 10, 15842. doi: 10.1038/s41598-020-72698-w.
189. Guo Y, Miao X, Sun X, Li L, Zhou A, Zhu X, Xu Y, Wang Q, Li Z, and Fan Z. Zinc finger

transcription factor Egf1 promotes non-alcoholic fatty liver disease. *JHEP Rep.* (2023) 5, 100724. doi: 10.1016/j.jhepr.2023.100724.
190. Sid V, Siow YL, Shang Y, Woo CW, and O K. High-fat diet consumption reduces hepatic folate transporter expression via nuclear respiratory factor-1. *J. Mol. Med. (Berl.)* (2018) 96, 1203–1213. doi: 10.1007/s00109-018-1688-8.
191. Su T, Liu P, Ti X, Wu S, Xue X, Wang Z, Dioum E, and Zhang Q. HIF1α, EGR1 and SP1 co-regulate the erythropoietin receptor expression under hypoxia: an essential role in the growth of non-small cell lung cancer cells. *Cell Commun. Signal.* (2019) 17, 152. doi: 10.1186/s12964-019-0458-8.
192. Doetzlhofer A, Rotheneder H, Lagger G, Koranda M, Kurtev V, Brosch G, Wintersberger E, and Seiser C. Histone deacetylase 1 can repress transcription by binding to Sp1. *Mol. Cell. Biol.* (1999) 19, 5504–5511. doi: 10.1128/MCB.19.8.5504.
193. Zeng H, Zhang JM, Du Y, Wang J, Ren Y, Li M, Li H, Cai Z, Chu Q, and Yang C. Crosstalk between ATF4 and MTA1/HDAC1 promotes osteosarcoma progression. *Oncotarget* (2016) 7, 7329–7342. doi: 10.18632/oncotarget.6940.
194. Fojas de Borja P, Collins NK, Du P, Azizkhan-Clifford J, and Mudryj M. Cyclin A-CDK phosphorylates Sp1 and enhances Sp1-mediated transcription. *EMBO J.* (2001) 20, 5737–5747. doi: 10.1093/emboj/20.20.5737.
195. Guo K, Andrés V, and Walsh K. Nitric oxide-induced downregulation of Cdk2 activity and cyclin A gene transcription in vascular smooth muscle cells. *Circulation* (1998) 97, 2066–2072. doi: 10.1161/01.cir.97.20.2066.
196. Chung SS, Kim JH, Park HS, Choi HH, Lee KW, Cho YM, Lee HK, and Park KS. Activation of PPARgamma negatively regulates O-GlcNAcylation of Sp1. *Biochem. Biophys. Res. Commun.* (2008) 372, 713–718. doi: 10.1016/j.bbrc.2008.05.096.
197. Wollaston-Hayden EE, Harris RB, Liu B, Bridger R, Xu Y, and Wells L. Global O-GlcNAc levels modulate transcription of the adipocyte secretome during chronic insulin resistance. *Front. Endocrinol. (Lausanne)* (2015) 5, 223. doi: 10.3389/fendo.2014.00223.
198. Zhang Y, Qu Y, Niu T, Wang H, and Liu K. O-GlcNAc modification of Sp1 mediates hyperglycaemia-induced ICAM-1 up-regulation in endothelial cells. *Biochem. Biophys. Res. Commun.* (2017) 484, 79–84. doi: 10.1016/j.bbrc.2017.01.068.
199. Ye X, Liu H, Gong YS, and Liu SF. LPS down-regulates specificity protein 1 activity by activating NF-κB pathway in endotoxemic mice. *PLoS One* (2015) 10, e0130317. doi: 10.1371/journal.pone.0130317.
200. Ruan H, Hacohen N, Golub TR, Van Parijs L, and Lodish HF. Tumor necrosis factor-alpha suppresses adipocyte-specific genes and activates expression of preadipocyte genes in 3T3-L1 adipocytes: nuclear factor-kappaB activation by TNF-alpha is obligatory. *Diabetes* (2002) 51, 1319−1336. doi: 10.2337/diabetes.51.5.1319.
201. Parameswaran N and Patial S. Tumor necrosis factor-α signaling in macrophages. *Crit. Rev. Eukaryot. Gene Expr.* (2010) 20, 87−103. doi: 10.1615/critreveukargeneexpr.v20.i2.10.
202. Arruda AP, Milanski M, Coope A, Torsoni AS, Ropelle E, Carvalho DP, Carvalheira JB, and Velloso LA. Low-grade hypothalamic inflammation leads to defective thermogenesis, insulin resistance, and impaired insulin secretion. *Endocrinology* (2011) 152, 1314−1326. doi: 10.1210/en.2010-0659.
203. Aymeric L, Apetoh L, Ghiringhelli F, Tesniere A, Martins I, Kroemer G, Smyth MJ, and Zitvogel L. Tumor cell death and ATP release prime dendritic cells and efficient anticancer immunity. *Cancer Res.* (2010) 70, 855−858. doi: 10.1158/0008-5472.CAN-09-3566.
204. Coutinho-Silva R and Ojcius DM. Role of extracellular nucleotides in the immune response against intracellular bacteria and protozoan parasites. *Microbes Infect.* (2012) 14, 1271−1277. doi: 10.1016/j.micinf.2012.05.009.
205. Jain S, Pydi SP, Toti KS, Robaye B, Idzko M, Gavrilova O, Wess J, and Jacobson KA. Lack of

adipocyte purinergic P2Y6 receptor greatly improves whole body glucose homeostasis. *Proc. Natl. Acad. Sci. U. S. A.* (2020) 117, 30763−30774. doi: 10.1073/pnas.2006578117.
206. Plomgaard P, Nielsen AR, Fischer CP, Mortensen OH, Broholm C, Penkowa M, Krogh-Madsen R, Erikstrup C, Lindegaard B, Petersen AM, et al. Associations between insulin resistance and TNF-alpha in plasma, skeletal muscle and adipose tissue in humans with and without type 2 diabetes. *Diabetologia* (2007) 50, 2562−2571. doi: 10.1007/s00125-007-0834-6.
207. Yamamoto T, Inokuchi T, Ka T, Yamamoto A, Takahashi S, Tsutsumi Z, Tamada D, Okuda C, and Moriwaki Y. Relationship between plasma uridine and insulin resistance in patients with non-insulin-dependent diabetes mellitus. *Nucleosides Nucleotides Nucleic Acids* (2010) 29, 504−508. doi: 10.1080/15257771003740986.
208. Rastaldo R, Pagliaro P, Cappello S, Penna C, Mancardi D, Westerhof N, and Losano G. Nitric oxide and cardiac function. *Life Sci.* (2007) 81, 779−793. doi: 10.1016/j.lfs.2007.07.019.
209. Abdelrahim M, Liu S, and Safe S. Induction of endoplasmic reticulum-induced stress genes in Panc-1 pancreatic cancer cells is dependent on Sp proteins. *J. Biol. Chem.* (2005) 280, 16508−16513. doi: 10.1074/jbc.C500030200.
210. Donati G, Imbriano C, and Mantovani R. Dynamic recruitment of transcription factors and epigenetic changes on the ER stress response gene promoters. *Nucleic Acids Res.* (2006) 34, 3116−3127. doi: 10.1093/nar/gkl304.
211. Weyer C, Foley JE, Bogardus C, Tataranni PA, and Pratley RE. Enlarged subcutaneous abdominal adipocyte size, but not obesity itself, predicts type II diabetes independent of insulin resistance. *Diabetologia* (2000) 43, 1498−1506. doi: 10.1007/s001250051560.

Acknowledgements

This research was supported by Monbukagakushō (MEXT) Research Scholarship from The Ministry of Education, Culture, Sports, Science and Technology, Japan.

First of all, I would like to express the deepest appreciation to Dr. Kazuo Inoue, my doctoral supervisor and the Professor of the Laboratory of Physiological Function of Food from the Division of Food Science and Biotechnology, Kyoto University, for his guidance, mentorship, and encouragement as well as genuine generosity during the course of the study.

I would also like to express my gratitude to the sub-chief examiner of the dissertation committee, Dr. Tsutomu Sasaki, Professor of the Laboratory of Nutrition Chemistry from the same division at Kyoto University, for his stimulating and fruitful discussion. The conversations after the defense inspired me to think comprehensively about my research.

I am also grateful to the Board of Professors of the Division of Food Science and Biotechnology: Dr. Kazuhiro Irie, Professor of the Laboratory of Organic Chemistry in Life Science; Dr. Fumito Tani, Professor of the Laboratory of Bioengineering; Dr. Kiyoshi Yasukawa, Professor of the Laboratory of Enzyme Chemistry; and Dr. Wataru Hashimoto, Professor of the Laboratory of Basic and Applied Molecular Biotechnology, for their invaluable feedback on my research and their guidance, which has enabled me to complete my PhD.

I would like to express my sincere gratitude to Dr. Tsuyoshi Goto, Associate Professor of the same Laboratory, for his countless feedback and advice during the doctoral course. He continuously provided encouragement and was always willing and enthusiastic to assist in any way he could

throughout the research. His contribution to my research is truly appreciated.

I also extend my thanks to Dr. Haruya Takahashi, Assistant Professor of my laboratory, Dr. Kousaku Ohinata, and Dr. Takumi Yokokawa, Associate Professor and Assistant Professor, respectively, of the Laboratory of Physiological Function of Food from the Division of Food Science and Biotechnology, Kyoto University. Their invaluable feedback and interest in my research have led to fruitful discussion of the study and enabled me to complete my dissertation.

I would also like to thank Ms. Kazue Yano, secretary of the same laboratory, for providing secretarial and administrative support for the laboratory.

I would like to express my sincere appreciation to Dr. Teruo Kawada, retired Professor of the Laboratory of Molecular Function of Food from the Division of Food Science and Biotechnology, Kyoto University, for giving me the opportunity to do research at Kyoto University.

I would like to express my gratitude to the participants of this study. I extend my deepest appreciation to Dr. Huei-Fen Jheng from the Research and Development Division, National Laboratory Animal Center, National Applied Research Laboratories, Taipei, Taiwan; Dr. Wataru Nomura, Assistant Professor of the Laboratory of Molecular Microbiology from the Division of Applied Life Sciences, Kyoto University; Dr. Shinsuke Mohri, Assistant professor from the Laboratory of Medical Physiology and Metabolism, Department of Biomedical Sciences, College of Life Sciences, Ritsumeikan University; Dr. Takeshi Ara from the Bioinformation and DNA Data Bank of Japan Center, National Institute of Genetics; Rina Yu, Professor from Department of Food Science and Nutrition, University of Ulsan, Republic of Korea; Yuko Okamatsu-Ogura, Kazuhiro Kimura, Masayuki Saito, Associate professor, Professor, Professor Emeritus from the Laboratory of Biochemistry, Departments of Basic

Veterinary Sciences, Faculty of Veterinary Medicine, Hokkaido University; Shigenobu Matsumura, Associate Professor from Division of Human Life and Ecology, Graduate School of Human Life and Ecology, Osaka Metropolitan University, as well as Hiroto Minamino from Department of Diabetes, Endocrinology, and Nutrition, Graduate School of Medicine, Kyoto University, for their supports and invaluable comments on my research. Their willingness to share their knowledge and expertise added depth and richness to my research.

I would like to sincerely appreciate Dr. Satoko Kawarasaki and Dr. Su-Ping Ng from the same laboratory for their passion for their research. They enable me to keep doing my doctoral course. My thanks also go to all members of the same laboratory: Masaki Asano (Assistant Technical Staff), Zheng Ni, Kouta Okudo, Yusuke Yoshiko, Shunta Numano, Mai Takada, and Takumi Kishimoto for creating a pleasant, friendly, supportive, and warm laboratory environment.

Lastly, but most sincere, thanks go to my family for their love, like an oasis in the desert.

Jungin Kwon

List of Publications

Original papers

- **Kwon J**, Aoki Y, Takahashi H, Nakata R, Kawarasaki S, Ni Z, Yu R, Inoue H, Inoue K, Kawada T, Goto T. Inflammation-induced nitric oxide suppresses PPARα expression and function via downregulation of Sp1 transcriptional activity in adipocytes. *Biochim Biophys Acta Gene Regul Mech.* (2023) 1866(4):194987. doi: 10.1016/j.bbagrm.2023.194987.

- **Kwon J**, Yeh YS, Kawarasaki S, Minamino H, Fujita Y, Okamatsu-Ogura Y, Takahashi H, Nomura W, Matsumura S, Yu R, Kimura K, Saito M, Inagaki N, Inoue K, Kawada T, Goto T. Mevalonate biosynthesis pathway regulates the development and survival of brown adipocytes. *iScience.* (2023) 26(3):106161. doi: 10.1016/j.isci.2023.106161.

Related papers

- Yeh YS, Iwase M, Kawarasaki S, **Kwon J**, Rodriguez-Velez A, Zhang X, Jeong SJ, Goto T, Razani B. Subcutaneous transplantation of white adipose tissue. *Methods Mol Biol.* (2023) 2662: 183–192. doi: 10.1007/978-1-0716-3167-6_16.

- Jheng HF, Takase M, Kawarasaki S, Ni Z, Mohri S, Hayashi K, Izumi A, Sasaki K, Shinyama Y, **Kwon J**, Ng SP, Takahashi H, Nomura W, Yu R, Ochiai K, Inoue K, Kawada T, Goto T. 8-Prenyl daidzein and 8-prenyl genistein from germinated soybean modulate inflammatory response in activated macrophages. *Biosci Biotechnol Biochem.* (2023) 87(7): 747–757. doi: 10.1093/bbb/zbad041.

- Kawarasaki S, Matsuo K, Kuwata H, Zhou L, **Kwon J**, Ni Z, Takahashi H, Nomura W, Kenmotsu H, Inoue K, Kawada T, Goto T. Screening of flavor compounds using Ucp1-luciferase reporter

beige adipocytes identified 5-methylquinoxaline as a novel UCP1-inducing compound. *Biosci Biotechnol Biochem.* (2022) 86(3): 380–389. doi: 10.1093/bbb/zbab216.

- Kawarasaki S, Sawazaki H, Iijima H, Ng SP, **Kwon J**, Mohri S, Iwase M, Jheng HF, Takahashi H, Nomura W, Inoue K, Kawada T, and Goto T. Comparative analysis of the preventive effects of canagliflozin, a sodium-glucose co-transporter-2 inhibitor, on body weight gain between oral gavage and dietary administration by focusing on fatty acid metabolism. *Diabetes Metab Syndr Obes.* (2020) 13: 4353–4359. doi: 10.2147/DMSO.S269916.

- Yuliana A, Daijo A, Jheng HF, **Kwon J**, Nomura W, Takahashi H, Ara T, KawadaT, and Goto T. Endoplasmic reticulum stress impaired uncoupling protein 1 expression via the suppression of peroxisome proliferator-activated receptor γ binding activity in mice beige adipocytes. *Int J Mol Sci.* (2019) 20(2): 274. doi: 10.3390/ijms20020274.

- Yeh YS, Jheng HF, Iwase M, Kim M, Mohri S, **Kwon J**, Kawarasaki S, Li Y, Takahashi H, Ara T, Nomura W, Kawada T, and Goto T. The mevalonate pathway is indispensable for adipocyte survival. *iScience.* (2018) 9: 175–191. doi: 10.1016/j.isci.2018.10.019.

- Matsu-Ura T, Baek M, **Kwon J**, Hong C. Efficient gene editing in *Neurospora crassa* with CRISPR technology. *Fungal Biol Biotechnol.* (2015) 2: 4. doi: 10.1186/s40694-015-0015-1.